DEVELOPMENT AND APPLICATION OF A MODEL FOR ESTIMATING THE EFFICIENCY AND CARBON FOOTPRINT OF REFRIGERATION SYSTEMS BY CONSIDERING THE IMPACT OF FOULING ON CONDENSER PERFORMANCE.

A thesis presented for fulfillment of the requirements for the degree of

Master of Philosophy

In

Energy Management

At Massey University, Palmerston North, New Zealand

Stephen M. Milgate

2011

Abstract

Refrigeration systems on industrial plants such as dairy processing facilities are major consumers of energy. The higher the efficiency of these systems the lower the cost of electricity and subsequent carbon emissions from electricity produced from fossil fuels.

Traditionally chemical treatment of cooling loops for refrigeration systems has been undertaken in a reactive manner. The treatment regime is only changed when there is a detrimental effect on the system such as the development of corrosion, scale or biofilm. Often this results in medium to long term losses in efficiency before the situation is rectified.

A predictive model has been developed that has the potential to allow real time control of chemical treatment for cooling loops. The model predicts the film thickness for common fouling materials found in cooling systems and the heat transfer efficiency losses associated with this fouling. Such a predictive model can be used in conjunction with monitoring of the apparent heat transfer efficiency to infer the film thickness and therefore guide chemical treatment programmes.

The model was tested against foulant efficiency relationships published by Qureshi and Zubair, Macleod - Smith and The Carrier Refrigeration Handbook. In all three cases the predictive model produced results that agreed with the results for each of these sources.

The model was also tested using the reticulated ammonia refrigeration system at Fonterra Whareroa. Psychrometric, climatic, data logged temperatures and sensor data from the Whareroa system database were used to calculate the efficiency of one of the refrigeration system's condensers (EC1). Resulting heat of rejection values and an estimated thermal conduction constant (k) based on a deposit analysis were used as inputs for the model to calculate the predicted foulant film thickness. Inspection of the evaporative condenser during the June

2010 shut determined the model had predicted the foulant film thickness to within 6% of the measured 1.62mm.

An energy balance was completed on the reticulated ammonia refrigeration system at Whareroa to provide a better understanding of the system dynamics. Unfortunately it was not possible to obtain complete agreement between heat load and heat of rejection for the ammonia system – the level of agreement ranged from 8.9 to 30.2%. This variability seems to be explained by incomplete monitoring of the condenser fan speed.

Although the predictive model produced results that agreed with three other researchers the level of efficiency determined by the model is dependent on the accuracy of a number of variables including the thermal conductivity value (k-value) chosen for the foulant material creating the insulating film on the evaporative condenser coils. This is easy to determine for a pure compound but there is no model available to predict the thermal conductivity of a composite fouling material. Consequently this would be one improvement that could be made to the model in the future.

Model capabilities would also be enhanced by incorporating the commercial version of EES. This would allow the model to be automated for 'on-line' real time system monitoring.

The evaporative condensers at Fonterra Whareroa that were used for this study are 'base load' heat of rejection units, i.e. they are always fully loaded or turned off. Consequently it is recommended that the model is further tested on refrigeration systems with variable loads to determine the accuracy for partial load situations, and also on systems with a range of fouling materials.

Acknowledgements

I would like to thank my thesis supervisor Dr Richard Love for his patience, guidance and encouragement throughout this project.

A big thank you must also go to Dr Kevin Gehan at Nalco for his mentoring and encouragement.

I would also like to acknowledge the constant assistance that I received from Fonterra Whareroa during the course of this project. In particular, special thanks goes to Jack Ballagh, Rob Arnoll and Andrew Richards for allowing me access to commissioning documentation for the ammonia refrigeration system and ongoing access to the I-history database.

Finally I would like to thank my partner Mandy Armstrong for her enduring patience, support and encouragement.

Table of Contents

List of Figures

List of Tables

CHAPTER 1 INTRODUCTION

1.1 Introduction

Refrigeration has played an important role in the development of the New Zealand economy. The meat processing and dairy export business which began in 1882 (International business forum, 2009), would not have been possible without the advent of refrigeration.

New Zealander's lives are impacted by refrigeration every day. Heat pumps and air conditioning are used to cool and heat living and work spaces, and to preserve our food through the use of chillers and freezers. Refrigeration is also used to extract heat from industrial processes through the use of equipment such as plate heat exchangers, compressors and cooling towers.

During most types of refrigeration heat is transferred from the material that requires cooling to another material – the 'coolant' or 'refrigerant'. The rate of heat transfer between the two materials is proportional to the temperature difference between the two materials. Any resistance to heat transfer created by 'fouling' of the heat transfer surfaces will have a detrimental effect on the efficiency of the transfer of heat and may create issues for the process the refrigeration system is connected to.

The mechanical vapour compression refrigeration process is a cyclic thermodynamic process that combines four stages: expansion, vapourisation, compression and condensation. The refrigerant experiences changes in its pressure, temperature and state during the cycle.

Each of the four stages is associated with a component of the refrigeration system. The descriptions below for each stage refer to the ideal cycle situation (the numbers on Figure 1 refer to the relevant component description):

1) Metering device (expansion) that ‘throttles’ the saturated refrigerant and causes a reduction in pressure and temperature while maintaining a constant enthalpy (isenthalpic). Also known as expansion or throttling valves.
2) An evaporator (vapourisation) is the heat exchanger where heat is captured from the environment requiring cooling. The uptake of heat causes the refrigerant to vapourise resulting in an increase in enthalpy equivalent to the latent heat of evaporation (vapourisation). The process occurs at constant temperature and pressure so it is an isothermal and isobaric process.
3) A compressor (compression) separates the low pressure (suction) side of the system from the high pressure (discharge) side of the system. The refrigerant is compressed from the saturation pressure in the evaporator to the saturation pressure within the compressor. In an ideal situation this process occurs at constant entropy (isentropic).
4) A condenser (condensation) is another heat exchanger that rejects heat from the compressed vapour to the external environment, reducing the superheated vapour (refrigerant) to a liquid. The heat rejected is equivalent to the heat of evaporation plus the heat of compression.

In reality the refrigeration process does not fully duplicate the ideal cycle described above. The two primary reasons for this are due to the dynamics of evaporation and condensation. Refrigerant leaving the evaporator is superheated, i.e. at a higher temperature than the low pressure saturation temperature. The refrigerant leaving the condenser is subcooled, i.e. colder than the high pressure saturation temperature. This is shown on the Mollier diagram in Figure 1 by points C, C’ (superheating) and A, A’ (subcooling) respectively. The refrigerant leaving the expansion valve is a mixture of vapour and liquid. This is shown in figure 1 as point B, which is within the saturation envelope. In large systems the liquid refrigerant leaving the expansion valve is separated from the vapour, and only the liquid is sent through the evaporator.

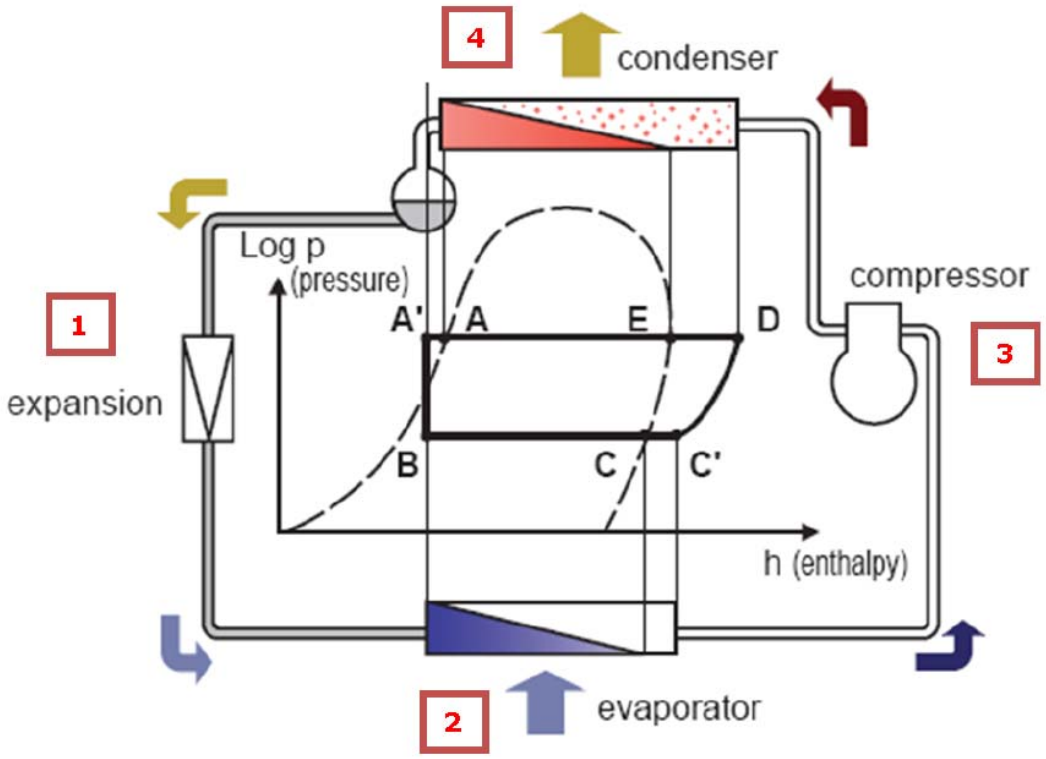

Figure 1: The Refrigeration cycle and associated Mollier diagram

Source: (Broeck, 2007)

Referring to the Mollier diagram in Figure 1, the expansion stage is represented by points A' to B, the evaporation stage by points B to C', the compression stage by points C' to D and the condensation stage by points D to A'.

The main energy input into the refrigeration system is to run the compressor. If the system is running at below optimum efficiency then more energy will be required to compress the refrigerant vapour to achieve the same amount of cooling. A key determinant of the efficiency of the system is the effectiveness with which the condenser rejects heat from the system. A reduction in the effectiveness of rejecting heat will be indicated by an increase in the condensation temperature. As the condensation temperature rises the compressor has to work harder to achieve the same level of cooling. Consequently, it is very important to minimise the condensation temperature in a refrigeration system so that energy use can be optimised.

In many situations an intermediate step is used to transfer heat from a process or environment to the refrigeration system. Water transfers heat from the process or environment that requires cooling to the evaporator where the heat load is transferred to the refrigerant stage. For many moderate temperature (4-200°C) industrial processes (Nalco, 1988) water is the preferred heat transfer medium to use in this situation due to its availability and high heat capacity.

Antifreeze agents are added to depress the freezing point of water for applications at or below 0°C. These agents include calcium and sodium chloride, methanol, glycerin, ethylene and propylene glycol. In many moderate temperature applications water is also used to transfer the heat rejected at the condenser to the environment. These systems are often called 'cooling water systems'.

1.2 Cooling water system chemical treatment

When water is used as a heat transfer medium treatment chemicals are often added for a number of reasons:

- To prolong its usefulness and therefore reduce waste (closed loops).
- To depress the freezing point of water, as noted above.
- To attenuate the corrosive or scaling effects associated with a particular water source (corrosion and scale inhibitors).
- For the reduction and removal of micro-organisms that may lead to fouling, corrosion (biocides and bio-dispersants) and a build-up of harmful pathogens such as Legionella.

An explanation of how these water treatment chemicals function is described below:

1.2.1 Corrosion inhibitors

Corrosion occurs when conditions allow an electrical cell or "corrosion circuit" to develop. Chemical reactions occur at the anode to remove metal, and at the cathode to remove oxygen.

An effective corrosion control programme usually depends on specific inhibitors for stopping the anodic reaction, slowing the cathodic reaction, or both. Typically, inhibitors used for corrosion protection in cooling water systems are chemical compounds as summarised in Table 1. Although these inhibitors are identified as either anodic or cathodic, the exact mechanisms by which they function are not precisely known. In several instances, an inhibitor may exhibit both anodic and cathodic characteristics, but one may predominate (Nalco, 1988).

Table 1: Typical Corrosion Inhibitors

Principally anodic	Principally cathodic	Both anodic and cathodic
Chromate	Calcium carbonate	Organic filming amines
Orthophosphate	Polyphosphate	Phosphonates
Nitrite	Zinc	
Silicate		

Source: (Nalco, 1988), (p 20.17)

When inhibitors were first introduced for the treatment of water systems, they were frequently composed of single active components (e.g. chromate). Over the years, some ingredients have been shown to improve the performances of others by the principle of synergism. For example, chromate by itself requires a concentration of 200 to 300 ppm to be effective as a corrosion inhibitor but if it is combined with small quantities of zinc it is effective at 20 to 30 ppm.

1.2.2 Scale inhibitors

Scale forms where there is a critical concentration of scale-forming minerals such as calcium, magnesium and silica and the chemical conditions are suitable for deposition to occur. Scale tends to form in hot regions of the cooling system because scale-forming salts solubility reduces with increase in temperature.

Scale inhibitors act in several different ways to stop scale formation as summarised in Table 2.

Table 2: Typical scale inhibitors

Scale inhibitor	Primary mode of action
Phosphonates	Scale conditioning
Poly-phosphonates, EDTA	Threshold inhibition
Acrylic polymers, lignins, tannins	Scale conditioning
Anionic polymers	Threshold inhibition

Source: (Nalco, 1988), (pp21.11-13)

Threshold inhibition chemicals prevent scale formation by keeping the scale-forming minerals in solution and not allowing a deposit to form. Scale conditioners modify the crystal structure of scale, creating bulky, transportable sludge instead of a hard deposit.

1.2.3 Biocides

The purpose of a cooling water biological treatment programme is to control the growth of micro-organisms (bacteria, algae, fungi, and protozoa) and macro-organisms (eg. mussels and clams) in cooling water systems. These organisms can cause serious problems including loss of heat transfer efficiency, corrosion, flow restriction, and public health issues.

Treatment often requires the use of biocides to kill microbe colonies and dispersants of concentrated surfactants to loosen and wash them away. Biocides can be classed as oxidising and non-oxidising. Oxidising biocides oxidise important cellular components in micro-organisms resulting in death of the organism. Non-oxidisers react with specific cell components within a micro-organism to ultimately destroy that cell. Table 3 summarises typical chemical compounds used as biocides.

Table 3: Typical biocides

Oxidising Biocides	Non-oxidising biocides
Chlorine gas	Isothiazolone
Sodium hypochlorite (bleach)	Dibromonitiloproprionamide (DBMPA)
Sodium bromide	Glutaraldehyde
Chlorine dioxide	Alkyl Dimethyl Benzyl Ammonium Chloride (Quaternary ammonium compounds)
Ozone	Carbamates
Bromochlorodimethylhydantoin	Terbuthylazine
	Methylene Bis-Thiocyanate

Source: (Nalco, 1988), (pp 22.1-16)

Over time a colony of micro-organisms will develop a resistance to a particular biocide. Consequently it is important to use a combination of two different biocides (usually an oxidising and non-oxidising biocide) to maintain good long term microbiological control of a specific water system.

1.2.4 Treatment programme management

It makes good economic sense to optimise the use of these water treatment chemicals. In New Zealand approximately $50 million dollars is spent on water treatment chemicals per annum to protect industrial plant from microbiological activity, scale formation and corrosion. Many industrial plants such as Fonterra Whareroa would spend in excess of $500,000 per annum for chemicals to keep their cooling water systems in optimum condition.

A large percentage of the chemicals used for the treatment of cooling water are not good for the environment. Biocides are designed to kill living cells so they are potentially hazardous to people and the environment, particularly waterways, if not managed appropriately. Several of the corrosion inhibitors are based on metals such as zinc and chromium, which also have a negative impact on the environment due to their toxicity if poorly managed.

The majority of methods used to control the rate of addition of inhibitors and biocides are based on the concentrating effects of cooling systems where evaporation is the primary means of heat removal. As water evaporates the impurities that are dissolved or suspended in the water are left behind. As the rate of evaporation increases there is a proportional increase in the concentration of impurities. The level of impurities in a system is controlled by the removal of 'cycled' water (bleeding) from the system and replacing it with fresh (makeup) water at a flow rate that maintains a constant level of contaminants. Generally the dissolved contaminant level is measured by conductivity and the chemicals are dosed proportional to makeup water flow.

1.3 The project environment

This project will focus on the refrigeration system at Fonterra Whareroa situated at Hawera in the Taranaki region of New Zealand.

Fonterra Whareroa is an example of a dairy processing plant that carries out industrial milk processing to produce cheese, milk powder, whey protein products, casein and butter (refer Figure 2). Electricity is also generated on-site through the use of steam turbines.

Chilled water is used to cool milk arriving on site to 5°C or less to inhibit the growth of micro-organisms. Chilled water is then used in other dairy process

sequences such as cooling after pasteurisation, Ultrafiltration (UF), and cooling of silos.

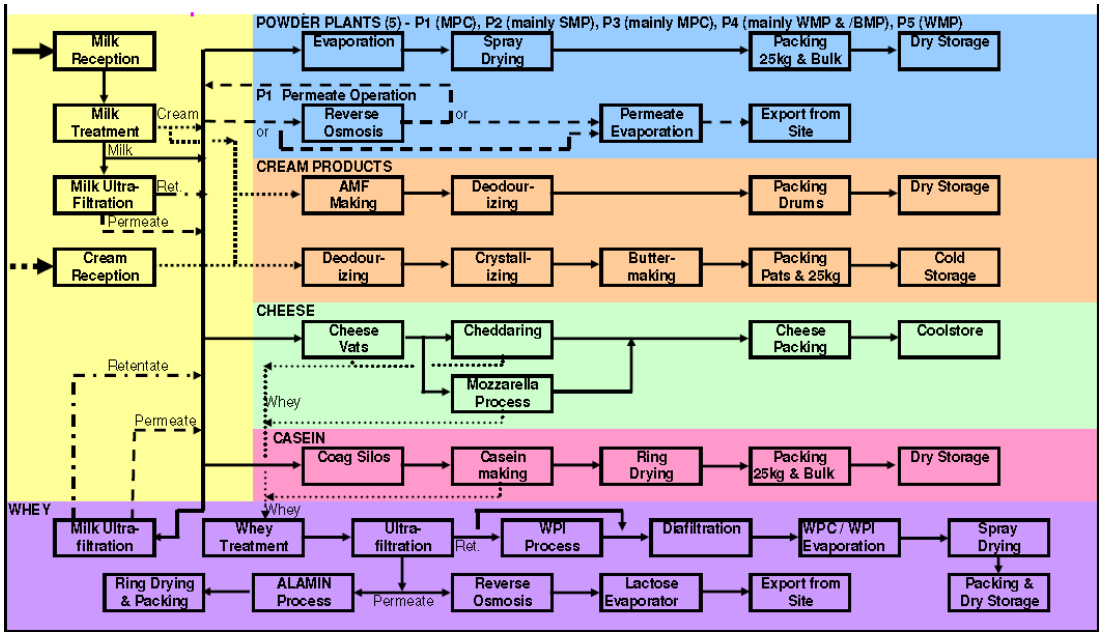

Source: Fonterra Whareroa Engineering Department

Figure 2: Basic milk processing flow diagram for the Fonterra Whareroa plant

Heat is transferred from the chilled water to the ammonia in the reticulated refrigeration circuit using counter current flow plate heat exchangers.

Figure 3 provides an example of the seasonal heat load profile through the plant. The implications of heat load and heat capacity for the plant are discussed further in Chapter 3.

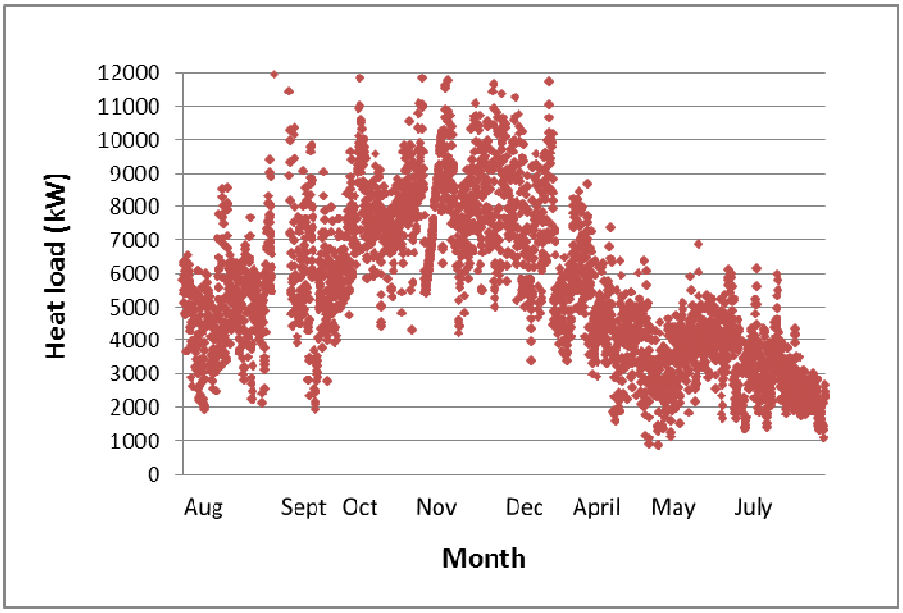

Figure 3: Example of seasonal heat load profile from processing plants to chilled water at Fonterra Whareroa for the period August 2009 to July 2010.

1.4 Energy management

Under the Kyoto Protocol New Zealand has made a commitment to reduce its CO_2-equivalent[1] (CO_2-e) emissions to pre-1990 levels. If this is to become a reality, or more realistically if the trend of increased CO_2-e is to be reversed then industry will need to be more discerning about electricity generation and use.

Figure 4 provides a summary of the use of fuels for thermal energy generation for the period 1990 to 2007. The use of gas and coal has increased significantly during this 17-year period. Gas use has increased by 2.2% per annum and coal has increased by 9.9% per annum. This increase has contributed significantly to the increase in CO_2-e emissions per MegaWatt hour (MWhr) of electricity produced from 0.12 tonsCO_2-e/ MWhr in 1990 to 0.17 tonsCO_2-e/ MWhr in 2007 for New Zealand (Table 5).

[1] **Greenhouse gas emissions are presented as carbon dioxide equivalents (CO_2-e) from the direct greenhouse gases carbon dioxide (CO_2), Methane (CH_4) and Nitrous oxide (N_2O), based on their global warming potential.**

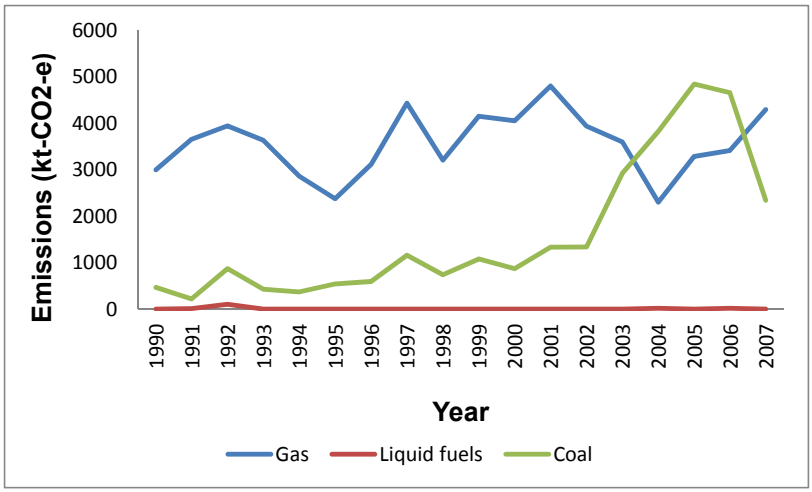

Figure 4: Thermal electricity generation emissions by fuel type for New Zealand (kt CO_2 equivalents)

Source: (New Zealand Ministry of Economic Development, 2008)

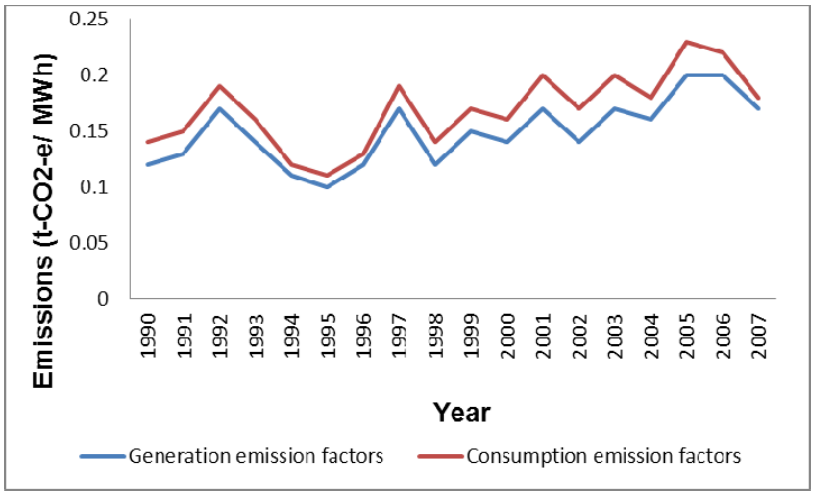

Figure 5: Emission factors for electricity generation and consumption for New Zealand.

Source: (New Zealand Ministry of Economic Development, 2008)

The CO_2-e emission factor for Whareroa is 0.634t per MWhr (Fonterra, 2010) due to the high level of CO_2 in the gas that the plant uses for Cogeneration. All other Fonterra plants use 0.22 t CO_2-e per MWh.

Refrigeration is a significant user of electricity at Fonterra Whareroa. The refrigeration system uses approximately 10% of the total electricity used on site.

Optimising the efficiency of the refrigeration plant will assist Whareroa to make meaningful reductions in electricity use and CO_2-e emissions.

As previously stated the cost of treating the system's used for cooling applications at Fonterra Whareroa is approximately $500,000 per annum. However the dose rate required to treat these system's is very low, in the order of 10 to 20 ppm (0.001 to 0.002%). Therefore the imbedded 'Carbon footprint' associated with the production and manufacture of these treatment chemicals is negligible when compared to the 'Carbon footprint' associated with the energy used to power the Refrigeration system. Consequently, for this study any CO_2-e produced in the manufacture of the treatment chemicals has been ignored.

1.5 Problem statement

The dosing of treatment chemicals in a ratio proportional to makeup water flow does not consider the condition of the system. If the heat transfer surfaces are becoming fouled the first indication is a loss in process efficiency and in many cases this is too late.

An added complication is that the efficiency ratings of evaporative condensers integrated into refrigeration systems are based on 'design' parameters. Design efficiency values provided by manufacturers for these condensers are based on maximum capacity heat loads. When the condenser is not fully loaded it is difficult to quantify the efficiency of this partially loaded unit because the efficiency relationship is not linear. This is because evaporative condensers reject heat by a combination of sensible heat transfer from the water film on the outside of the coil to the air and latent heat through evaporation of the water film to the air. Both heat and mass transfer mechanisms must be considered simultaneously to quantify the efficiency of the condenser (ASHRAE, 2008)

1.6 Objectives

The primary objective of this project is to develop a control algorithm that manages chemical addition by assessing the efficiency of the heat transfer process at all load levels and then taking any necessary remedial action in real time.

This study will focus on the condensing component of the refrigeration cycle. The rationale being, that the condenser is often a major determinant of refrigeration efficiency and power consumption due to its function of rejecting the heat of evaporation plus the heat of compression. Although changes in condenser temperature do not have as great an effect on refrigeration cycle performance as changes in vapourisation temperature at the evaporator (Dossat & Horan, 2001, pp127-129), optimising condenser efficiency reduces the saturation condensing temperature (and therefore pressure), resulting in lower energy use by the compressor(s).

A reduction in condenser efficiency results in a loss in heat rejection capacity which ultimately leads to an increase in the saturation temperature (pressure) of the condenser. The resulting higher discharge pressure places an increased load on the condenser. Obviously if the condenser cannot reject the total heat load a 'limiting factor' is created that will ultimately dictate a reduction in heat load from the process, i.e. a slowdown in production rate if heat rejection capacities are exceeded.

The specific objectives of this study are to:

1. Complete a comprehensive literature search to determine the techniques that are currently in use for estimating partial load heat transfer efficiencies. Particular emphasis will be placed on models that consider the effects of water side fouling on condenser efficiency.

2. Complete an energy balance and process dynamics study of an existing manufacturing facility so that the site can be used for model testing. This understanding of the system will also be used to monitor total system performance when a single parameter has been modified.

3. Assess identified models using condensers at known heat load levels.

4. Quantify the economic and environmental impacts of chemical dosing systems when the model is used.

5. Provide recommendations for potential refinements to the models tested.

1.7 Summary

Refrigeration is extremely important to the economy of New Zealand. It is also a significant user of energy.

The mechanical vapour compression refrigeration cycle is a four-stage process consisting of expansion of refrigerant to a liquid at low pressure, evaporation to a vapour to uptake energy (heat), and compression of the vapour to a higher pressure providing a manageable condensation temperature at the condenser where the energy is rejected from the system.

The use of treatment chemicals and good management practices allow industry to optimise the efficiency of these systems and in doing so reduce the environmental impact through CO_2 emissions caused by electricity generation from fossil fuels.

This project will focus on developing a model that can be utilised as a tool for monitoring refrigeration system efficiency at varying loads to allow optimisation of energy use.

Figure 6 provides a flow diagram for the development of this project:

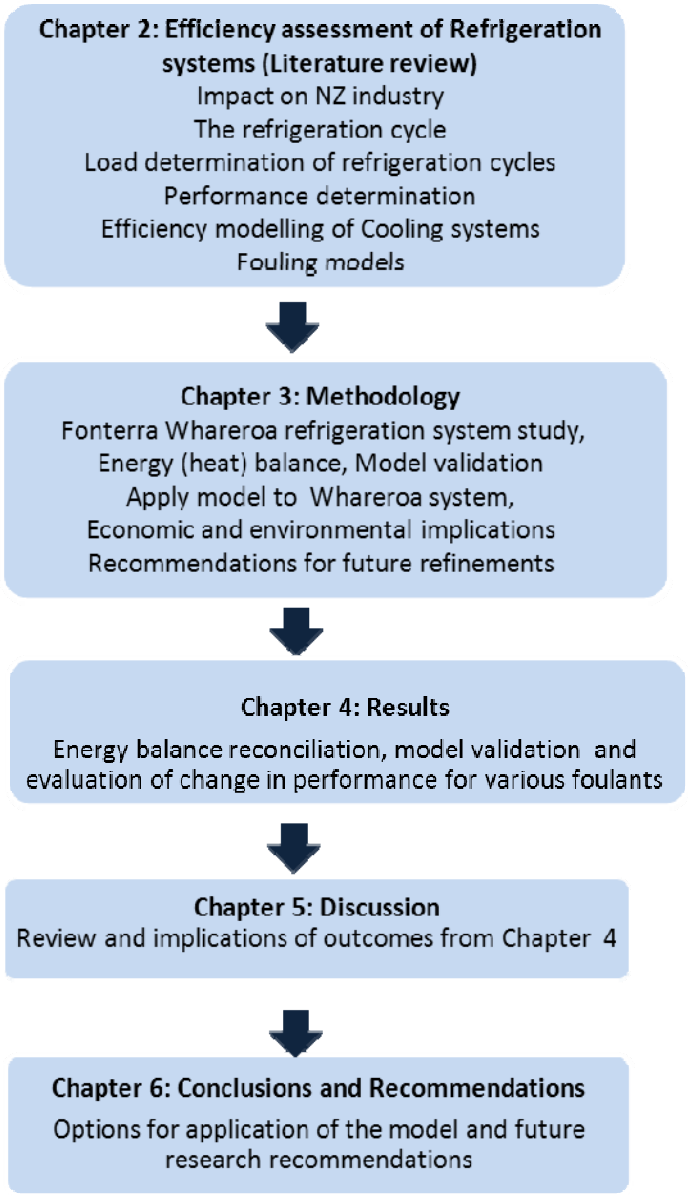

Figure 6: Flow diagram for the development of the thesis

CHAPTER 2 EFFICIENCY ASSESSMENT OF REFRIGERATION SYSTEMS

2.1 Background

Refrigeration processes are a significant user of energy on industrial sites. As an example, approximately 10% of the energy budget of a milk (dairy) processing site is consumed by the compressors that drive the refrigeration plant. Consequently, efficiency losses could have a significant impact on the economic viability and indirect environmental impact for industrial plants with refrigeration systems due to increased electricity demand.

The performance of a refrigeration cycle and its associated cooling processes can be precisely defined using the laws of thermodynamics. There are two main energy inputs to the refrigeration cycle (Dossat & Horan, 2001):

- The energy required to vapourise (and superheat) the liquid refrigerant in the evaporator ($\boldsymbol{Q_e}$) (kW)
- The energy required to compress the low pressure refrigerant vapour to a high pressure in the compressor ($\boldsymbol{W_{comp}}$) (kW)

$\boldsymbol{Q_e}$ represents the cooling that is done by the refrigerant system. $\boldsymbol{W_{comp}}$ represents the energy input to the compressor: in fact, due to the inefficiencies of the compressor motor, slightly more electrical energy will be required. The sum of the energy $\boldsymbol{Q_e}$ and $\boldsymbol{W_{comp}}$ is rejected to the external environment at the condenser. That is, there is one main energy output ($\boldsymbol{Q_c}$). The magnitude of $\boldsymbol{Q_c}$ is simply given by the first law of thermodynamics:

$$\boldsymbol{Q_c = Q_e + W_{comp}} \quad \textbf{(1)}$$

Where the energy flow for each process is given by:

$$Q = m_r \triangle h \ (kW) \quad \textbf{(2)}$$

Q = heat transfer (kW)

m_r = mass flow rate of refrigerant (kg/s).

$\triangle h$ = refrigerant enthalpy change over the evaporator or the condenser (kJ/kg).

And $W_{comp} = mr \triangle h \ (kW)$ **(3)**

$\triangle h$ = refrigerant enthalpy change over the compressor (kJ/kg).

Depending on the exact system configuration there is also electrical energy input to run the condenser fans, various pumps and peripheral devices. However, the compressor is the main electrical energy consumer in the refrigeration cycle (typically greater than 75%).

When there is no change in phase but a change in temperature (sensible heat), the energy balance for this situation may be given by:

$$Q = m_r \, Cp \triangle T \ (kW) \quad \textbf{(4)}$$

Where m_r = mass flow rate of refrigerant (kg/s)

Cp = specific heat of refrigerant (or other substance) (kJ/kg °C)

$\triangle T$ = change in temperature at condenser or evaporator (°C)

2.2 Heat rejection capacity of evaporative condensers and cooling towers

The main focus of this study will be on the condensing component of the refrigeration cycle. This is because the condenser(s) are the point where the combined heat load from the processes of evaporation and compression are rejected to the external environment and consequently where a chemical water treatment programme will influence the efficiency of the refrigeration system. Ultimately, the primary objective of this thesis is to provide a tool for monitoring any reduction in efficiency of the condenser in real time so that the internal water treatment of the water side of the heat exchanger can be adjusted to correct this situation.

It is also simpler working with the cooling loop of the condenser than the chilled water at the evaporators because there are no added complications from the process to consider.

Air cooled condensers, open cooling towers and evaporative condensers are all options for removing heat from a refrigeration system. In contrast to open cooling towers and evaporative condensers, air cooled condensers work against dry bulb temperature and therefore are less effective than wet bulb devices. This project will not be considering air cooled condensers because they do not use water and therefore do not require chemical treatment.

Open cooling towers and evaporative condensers are both used to transfer heat from a process such as a refrigeration system to the environment through evaporation of water on the surface of metal tubes. The evaporation of this surface water cools the tubes, which contain high temperature refrigerant, cooling the refrigerant vapour until it reaches the saturation temperature (assuming it is superheated, which is typical). On reaching the saturation temperature, the refrigerant is condensed. Once it is liquid, the refrigerant may be further subcooled (reduced in temperature below the saturation

temperature). Typically (for a standard system operating in New Zealand conditions), the refrigerant will have a saturation temperature of around 30 °C.

Assuming that the heat transfer surfaces are clean, the main determinant of efficiency is the ability of the atmosphere to absorb the vapour evaporated at the heat transfer surface. This is the reason why open cooling towers and evaporative condensers are sometimes termed 'wet bulb sensitive devices'.

This 'wet bulb sensitivity' can be explained through application of the equation for heat transfer through a heat transfer surface.

$$Q = UA(\Delta T)lm \qquad \textbf{(5)}$$

Where Q = Heat flow (kW)

U = Overall heat transfer coefficient (kW/m^2 K)

A = Heat transfer area (m^2)

$(\Delta T)lm$ = Log mean temperature difference

Assuming design conditions, if U is fixed and A is fixed then $(\Delta T)_{lm}$ is the only variable that can vary. $(\Delta T)_{lm}$ is dependent on the WB temperature of the air entering the condenser. Hence the condenser is sensitive to changes in WB temperature.

The main factor that determines the quantity of heat that can be rejected from a process using evaporation, also termed its capacity, is the atmosphere's ability to absorb the vapour that is being evaporated. The primary atmospheric property that describes this is the relative humidity.

Relative humidity (RH) is defined (Dossat & Horan, 2001, p319) as the ratio of the partial pressure of the water vapour in the atmosphere to the saturation pressure of the water vapour at the current dry bulb temperature. As RH increases, the atmosphere's ability to absorb more water vapour decreases, resulting in a reduction in the efficiency of an evaporative cooling device, such

as an evaporative condenser or open cooling tower. The limit occurs when the atmosphere cannot absorb any more water vapour (i.e. humidity is 100%), then the process of evaporation cannot occur.

In practical terms the wet bulb temperature (WB) is often used to determine the relative humidity of an environment because it is easier to measure. The wet bulb temperature is the temperature measured by a thermometer with a wetted wick. A thermometer with a wetted wick is cooled (by evaporation) to below the temperature measured by a dry bulb thermometer. The difference between the Dry Bulb and the Wet Bulb temperatures is termed the 'wet bulb depression' and this is directly related to the RH. The greater the wet bulb depression, the more evaporative cooling of the wick has occurred, hence the lower the relative humidity. As the wet bulb depression increases so too does the evaporation rate of the condenser. This will result in an increase in the efficiency of the open cooling tower or evaporative condenser.

Table 4 summarises the difference in characteristics for air at 20°C (DB) and atmospheric pressure for two different relative humidities: 50% and 90%. At 50% RH the WB temperature is 13.8°C, giving a wet bulb depression of 6.2. In comparison, at 90% RH the same environment yields a wet bulb depression of 1.14. Therefore the change (increase) in RH has moved the saturation curve closer to the constant relative humidity curve.

Table 4: Thermodynamic properties of air at 20°C for relative humidities of 50% and 90% at atmospheric conditions (STP)

Variable	***RH 50%***	***RH 90%***
Pressure (kPa)	101.3	101.3
Wet bulb temperature (°C)	13.78	18.86
Humidity ratio (kg/kg)	0.0073	0.0132

This relationship can also be illustrated using an Is plot. In Figure 7 below, point A shows the intersection of the DB curve at a value of 20°C with the RH

curve for 50%. The corresponding humidity ratio (x axis) is 0.0073 kg/kg. Therefore the amount of water that the air under these conditions can absorb before saturation is 0.0148-0.0073 = 0.0075 kg of water per kg of dry air.

In comparison at point B, the intersection of the DB curve at a value of 20°C with the RH curve for 90%, the humidity ratio is 0.0132 kg/kg. So, the amount of water that the air under these conditions can absorb before saturation is 0.0148-0.0132=0.0016 kg of water per kg of dry air, i.e. 0.0059 kg per kg of dry air less than at 50% RH.

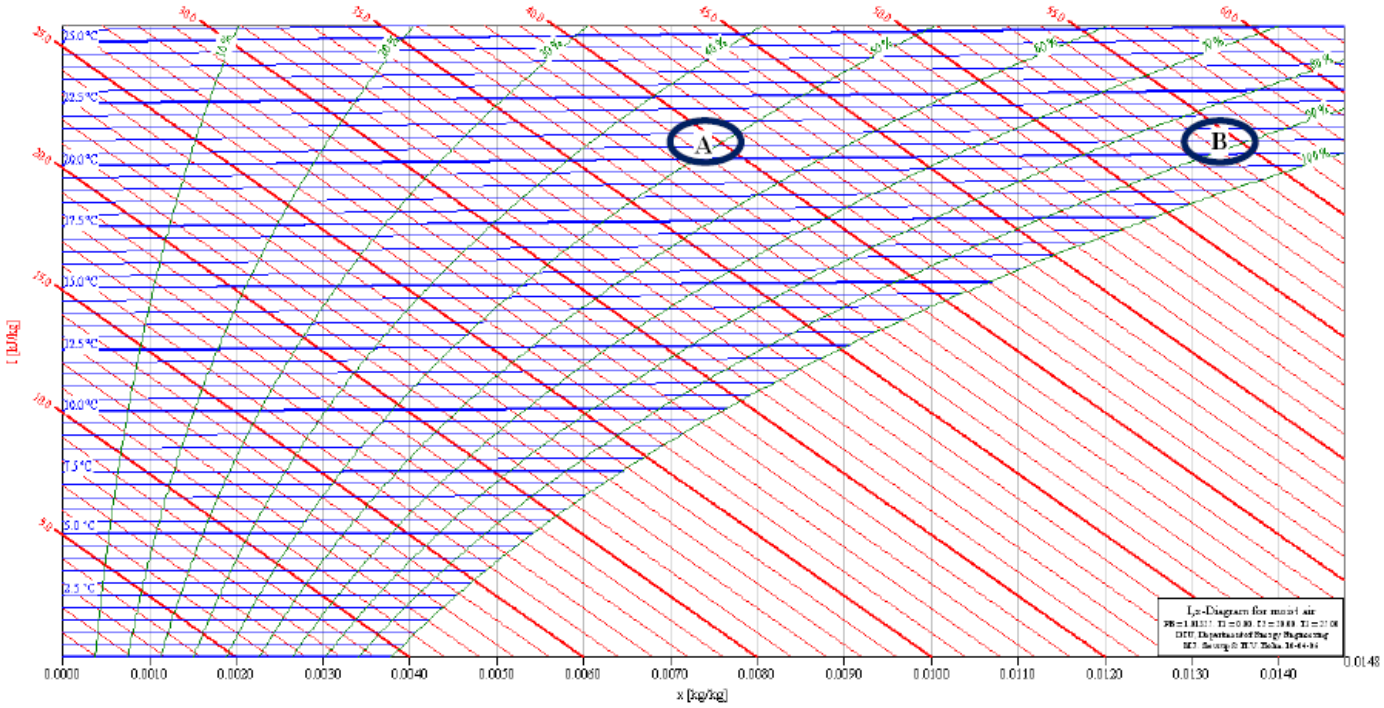

Figure 7: Is plot for air at atmospheric conditions.

Point A shows the intersection of the DB curve at a value of 20℃ with the RH curve for 50%. The corresponding humidity ratio (x axis) is 0.0073 kg/kg. Therefore the amount of water that the air under these conditions can absorb before saturation is 0.0148-0.0073 = 0.0075 kg of water per kg of dry air.

In comparison at point B, the intersection of the DB curve at a value of 20℃ with the RH curve for 90%, the humidity ratio is 0.0132 kg/kg. So, the amount of water that the air under these conditions can absorb before saturation is 0.0148-0.0132=0.0016 kg of water per kg of dry air, i.e. 0.0059 kg per kg of dry air less than at 50% RH.

2.3 Cooling Towers

In principle a cooling tower cools water by evaporation. Cooling towers reject heat through both mass (water particles) and heat transfer (latent heat) mechanisms. Two basic types of evaporative cooling devices are used by industry (ASHRAE, 2008). The first of these, the direct-contact or open cooling tower, exposes water directly to the cooling atmosphere and transfers the system heat load directly to the atmosphere. The second is the closed-circuit cooling tower, also called an Evaporative Condenser. Closed-circuit cooling towers indirectly contact the heat transfer fluid or vapour with the atmosphere.

If we refer to equation **(5):** $\boldsymbol{Q = UA(\Delta T)lm}$ the essential points are that for the evaporative condenser we only need to consider one calculation that accounts for both the wet bulb temperature and the refrigerant condensing temperature. In comparison for the open cooling tower we need to consider two calculations. One equation is at the cooling tower that accounts for the wet bulb temperature and cooling water temperature. The second equation is at the condenser which accounts for the cooling water temperature and the refrigerant temperature. The issue here is that the condensing temperature of the refrigerant cannot get as close to the wet bulb temperature, which results in a higher operating cost due to the refrigerant condensing at a higher pressure.

2.3.1 The Evaporative Condenser

An evaporative condenser is an evaporative cooling device that cools a refrigerant (or process fluid) through the mechanism of heat transfer. The evaporative condenser combines the cooling strategy of an air cooled condenser (sensible heat) with that of an open cooling tower (latent heat). Water is sprayed onto coils containing the vapourised refrigerant returning from the process it is cooling. It is

important that the spray completely wets the coil to optimise the efficiency of the heat transfer surface.

The refrigerant condenses and the heat of condensation is transferred through the wall of the coil to evaporate the water. The evaporated water is then absorbed by the air in the condenser. This air is then driven out into the environment using air fans (refer Figure 8 below) which also draw in dry air. The efficiency of the condenser increases as the quantity of air through the unit increases. In practical terms the air flow through the condenser is limited by the power requirements of the fan and the maximum air velocity that can be permitted without carryover of water droplets.

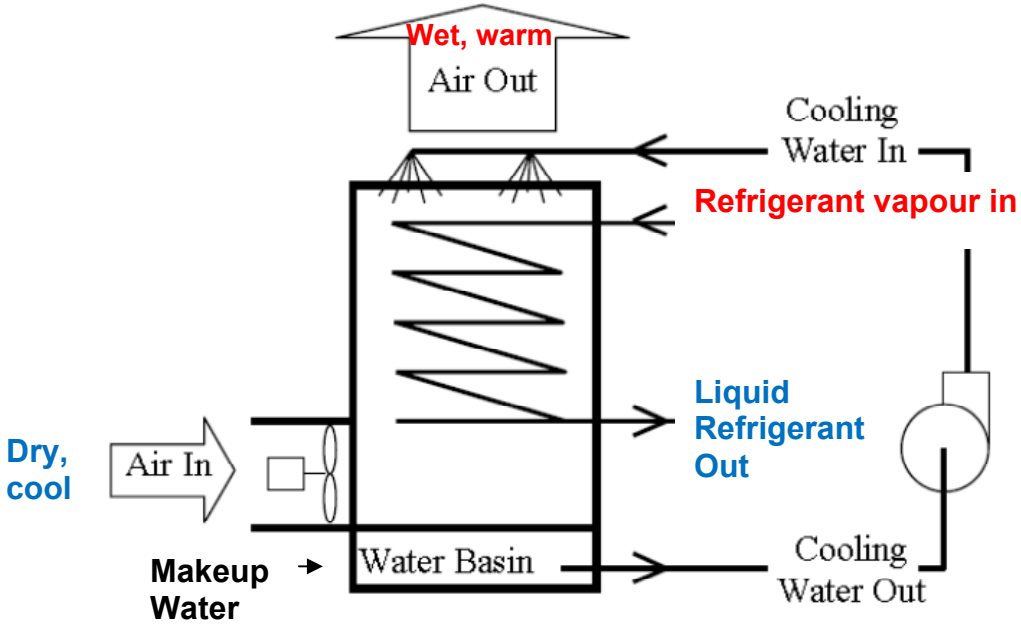

Figure 8: An Evaporative Condenser

Source: (Manske, Reindl, & Klein, 2001)

2.3.2 The open cooling tower

There are several design configurations for open cooling towers. Figure 9 demonstrates the general operational principles. Cooling water transferring the heat load from the process is distributed as a spray at the top of the tower, where it flows down through a fill packing that is used to maximise the surface area of the evaporation zone. Air is forced up through the fill using a fan and the heat of evaporation is removed from the water on the fill. The cooler water is then collected in the 'cold well' at the base of the tower before being re-circulated to the process. Water lost through evaporation is made up by the addition of fresh 'makeup' water to the cold well to maintain a constant level.

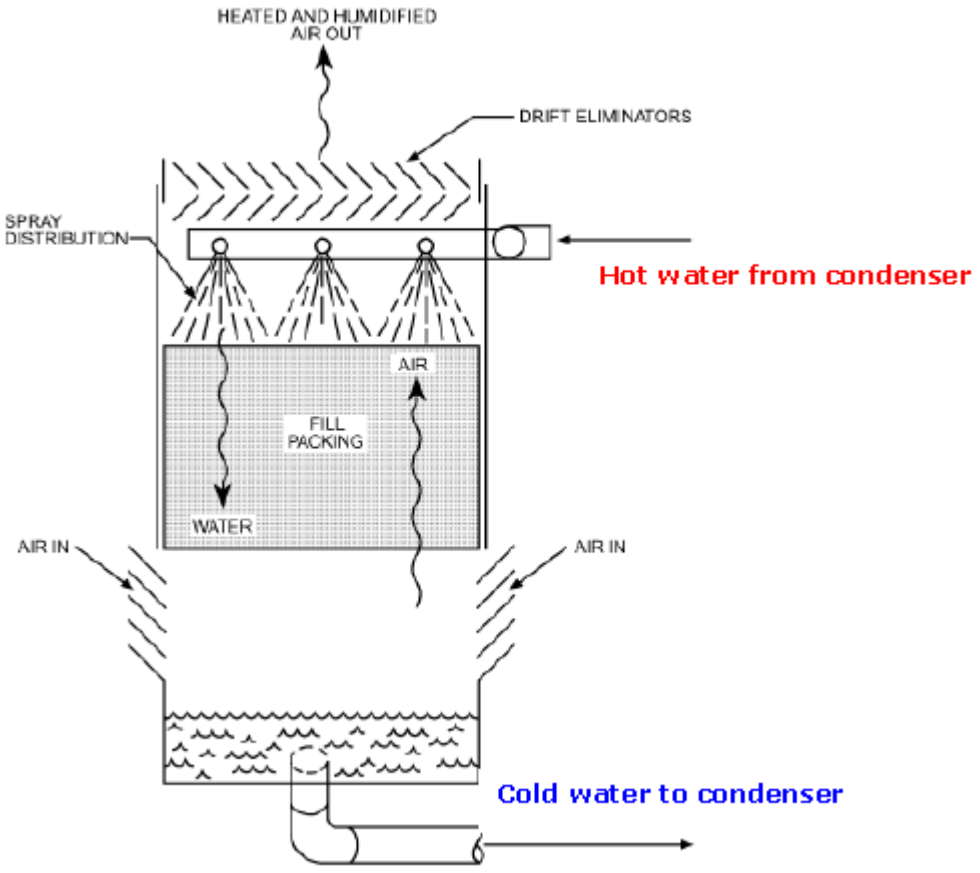

Figure 9: Direct-Contact or Open Cooling Tower

Source: (ASHRAE, Chapter 38: CONDENSERS, 2008)

2.4 Performance determination

There are a few different ways to view the efficiency of the refrigeration cycle and they are all inter-related. The Coefficient of Performance (*COP*) is a common measure of a refrigeration system's overall energy efficiency. *COP* is defined in several ways in the literature, although all are the ratio of cooling done to work done by the compressor that is required to do that cooling. The various *COP* definitions differ in what is considered to be the "work done by the compressor". For this project the following definition will be used:

$$COP = \frac{Q_e}{Q_c} \qquad \textbf{(6)}$$

The higher the value of *COP*, the greater the energy efficiency of the system.

Another metric for measuring the performance of a refrigeration system is the Heat Rejection Factor (*HRF*). *HRF* is a ratio of the heat rejected at the condenser to the heat accepted at the evaporator. The actual *HRF* a particular condenser is capable of can be described as a function of the outside air wet bulb temperature. Manske, Reindl, & Klein (2001, p19), provide a procedure for optimising this relationship (Appendix 1) as it is system and site specific.

Any change in the *HRF* may indicate a change in the heat transfer characteristics of the condenser.

The actual heat rejected at the evaporative condenser is determined by dividing the nominal heat rejection capacity by the *HRF*.

$$\boldsymbol{Q_C = \frac{N_C}{HRF\ (Twb,SCT)}} \quad \textbf{(7)}$$

and $$\boldsymbol{Q_C = Q_e HRF} \quad \textbf{(8)}$$

Where $\boldsymbol{N_c}$ is the Nominal capacity is the design capacity defined by the manufacturer of the evaporative condenser.

$\boldsymbol{HRF}$ is the heat rejection factor at a particular wet bulb temperature and saturation condensing temperature.

$\boldsymbol{N_c}$ and $\boldsymbol{HRF}$ at a specific wet bulb and SCT are commonly supplied by the manufacturer (refer Appendix 2 for the typical procedure).

The relationship of $\boldsymbol{HRF}$ to $\boldsymbol{COP}$ is:

$$\boldsymbol{HRF = \frac{Q_C}{Q_e}} \quad \textbf{(9)}$$

and $$\boldsymbol{W_{comp} = Q_C - Q_e} \quad \textbf{(1)}$$

Combining these equations:

$$\boldsymbol{HRF = \frac{W_{comp}+Q_e}{Q_e} = \frac{W_{comp}}{Q_e} + 1 = \frac{1}{COP} + 1} \quad \textbf{(10)}$$

Where $\boldsymbol{W_{comp}}$ is the work done by the compressor.

In summary, the efficiency of the refrigeration cycle varies in response to changes in the saturation temperature of the refrigerant at the condenser. If the saturation temperature at the evaporator remains constant (constant suction pressure), the

efficiency of the cycle decreases as the SCT (at the condenser) increases. This increase will be realised when the heat transfer capacity of the condenser is reached. If any fouling of the heat transfer surfaces is present, then this heat capacity of the condenser will be reached at a lower Heat of Rejection (HOR) level than the manufacturer's design specifications.

2.5 Efficiency Modelling

A survey of the literature indicates only a limited number of studies that focus on the performance of evaporative condensers. However, Ettouney, El-Dessouky, Bouhamra, & Al-Azmi (2001), provide an excellent summary of the development of modelling for evaporative condensers, from the very early models developed by Goodman (1938) and Thompsen (1946) to the predictive model developed by Peterson, Glasser, & Williams (1988).

A number of recently developed models that focus on efficiency of evaporative condensers have been reviewed. Brownell (1998), Manske, Reindl, & Klein (2001), Ettouney, El-Dessouky, Bouhamra, & Al-Azmi (2001), and Qureshi & Zubair (2006), have all developed models to optimise the efficiency of wet cooling towers and evaporative condensers for industrial processes.

Brownell's model is based on an effectiveness approach that is defined as the ratio of the condenser capacity to its maximum possible capacity at the same operating conditions. Where maximum capacity is the capacity achieved with no fouling present.

Since evaporative condensers reject heat through both mass (latent) and sensible heat transfer mechanisms, the effectiveness factor (E_f) must be based on enthalpy, rather than temperature alone.

$$Ef = \frac{\textbf{Condenser capacity}}{\textbf{Maximum capacity}} = \frac{m_a(h_{air,\,out} - h_{air,\,in})}{m_a(h_{air,\,out(T_{refrigerant,\,SCT})} - h_{air,\,in})} \quad \textbf{(11)}$$

Where

E_f is the effectiveness of an evaporative condenser

$h_{air,\,in}$ is the enthalpy of ambient air drawn into the evaporative condenser.

$h_{air,\,out}$ is the enthalpy of air at the exit of the evaporative condenser.

$h_{air,\,out(T_{refrigerant,\,SCT})}$ is the enthalpy of saturated air at the refrigerant condensing temperature.

m_a mass flow rate of air (kg/s)

Manske (2001) incorporated the Brownell effectiveness approach into a research project that developed a model of a refrigeration system for optimising system performance. One of the findings of the study was that operating system head pressures that minimised the energy costs of the system were found to be a linear function of outdoor wet-bulb temperature.

Ettouney et al (2001) explained that the maximum amount of heat is removed from an evaporative condenser and hence effectiveness is maximised as the condensate temperature cools to the wet bulb temperature of the air in the condenser.

Qureshi and Zubair (2006) have also completed a comprehensive evaluation of the literature. Their review found that some of the early researchers made problematic assumptions such as assuming that the spray water temperature is constant. This results in a meaningless outcome as determined by Parker & Treybal (1961). They also explain that Webb & Villacres (1984) have developed three computer algorithms that have been used to perform rating calculations of three evaporative cooler heat exchangers. These algorithms are “useful for rating commercially

available heat exchangers at off-design conditions." Qureshi and Zubair's work develops this concept further.

Qureshi and Zubair's mathematical model explains the dynamics of evaporative coolers and condensers, and how these dynamics are affected by fouling. This approach is supported through previous work carried out by Dreyer (1988), Mizushina, Ito, & Miyashita (1967) and Webb & Villacres (1984).

The dynamics of this model are possibly best represented as a diagram which is provided as Figure 10 below.

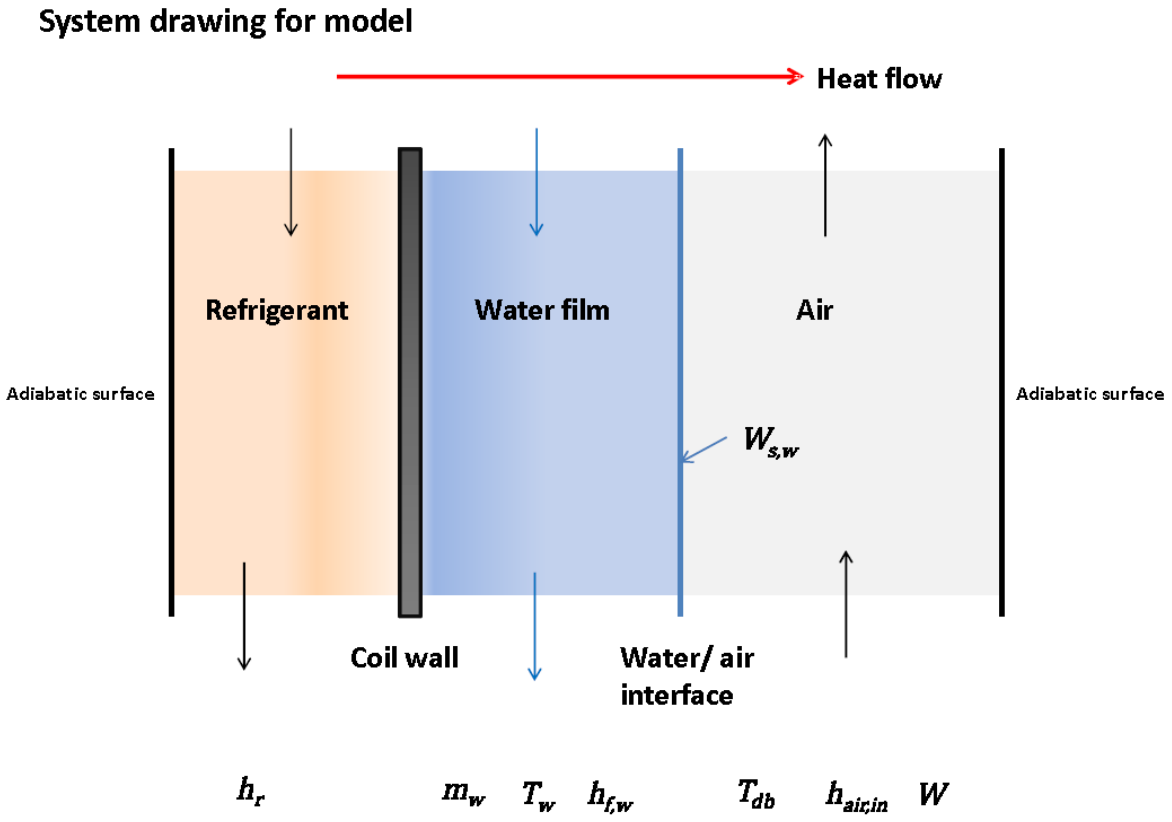

Figure 10: Dynamics of the Qureshi & Zubair model

The refrigerant condensers on the coil wall and the latent heat flows to the water film by means of conduction and convection. The heat is then transferred to the air stream by evaporation and mass transfer.

The Qureshi and Zubair model considers the flow of heat from the condensing refrigerant on the coil wall to the air flowing through the evaporative condenser. On condensing, the latent heat from the refrigerant flows through the coil wall by means of conduction and convection to the thin water film on the outside of the coil. The heat is then transferred to the air stream by means of evaporation and mass transfer.

The Qureshi and Zubair model proposes that the operation of an evaporative condenser can be described by five differential equations (nomenclature for these equations can be found in Appendix 4):

$$\frac{\partial W}{\partial A} = \frac{1}{m_a} dm_{wdA}$$

Represents the change in humidity over the area of the coil **(12)**

$$\frac{\partial mw}{\partial A} = hD(Wsint - W)$$

Represents the change in the mass low rate of water **(13)**

$$\frac{\partial ha}{\partial A} = \frac{hD}{ma}(hsint - ha)$$

Represents the change in the enthalpy of air **(14)**

$$\frac{\partial h_r}{\partial A} = \frac{U_{os}}{m_r}(T_r - T_{int})$$

Represents the change in refrigerant enthalpy **(15)**

$$\frac{\partial T_w}{\partial A} = \frac{1}{m_w C_{pw}}(m_a dh_{adA} - C_{pw} T_w dm_{wdA} - m_r dh_{rdA})$$

Represents the change in water temperature across the coil **(16)**

Integration of the differential equations allows us to calculate values for a range of operating conditions. The integrals proposed by Qureshi and Zubair are:

$$W = W_{in} + \int_0^{A1}(dWdA)dA \quad \textbf{(17)}$$

$$m_w = m_{wout} + \int_0^{A1}(dm_w dA)dA \quad \textbf{(18)}$$

$$h_a = h_{ain} + \int_0^{A1}(dh_a dA)dA \quad \textbf{(19)}$$

$$T_w = T_{wout} + \int_0^{A1}(dT_w dA)dA \quad \textbf{(20)}$$

$$h_r = h_{rout} + \int_0^{A1}(dh_r dA)dA \quad \textbf{(21)}$$

Qureshi and Zubair also make reference to an equation for effectiveness that is similar to the effectiveness approach proposed by Brownell (1998), and represented by Equation **(11)**, where effectiveness is defined as the ratio of the actual energy to the maximum possible energy transfer from the fluid in the coil. Brownell's approach differs from that of Qureshi and Zubair in that Brownell considers the enthalpy change of the air over the condenser whereas Qureshi and Zubair consider the enthalpy change of the refrigerant over the condenser. The Qureshi and Zubair effectiveness relationship is given by:

$$\varepsilon_{ec} = \frac{h_{rin} - h_{rout}}{h_{rin} - h_{win}} \quad \textbf{(22)}$$

Where h_{rin} = Enthalpy of refrigerant at inlet air temperature and pressure (kJ kg^{-1})

h_{rout} = Enthalpy of refrigerant at outlet air temperature and pressure (kJ kg^{-1})

h_{win} = Enthalpy of refrigerant at inlet air wet bulb temperature and pressure (kJ kg^{-1})

The primary outputs from Queshi and Zubair's study were:

- Mass flow ratio does not have a significant effect on system effectiveness.

- That the model was found to have good agreement with experimental data provided by other authors, e.g. the error was less than 6% when used to calculate the condensing temperature of the refrigerant.
- The model is a useful tool for design and rating calculations of evaporative coolers and evaporative condensers.

2.6 Fouling

Fouling is any build-up of material (scale, corrosion byproducts, entrained dirt or biofilm) on the heat transfer surfaces of the process or cooling side of a heat exchanger that creates a resistance to heat flow. Any reduction in heat flow through a process reduces the efficiency of that process. This ultimately increases energy costs and/or reduces output for this process. Fouling also increases the potential for corrosion and microbiological contamination of the system (e.g. Legionella).

In general terms, heat flow between fluids separated by a solid barrier can be represented mathematically by:

$$\boldsymbol{Q = UA(\Delta T)_{lm}} \quad \textbf{(4)}$$

The resistance to heat transfer is represented by the equation (ASHRAE, Chapter 38: CONDENSERS , 2008):

$$\frac{\mathbf{1}}{\boldsymbol{U}} = \frac{\mathbf{1}}{\boldsymbol{h_{inside}}} + \frac{\mathbf{1}}{\boldsymbol{h_{outside}}} + \frac{\boldsymbol{x}}{\boldsymbol{\lambda}} + \boldsymbol{R} \quad \textbf{(23)}$$

Where U = Overall heat transfer coefficient (kW/m^2 K)

h_{inside} = Film heat transfer coefficient on the outside of the surface (kW/m^2 K)

$h_{outside}$ = Film heat transfer coefficient on the inside of the surface (kW/m^2 K)

λ = Thermal conductivity of the material (kW/m/ K)

R = Resistance of the fouling layer (kW/m/ K)

x = Thickness of layer (m)

Equation **(23)** indicates that as the resistance of the fouling layer (***R***) increases the overall heat transfer coefficient (***U***) decreases; consequently either the rate of heat transfer (***Q***) decreases or the temperature difference over the condenser ($(\Delta T)_{lm}$) must increase to maintain a constant rate of heat transfer. It should be noted that the resistance (fouling) on both sides of the solid barrier have been considered. However, it is assumed that the resistance on the refrigerant side is negligible and therefore only the fouling on the water side will be considered in this study.

Gehan (2005) developed a "Wet Surface Air Cooler (WSAC) Performance Monitoring" tool to determine the effect of scaling (increased thermal resistance) on the Heat Transfer Coefficient ***U*** for condensing steam systems, e.g. surface condensers. Gehan's modelling approach may also be applicable to the water side of an evaporative condenser, where water is evaporating, if the appropriate heat transfer coefficients are used to calculate the overall design heat transfer coefficient U_{clean}.

Gehan determined that the fouled heat transfer coefficient has a relationship to the total thickness of calcium scale (δ) as follows:

$$U_{fouled} = \frac{1}{1/U_{clean}} + 0.417\delta \qquad \textbf{(24)}$$

Where U_{clean} = design or clean U (kW/m^2 K)

U_{fouled} = fouled or non-clean U

δ = Total radial thickness of scale deposit on coil (m)

Qureshi and Zubair have also developed a fouling model for evaporative cooler and condenser tubes (2004) that is a refinement of previous work by Kern & Seaton (1959), Mizushina, Ito, & Miyashita (1967), Webb & Villacres (1984), Dreyer (1988), Macleod-Smith, September (2003) and incorporates the fouling growth model developed by Khan, Qureshi, & Zubair (2004).

This model shows a good correlation between normalised fill performance index ($\eta_{Q,norm}$), due to fouling as a function of weight gain when applied to experimental data. The model was developed for cooling towers but the authors suggest that the model could also be applied to evaporative condensers due to their similar characteristics.

The model can be written as:

$$\eta_{Q,norm} = \frac{(Q_{clean} - Q_{fouled})}{Q_{clean}} = C_1\left(1 - exp\left(\frac{\delta}{C_2}\right)\right) \quad \textbf{(25)}$$

Where C_1 and C_2 are constants depending on the fouling characteristics of the evaporative condenser (see Appendix 4 for nomenclature). δ again, represents the total film thickness of scaling material, C_1 represents the increase in condenser performance index when the fouling reaches its asymptotic value ($\eta_{Cr} = nC1$), and C_2 represents the thickness where the performance has decreased to 63.2% of the asymptotic value due to fouling. A linear description of this model is:

$$\ln\left(\frac{1}{1-\frac{\eta_{Q\,norm}}{C_1}}\right) = \left(\frac{\delta}{C_2}\right) \qquad (26)$$

The model was compared to experimental data provided by Macleod-Smith (September, 2003) and found to have a best fit (coefficient of determination, R^2 = 0.999) when n = 0.76. Macleod-Smith showed that a calcium carbonate scale thickness of 2.4mm (δ =0.0024m) will reduce the capacity of an evaporative condenser by 55%. This value is only applicable to the condenser configuration used by Macleod-Smith and will vary for other configurations.

The primary outcomes of this work were:

- Recirculating water temperature was a better determinant of evaporative cooler performance than inlet wet bulb temperature.
- Decrease in effectiveness due to fouling is over 50% and 75% for condensers and evaporative coolers respectively when the fouling is increased to the asymptotic value, i.e. 2.4mm for $CaCO_3$ scale.

2.7 Sustainability of industrial processes

The result of increased energy costs through reduced efficiency is to decrease the economic sustainability of businesses when energy is a large component of their variable costs of production. This in turn motivates these businesses to focus on projects that will optimise this cost.

Projects that enhance the mechanism of heat transfer would fit into this category. Consequently, any procedures that remove the possibility of fouling on heat transfer surfaces should be viewed positively by industry.

The cost of energy continues to increase as the cost of oil, infrastructural and variable costs increase. Figure 11 shows that the cost of electricity to New Zealand industry has increased by 947.72% from 1974 to 2007 and 50.65% in the ten years to 2007.

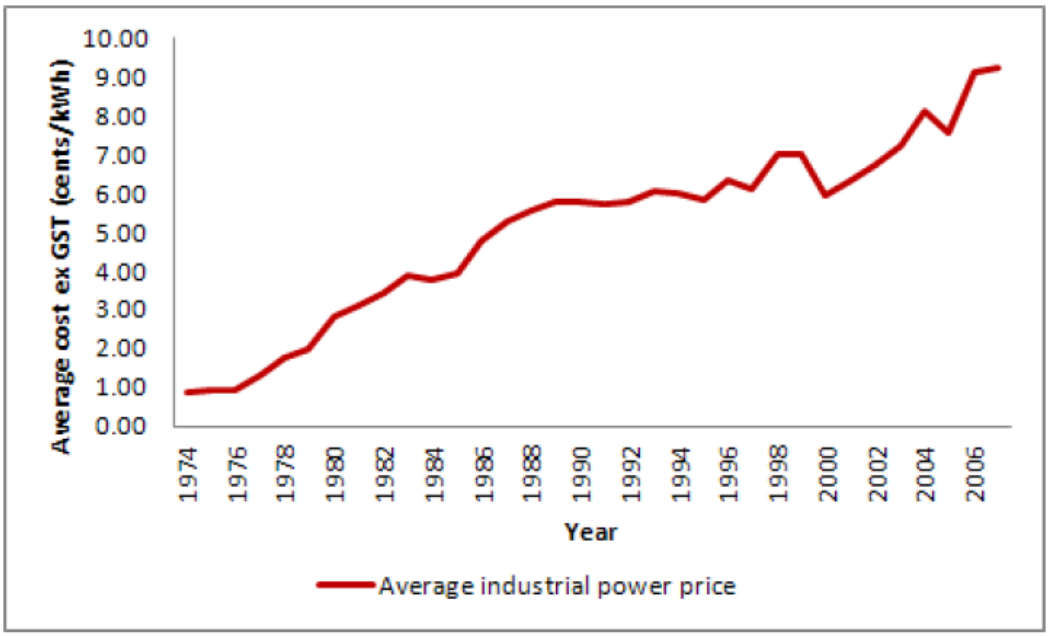

Figure 11: Industrial electricity prices for New Zealand (Real 2007 prices)

Source: MED Energy data 2007

Error! Reference source not found. gives a comparison of international industrial electricity prices for the period 1995 to 2007.

The cost of electricity to NZ industry has increased by 56% in the period 1995 to 2007. When compared to the other countries surveyed this is the third highest rate of increase. The result of this large increase is to project the comparative international cost of electricity to NZ industry from a low level in 1995 to the highest comparative cost in 2006.

Table 5: Comparison of international industrial electricity prices for the period 1995 to 2007.

Country	1995	2007	%Change
Australia	99.9	110.7	10.8%
Canada	76.7	132.0	72.1%
Germany	99.0	132.1	33.4%
Japan	101.5	115.2	13.5%
New Zealand	**87.4**	**136.6**	**56.3%**
UK	86.1	127.0	47.5%
USA	88.2	141.4	60.3%
OECD	88.1	130.1	47.7%

Source: IEA *Energy Prices and Taxes Fourth Quarter 2007 (NZD per MWh)*

This project will endeavour to make comparisons of the cost of energy with reductions in efficiency of cooling towers in general and evaporative condensers, specifically.

2.8 Summary

An energy balance can be performed over a refrigeration system using elementary thermodynamics. Assuming negligible heat losses and gains elsewhere in the system, the total heat rejected at the condenser is the sum of the heat of evaporation that is used to cool an external system plus the work done by the compressor(s).

This project focuses on the condensing portion due the major impact that this stage has on energy use of the refrigeration system together with the fact that this is the part of the system that can be seriously affected by water-side fouling issues.

The primary objective of this thesis is to provide a tool for monitoring any reduction in efficiency of the condenser in real time so that the internal water treatment of the water-side of the heat exchanger can be adjusted to correct this situation.

For many large scale refrigeration systems, the main mechanism used by the condenser to reject heat to the environment is evaporation of water. This system is often implemented as a complete unit (an evaporative condenser) or the condenser may be cooled with cooling water generated in a remote cooling tower through evaporation of water (condenser plus cooling tower system).

Evaporation efficiency is influenced significantly by the external environment's ability to absorb heat. The main factor influencing heat absorption is the water content of the air. As the moisture content (relative humidity) of the air increases so too does the air's ability to absorb heat. A common measure of moisture content is the wet bulb temperature. Consequently, cooling towers in general are often referred to as 'wet bulb devices'.

The efficiency of open system evaporative cooling device such as an evaporative condenser can be determined in several ways. This project will utilise the 'effectiveness approach' developed by Brownell (1998). This approach is based on an enthalpy balance to account for the fact that evaporative condensers reject heat through both mass (latent) and sensible heat transfer mechanisms.

The project also utilises the modeling of Qureshi and Zubair (2005) to define the dynamics of an evaporative condenser. This model was used because it is the most recent and comprehensive work on efficiency determination of evaporative condensers.

Electricity costs to New Zealand industry have risen by 56% in the period 1995 to 2006. These costs are still increasing and will continue to do so at an ever increasing rate as demand and cost of generation rise. Any tool that allows

industry to optimise energy efficiency will help to mitigate the impact of these costs and also reduce the carbon footprint of New Zealand industry.

CHAPTER 3 METHODOLOGY

3.1 Introduction

The main focus of this project is to identify the best approach for monitoring cooling tower efficiency. This approach will then be used to develop an algorithm to manage water-side fouling issues in real time.

As stated in Chapter 1, the objectives of this project are to:

1) Complete a comprehensive literature search to determine the techniques that are currently in use for estimating partial load heat transfer efficiencies, with particular emphasis on models that consider the effects of water-side fouling on condenser efficiency.

2) Complete an energy balance and process dynamics study of an existing manufacturing facility so that the site can be used for model testing. This understanding of the system will also be used to monitor total system performance when a single parameter has been modified.

3) Assess identified models using condensers at known heat load levels.

4) Quantify the economic and environmental benefits associated with all models tested.

5) Provide recommendations for potential refinements to the models tested.

The initial priority was to identify a manufacturing facility that provided enough sophistication to test the models identified in the literature search and that also provided reliable monitoring equipment for recording what was occurring in the process. It was also imperative that the plant was easily accessible and that the plant would give permission for their confidential data to be used for research purposes. Fonterra Whareroa (Hawera) was chosen as the research site because it satisfied all these requirements. This site is currently the largest milk processing plant in the world. It processes 2.76 billion litres of milk per annum with a total peak milk rate of 13.6 million litres/day, producing 400,000 tonnes of product per annum (www.fonterra.com).

Fonterra have also given permission for the developed model to be tested at other sites such as Hautapu (Waikato) and Clandeboye (Timaru).

3.2 Limitations

The research review determined that there are a limited number of research projects described in the open literature that have focused on condenser efficiency. Consequently, this project is adding to a very small base.

The integrity of this project is reliant to a large degree on the accuracy and reliability of the monitoring equipment at Fonterra Whareroa. Each monitoring device on site is calibrated on a regular basis and is reported as the “Whareroa Instrument Works Report” (Fonterra, 2009). Table 6 is an excerpt from this report which shows the calibration information held about some of the chilled water flow rate instruments at the Whareroa site. Similar information is held for other instruments, and the full report can be found in the appendices (Appendix 5).

Table 6: Excerpt of "Whareroa Instrument Works Report".

Identifying instrument tags, manufacturer, error limit, calibration test date, next calibration date and output.

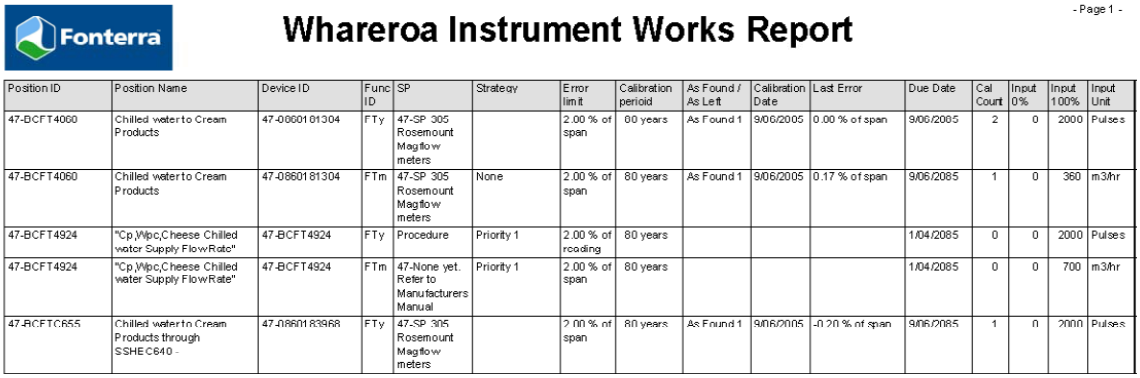

Fonterra

Whareroa Instrument Works Report

- Page 1 -

Position ID	Position Name	Device ID	Func ID	SP	Strategy	Error limit	Calibration period	As Found / As Left	Calibration Date	Last Error	Due Date	Cal Count	Input 0%	Input 100%	Input Unit
47-BCFT4060	Chilled water to Cream Products	47-0860181304	FTy	47-SP 305 Rosemount Magflow meters		2.00 % of span	80 years	As Found 1	9/06/2005	0.00 % of span	9/06/2085	2	0	2000	Pulses
47-BCFT4060	Chilled water to Cream Products	47-0860181304	FTm	47-SP 305 Rosemount Magflow meters	None	2.00 % of span	80 years	As Found 1	9/06/2005	0.17 % of span	9/06/2085	1	0	360	m3/hr
47-BCFT4924	"Cp,Wpc,Cheese Chilled water Supply FlowRate"	47-BCFT4924	FTy	Procedure	Priority 1	2.00 % of reading	80 years				1/04/2085	0	0	2000	Pulses
47-BCFT4924	"Cp,Wpc,Cheese Chilled water Supply FlowRate"	47-BCFT4924	FTm	47-None yet. Refer to Manufacturers Manual	Priority 1	2.00 % of span	80 years				1/04/2085	0	0	700	m3/hr
47-BCFTC655	Chilled water to Cream Products through SSHEC640 -	47-0860183968	FTy	47-SP 305 Rosemount Magflow meters		2.00 % of span	80 years	As Found 1	9/06/2005	-0.20 % of span	9/06/2085	1	0	2000	Pulses

The Whareroa Instrument Works Report (Fonterra, 2009) indicates surprisingly long calibration periods for some instruments (for example, the flow rate instruments in Table 6 supposedly do not need recalibration until 2085). When questioned about the long calibration periods the Fonterra Maintenance Coordinator claimed that as production is so dependent on the accuracy of these sensors, any sensor inaccuracy would be urgently noted and corrected as part of the analysis of production (Discussion with Jack Ballagh, June 2009). This strategy seems flawed, at face-value, because it seems to imply that product variance needs to occur before sensor inaccuracy is noted. This would be costly, as out-of-specification product is risked and sensor inaccuracy might also be difficult to diagnose when trouble-shooting the cause of product variation. It also seems problematic to calibrate these instruments during production periods (rather than during planned maintenance periods). However, it is assumed that these assurances are accurate and subsequent analysis of data gathered for this project (refer to Table 15) does indicate that the sensor data contained in I-history appears generally robust and consistent. Although, some of the chilled water flow rates may be questionable (see Discussion, section 4.5).

Fonterra capture all of their information from tagged sensor devices on their 'I-history' database. The reliability of the I-history database was integral to the

accuracy of this project. Tagged data was recovered from this database for several different monitoring periods. Table 7 provides details of the monitoring periods used for this project.

Table 7: I-history database data recovery details.

A list of tags used for each of these data extractions can be found in the appendices (Appendix 5). The hourly average is an average of two minute recording frequency for each tag.

Period	Frequency of data points
28th Jan 2008	Hourly average
28th Apr 2008 – 27th Apr 2009	Hourly average
1st Dec 2008 – 31st Dec 2008	Hourly average
29th Apr 2009 – 26th May 2009	Hourly average
18th Nov 2009 – 4th Feb 2010	Hourly average
4th Feb 2010 – 25th Apr 2010	Hourly average
3rd May 2010 – 24th May 2010	Hourly average
15th Jul 2010 – 30th Sep 2010	Hourly average
1st Nov 2010 – 15th Dec 2010	Hourly average

The I-history database returned useful data on all but one occasion. The temperature sensor for the BAC Evaporative Condenser #1, outlet water temperature failed for the 18th Nov 2009 – 4th Feb 2010 period.

Each data set was analysed using the 'Energy balance calculator spreadsheet' to determine the energy balance of the refrigeration system and the efficiency of the evaporative condenser. Refer to section 3.4.4 for details.

The load output from the compressors was deemed critical to the success of this project. In particular, the accuracy of the energy balance relied heavily on credible information from the condenser monitoring equipment. Consequently a study was

completed on the condensers that compared gauge ampere readings with data logged on the database. The study results can be found in the results section (4.2). However, in summary it was found that the gauge readings of the compressors complemented the data extracted from I-history.

All of the development work for this project has taken place on the ammonia refrigeration circuit at Whareroa. The hypothesis that the outcomes of this research are transferable to other processes has not been tested. However, it is likely that this model could be used for situational analysis of the refrigeration systems at other sites.

3.3 Assumptions

Several assumptions were made in terms of system efficiency and use of models from the literature.

3.3.1 System efficiency assumptions

Heat transfer across all heat exchanger units was assumed to proceed uniformly through all heat transfer surfaces within these units. In reality this is probably not the case but the average heat transfer across heat transfer surfaces is likely to be close to the assumed situation.

Within the EC5 refrigeration plant, six screw-type compressors are utilised for compression of the ammonia vapour. It is assumed that the compressor energy use efficiency (isentropic efficiency) of these compressors is as defined by the manufacturer's data. The specific isentropic efficiency of each compressor is calculated using the 'Energy balance calculator spreadsheet' (Love & Cleland, 2007) for each specific load level using the user specified function η_i. This function calculates the isentropic efficiency by calling on the pressure ratio, discharge temperature, load and compressor.

The pressure ratio is the ratio of discharge pressure to suction pressure; the discharge temperature is the temperature of the refrigerant leaving the compressor and the load is the fractional load of the compressor.

$$\eta_i = A(1) + A(2)PR + A(3)PR^2 + A(4)PR^3 + A(5)PR^4 + A(6)T_{dis} + A(7)T_{dis} + A(8)T_{dis}{}^2PR \quad \textbf{(27)}$$

Where η_i = isentropic efficiency

PR = pressure ratio (discharge pressure (kPa) / suction pressure (kPa))

$A(x)$ = manufacturer's performance factors

T_{dis} = temperature of refrigerant at discharge (°C)

The load on the compressors is dependent on the heat load placed on the refrigeration system by the processing plants. The compressors are managed to optimise their use, i.e. given a particular load, the compressors that are utilized are chosen to maximize the load on each compressor in order to increase efficiency. However, the compressors are often run at part load due to the staging constraints that are dictated by the sizing of the compressors. When the compressors are running at part load it is assumed that efficiency is determined by the Power Load Correction Factor relationship:

$$\eta_p = expB(1) + B(2)\,\%FLC + B(3)PR + B(4)FLC^2 + (5)PR^2 + B(6)PR\,\%FLC \quad \textbf{(28)}$$

Where η_p = part load efficiency

FLC = percent full load capacity

PR = pressure ratio

$B(x)$ = manufacturer's performance factors

It is also assumed that the pressure drops in the suction and discharge lines (pre and post compression) are negligible due to effective insulation of the pipes and utilisation of correct design characteristics such as pipe diameter.

3.3.2 Modelling assumptions

The model developed for the cooling tower utilises the work of Qureshi and Zubair (2006). The assumptions expressed by these researchers are adopted for this project:

- The system is in steady state.
- The apparatus and the cooling water re-circulating circuit are insulated from the surroundings.
- Radiation heat transfer is ignored.
- Negligible water loss due to drift.
- The heat and mass transfer co-efficients are constant within the tube bundle.
- Complete surface wetting of the tube bundle.
- The distribution of air and water is uniform at the inlets and this uniformity is maintained. Thus, the temperatures in the unit will only depend on the vertical position in the unit, which implies that the model is one-dimensional.
- The film temperature at the air-water interface (T_{int}) is equal to the bulk film temperature (T_w) i.e. ($T_{int}=T_w$).
- The re-circulating water temperature at the inlet ($T_{water,in}$) and the outlet are the same(T_{wout}) i.e. $T_{water,in} = T_{wout}$.
- The water film on the tubes is considered to be very thin, i.e. the air-water interface area is approximately equal to the outer surface area of dry tubes.

3.4 Energy Balance

The process for determining the energy balance of the Whareroa Refrigeration System was divided into several phases: system survey, data collection, energy calculations and rationalisation of the data to achieve an energy balance.

3.4.1 System Survey

The system survey scoped out and determined the mechanical components of the EC5 Refrigeration System at Fonterra Whareroa. This refrigeration system was originally commissioned in 1994.

The system is a single-stage pump recirculation ammonia (R717) plant comprising of a central ammonia engine room with six compressors connected to two vertical separation vessels. The liquid ammonia is circulated through five processing plants.

Figure 12 is a basic schematic diagram detailing the interaction of hot and cold utility through the refrigeration system.

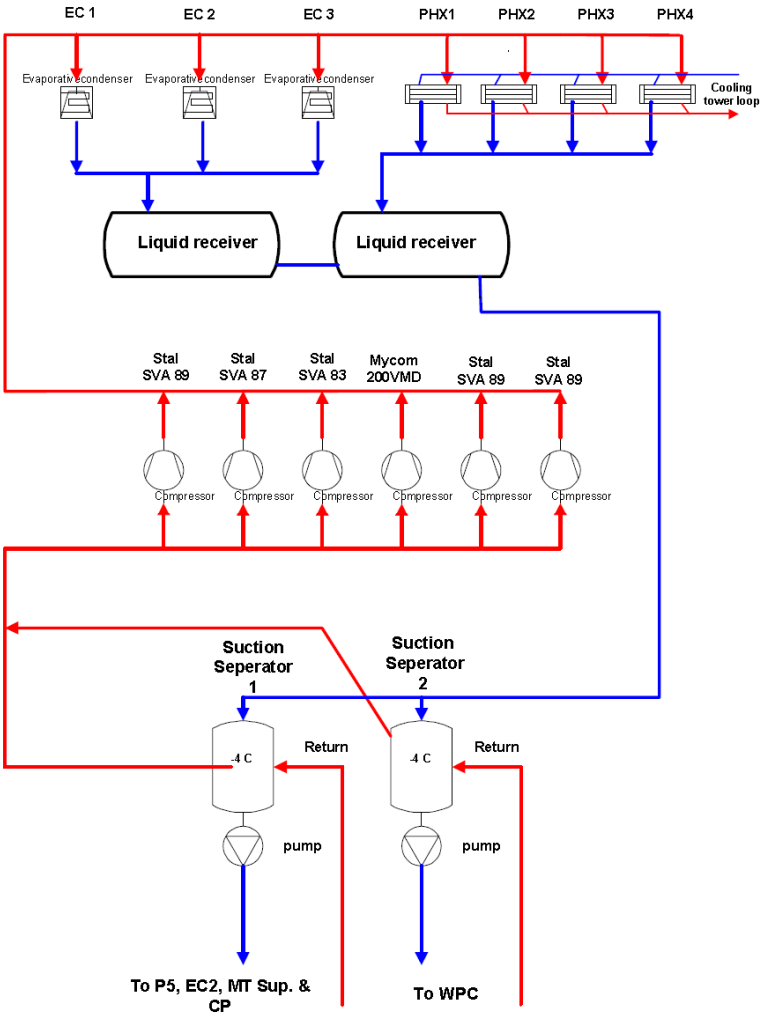

Figure 12: Basic plant diagram of the EC5 refrigeration system showing the vapourised refrigerant (Red line) and liquid ammonia (Blue line).

The heat carrying vapour returns from the processing plants to the suction separator. The compressors draw on this vapour and compress it from 2.7 barg to 10.7 barg. Resulting hot ammonia vapour is then condensed to approximately 35°C in the evaporative condensers or plate heat exchanger condensers. The heat of rejection is removed by condensing the refrigerant, cooling for the condensers is provided by evaporation of water either directly at the evaporative condensers, or at the cooling towers (for the plate heat exchangers).

Figure 13 is a pictorial representation of the EC5 Refrigeration System. The condenser component of the system contains 3 BAC evaporative condensers with a design heat rejection capacity of 7,628 kW and 4 Alfa Laval plate heat exchangers with a design heat rejection capacity of 18,076 kW (refer to Table 9 for details). Total design heat rejection capacity from the system is 25,704 kW.

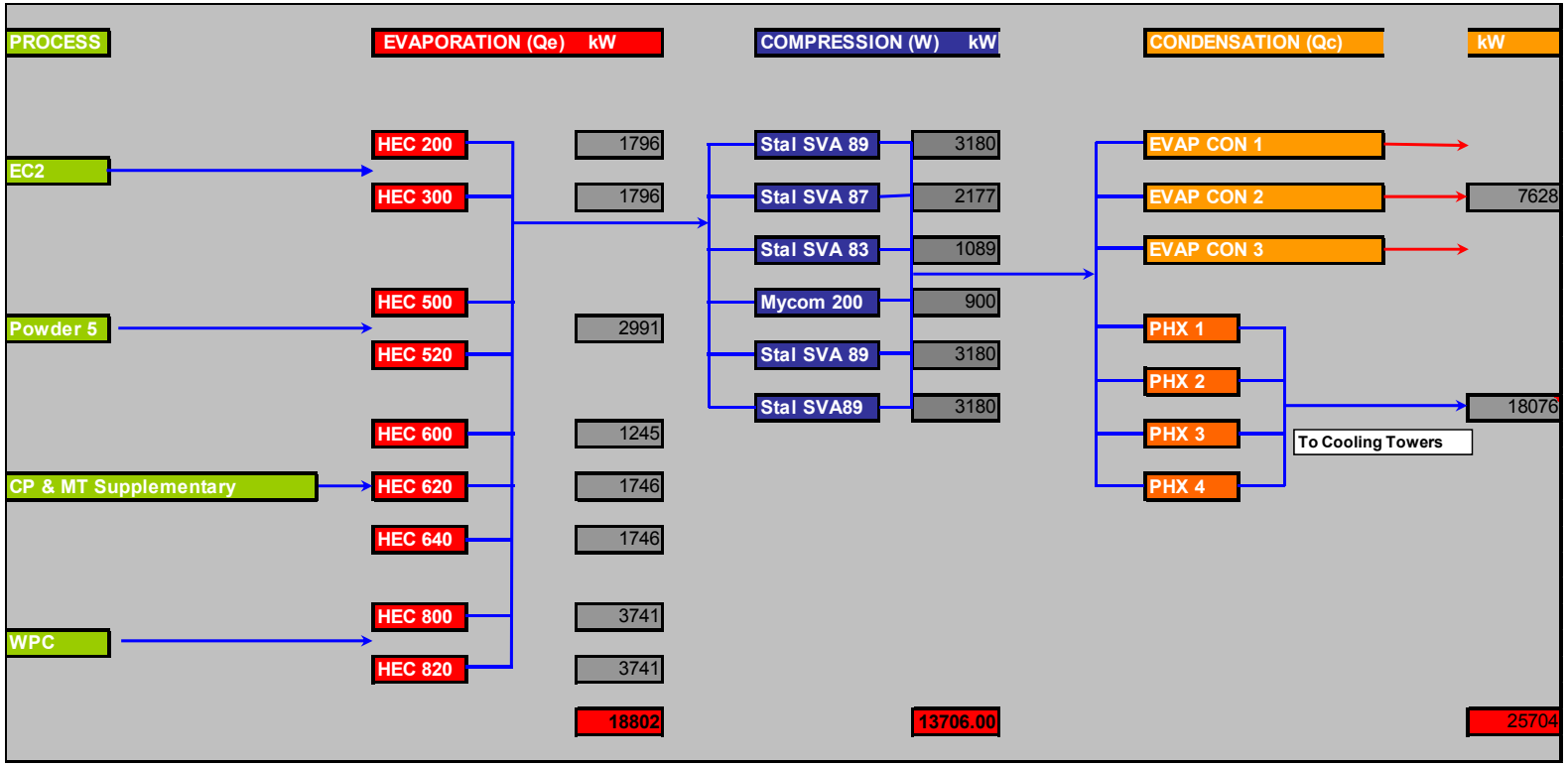

Figure 13: EC5 refrigeration system.

The heat load of each of the processes on the left enter the refrigeration system through the evaporators (HEC 200 to HEC 820). The ammonia is compressed by the six compressors and then the heat is rejected by the three evaporative condensers and four plate heat exchangers.

Table 8 shows the plate heat exchangers (PHE's) contained within each of the processing plants that comprise the evaporator component of the refrigeration plant. The heat exchangers are configured for counter-current flow.

Table 8: Refrigeration plant evaporators at Whareroa.

These plate heat exchangers are all employed to cool water using the evaporation of the low pressure NH3 utility. The cooled water is then pumped either directly (or via storage tanks) to process heat exchangers where it is used to cool product streams in each of the plants.

Plant	Number of PHE's	Saturation evaporation temperature (°C)	Chilled water temperatures (°C)	Total design cooling capacity (kW)[2]
Powder 5	2	-1.0	6.0 (in) 1.5 (out)	2,992
Energy Centre 2	2	-1.0	6.0 (in) 1.5 (out)	3,591
Milk Treatment (supplementary)	1	-1.0	7.0 (in) 1.5 (out)	1,245
Cream Products	2	-1.0	6.0 (in) 1.5 (out)	3,492
Whey Products	2	-1.0	6.0 (in) 1.5 (out)	7,483
Total	**9**			**18,802**

[2] All heat exchanger design heating and cooling capacity values were sourced from the plant commissioning documentation stored in the Energy Centre control room at Whareroa. Please refer to Appendix 7 for copies of these documents.

Table 9: Details of heat of rejection capacity of the Whareroa EC5 refrigeration system.

EC5 Condensers	Number	SCT (°C)	Ambient wet bulb temperature (°C)	Total design heat rejection capacity (kW)[1]
BAC VXC 400 Evaporative condenser (1552 kW*HOR*)	1	35	21	1,552
BAC VXC 800 Evaporative condenser (3038 kW*HOR*)	2	35	21	6,076
Alfa Laval Plate heat exchanger (4,519 kW *HOR*)	4	35	n/a	18,076
Total	**7**			**25,704**

Table 10: Details of compressor cooling capacity and power demand for the EC5 refrigeration system at Fonterra Whareroa

EC5 Compressors	Number	Power use at capacity (kW)	Total cooling capacity (kW)[1]
Stal SVA 89 (3,180 kW R)	3	1,995 (665)	9,540
Stal SVA 87 (2,177 kW R)	1	455	2,177
Stal SVA 83 (1,089 kW R)	1	235	1,089
Mycom 200VMD (900 kW R)	1	200	900
Total	**6**	**2,885**	**13,706**

Design Suction pressure – 268 kPa and Discharge pressure – 1255 kPa for all compressors.

Comparing Tables 9 and 10 it can be seen that the plant is not designed to meet the cooling requirement of all the plate heat exchangers at once, at design conditions. There is some buffer in the system, as the cooled water ultimately used for process cooling is stored in tanks, so it is possible for a large, temporary load to be met by depleting the stored chilled water. However, this constraint seems to mean that not all of the individual factories on site can be operated at once for extended periods of time.

Currently the total heat rejection capacity at the condensers is 13,706 kW plus the energy used by the compressors, i.e. 13,706 divided by the COP. If we take an average COP of 4.75 then the compressor energy use becomes 2,885 kW and the required heat rejection capacity is 16,591 kW. The significant spare condenser capacity, at design condition, means that there may be significant opportunity to save energy by reducing the discharge pressure of the compressors to a lower than design value as shown by Love, Cleland, & Merts (2008). The significant spare capacity also means that it may be possible, unless the system is closely monitored, for large efficiency declines (due to fouling) to occur unnoticed by site personnel. Unnoticed declines in efficiency are undesirable because it is a waste of capital (as it reduces the energy savings opportunities), and it may interfere with future site upgrades (if surplus condenser capacity is expected).

3.4.2 Data collection

Data used to analyse the selected models was obtained from four sources.

Design data for components of the Refrigeration system was obtained from supplier commissioning reports contained in system manuals situated in the Energy Centre Control Room at Whareroa. The system manuals also include information on the heat transfer equipment and compressors that have been retrofitted after commissioning. As previously mentioned, design specifications used were: Cooling Capacity (Heat Transfer capacity) for all nine evaporators, capacities for all six compressors, Heat of Rejection (*HOR*) rates for the three evaporative condensers and the *HOR* rates for the four plate heat exchanger condensers.

Process data was obtained from the Whareroa I-history database. The data collected comprised of flow rates of water through each PHE and cooling tower, temperature of water into and out of the PHE's, compressor loads and compressor suction and discharge pressures.

Psychrometric data for the site was obtained from the NIWA "National Climate database".[3] This website provided hourly ambient dry bulb temperature, wet bulb temperature, relative humidity and dew point from the Hawera weather station. Figure 14 indicates the location of the weather station relative to the Whareroa factory site. The closeness of the weather station (about 600 metres) means that it is likely an accurate indication of the conditions at the factory site. It is assumed that there are no significant micro-climate effects at the site. That is, it is assumed that the heat rejected by the various factory processes (including milk powder plants, a co-generation plant, and the refrigeration condensers) is rapidly dispersed into the wider environment.

[3] **http://cliflo.niwa.co.nz/pls/niwp/wgenf.genform1**

Figure 14: The position of the NIWA weather station relative to the Fonterra factory site at Whareroa.

The station is approximately 0.6 km from Whareroa and is at an altitude of 88 metres above Mean Sea Level (MSL). Fonterra Whareroa is at an altitude of 74 metres MSL. The map was sourced using Google Maps.

Psychrometric data for the Evaporative Condenser that was used to test the models was obtained from the weather station. The data obtained was dry bulb temperature, wet bulb temperature, relative humidity and dew point, all at hourly intervals.

Data tables were downloaded from the website as Microsoft 'Excel' spreadsheets. Table 11 provides an example:

Table 11: Excerpt of data downloaded from the NIWA "National Climate database" in Microsoft 'Excel' format.

Station information:

Name	Agent Number	Network Nu	Latitude (d	Longitude (	Height (m)	Posn_Prec	Observing
Hawera Aws	25222	E94622	-39.612	174.292	98	G	Metservice

Note: Position precision types are: "W" = based on whole minutes, "T" = estimated to tenth minute,
G = derived from gridref , "E" = error cases derived from gridref,
H = based on GPS readings (NZGD49), "D" = by definition i.e. grid points.

ScreenObs: Hourly

Station	Date(NZST)	Tair(C)	Twet(C)	RH(%)	Tdew(C)
Hawera Aws	20090429:1200	18.4	16.9	84.8	15.8
Hawera Aws	20090429:1300	20	16.2	66	13.5
Hawera Aws	20090429:1400	19	15.5	67	12.8
Hawera Aws	20090429:1500	16.2	14	77.3	12.2
Hawera Aws	20090429:1600	15	13.9	88	13
Hawera Aws	20090429:1700	14	13.5	94	13.1
Hawera Aws	20090429:1800	14.6	14	93.7	13.6
Hawera Aws	20090429:1900	15	14.1	90	13.4
Hawera Aws	20090429:2000	15	13.8	87	12.9
Hawera Aws	20090429:2100	15.4	14	85.1	12.9
Hawera Aws	20090429:2200	15	13.6	85	12.5
Hawera Aws	20090429:2300	15	13.9	88	13

Figure 15 is an example of the seasonal temperature profile for Whareroa showing variation in dry bulb and wet bulb temperatures. Dry bulb temperatures range from 25.9 to -2.6°C and wet bulb temperatures range from 21.4 to -3.1°C.

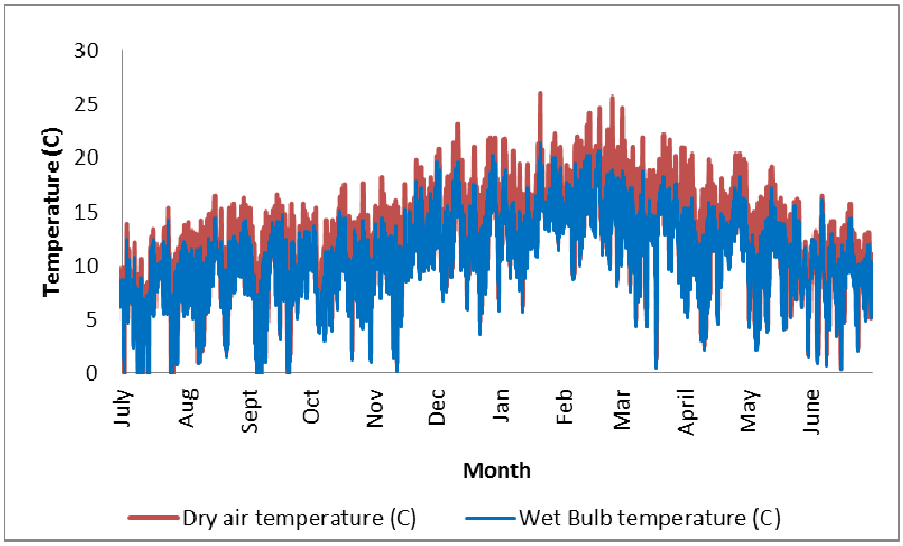

Figure 15: Seasonal temperature profile showing dry bulb and wet bulb temperatures for July 2009 to June 2010.

Temperature data was also measured over the condenser using a Comark Diligence EV N2004 datalogger made in the USA, using K type thermocouples. The data collected was Inlet ammonia temperature, Outlet ammonia temperature and dry bulb air temperature out of the Evaporative Condenser. Data was collected at hourly intervals and downloaded in Microsoft 'Excel' format. The datalogger was calibrated on an annual basis by ECEfast NZ Ltd and has an accuracy of +/-0.5 °C. Table 12 provides an example of the temperature data collected.

Table 12: Example of temperature measurements provided by the Comark Diligence EV N2004 datalogger.

Rec. No.	Date/Time	SCT Ch 1 (°C)	NH3 into condenser Ch 2 (°C)	Air leaving condenser Ch 3 (°C)	
498	9/08/2010 7:00:02 AM	10.8	50.2	23.4	
499	9/08/2010 8:00:02 AM	11.6	46.6	22.8	
500	9/08/2010 9:00:02 AM	9.2	44.0	22.6	
501	9/08/2010 10:00:02 AM	9.4	34.6	20.2	
502	9/08/2010 11:00:02 AM	10.8	38.2	20.6	
503	9/08/2010 12:00:02 PM	15.0	39.6	20.8	
504	9/08/2010 1:00:02 PM	13.4	47.2	23.0	
505	9/08/2010 2:00:02 PM	20.8	51.0	23.4	
506	9/08/2010 3:00:02 PM	25.2	51.4	23.4	
507	9/08/2010 4:00:02 PM	20.4	51.4	22.8	
508	9/08/2010 5:00:02 PM	17.4	49.4	22.6	

Figure 16 is an example of the temperatures measured for Ammonia in and out of the EC1 Evaporative condenser and the dry bulb air temperature out of the condenser.

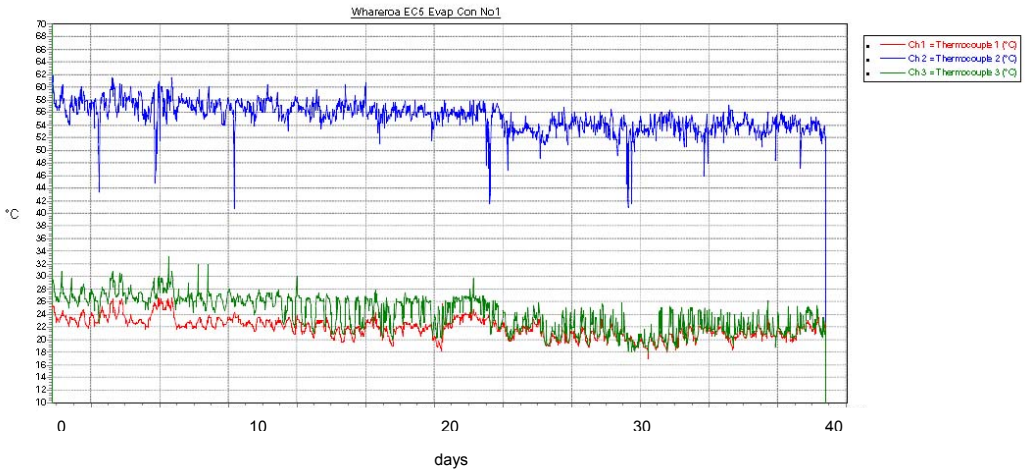

Figure 16: Example of the temperature output in graphical form from the 3 channel datalogger.

Thermocouple 1 (red) is air out of the Evaporative Condenser, Thermocouple 2 (blue) is the ammonia temperature into the condenser and Thermocouple 3 (green) is the ammonia temperature out of the condenser. The output is for a 40 day period.

3.4.3 Energy calculations

Heat load into the refrigeration system (cooling of the process chilled water) at the evaporators (see Table 3.3) was calculated using equation **(3)**:

$$Q = m_w Cp \triangle T (kW) \qquad \textbf{(3)}$$

Where m_w = Mass flow rate of chilled water (kg/s).

Cp = Specific Heat of water (4.18 kJ/kg °C)

$\triangle T$ = Change in temperature across the plate heat exchanger (PHE) (°C)

Efficiency of the Evaporative Condenser was calculated in Engineering Equation Solver' (EES), (S.A. Klein, F-Chart Software, 2009) from psychrometric data using Equation **(13)**:

$$E_f = \frac{\textbf{Condenser capacity}}{\textbf{Maximum capacity}} = \frac{m_a(h_{air,\,out} - h_{air,\,in})}{m_a(h_{air,\,out\,(T_{refrigerant,\,SCT})} - h_{air,\,in})} \quad \textbf{(13)}$$

Total Compressor capacity, Compressor total power consumption, COP, wasted power, estimated heat recovery and Compressor energy cost were calculated through utilization of the Compressor Scheduling Tool developed by Love & Cleland (2007)

Where COP was determined using equation **(5)**:

$$COP = \frac{Qe}{Qc}$$

The effect of fouling on evaporative condenser efficiency is calculated comparing the universal heat transfer coefficient U_{clean} with the fouled system U_{fouled} using equation **(26)**:

Equation for U_{clean} is:

$$\left(\frac{1}{U_{clean}\,A1}\right) = \left(\frac{1}{2\pi L}\right)\left(\frac{ln\left(\frac{r_{od}}{r_{id}}\right)}{k_{steel}}\right) + \frac{1}{h_{\,inside}\,A_{\,inside}} + \frac{1}{h_{\,outside}\,A_{\,outside}} \quad \textbf{(29)}$$

Where $A1$ is mean surface area of the coil

$A_{outside}$ is the outside surface area of the coil

A_{inside} is the inside area of the coil

r_{od} = outside diameter

r_{id} = inside diameter

k_{steel} is the thermal conductivity of the coil

And the equation for U_{fouled} is:

$$\frac{1}{U_{scale}A1} = \frac{1}{2\pi L}\left[\frac{\ln\left(\frac{r_{od}}{r_{id}}\right)}{k_{steel}} + \frac{\ln\left(\frac{rscale}{r_{od}}\right)}{k_{scale}}\right] + \frac{1}{h_{inside}A_{inside}} + \frac{1}{h_{outside}A_{outside}}$$

(30)

Where k_{scale} is the thermal conductivity of the fouling material.

The convective heat transfer coefficients h_{inside} and $h_{outside}$ were calculated from relationships defined by ASHRAE (ASHRAE, 2008) and (ASHRAE, 2009) using the following equations:

$$h_{inside} = \frac{N_u\, k_{ammonia,\,discharge}}{L}$$

(31)

$$h_{outside} = [(1012 + 9.19)\, T_{int}(2^{0.633})]/[\delta^{0.397}_{(1000)}]$$

(32)

Where

$$N_u = N_{u,\,lo}\left[(1 - x_{quality})^{0.8} + \frac{\left((3.8)\, x_{quality}^{0.76} \times (1 - x_{quality})^{0.04}\right)}{Pr^{0.38}}\right]$$

(33)

N_u = annular flow with uniform film distribution within the coil

$N_{u,\,lo}$ = 0.0023 $Re_l^{0.8} Pr_l^{0.4}$

$\mathbf{Re}_l = \frac{GD}{\mu_l}$ (G=mass velocity, D= diameter of coil)

$\mathbf{Pr}_l$ = Prandtl number = $\frac{cp\mu}{k}$ (cp=fluid specific heat,μ=fluid dynamic viscosity, k=fluid conductivity)

$\boldsymbol{x\ quality}$ = mass fraction of vapour

$$N_{u,\,lo} = (0.023)\, R_{eamm}^{0.8}\, Pr^{0.4} \tag{34}$$

$$R_{eamm} = \frac{M_{Velocity}\, r_{id}}{\mu_{amm}} \tag{35}$$

R_{eamm} = Reynolds number of ammonia

$M_{Velocity}$ = mass velocity of ammonia

r_{id} = inside diameter of coil

μ_{amm} = fluid dynamic viscosity of ammonia

$$Pr = \frac{P_{Discharge}}{P_c} \tag{36}$$

Pr = reduced pressure

$P_{Discharge}$ = the compressor discharge pressure

P_c = critical thermodynamic pressure of ammonia

$$R_{ea} = \frac{\rho_{air,\,in}\, V_{air}\, d_{tower}}{\mu_{air,\,in}} \tag{37}$$

R_{ea} = Reynolds number for air

$\rho_{air,\,in}$ = density of air in to condenser

V_{air} = velocity of air in condenser

d_{tower} = diameter of tower

$\mu_{air,\,in}$ = dynamic viscosity of air

All refrigerant property data was obtained from the database contained within EES. A complete nomenclature for these equations can be found in Appendix 4.

Thermal conductivities of common foulants were sourced from several references Hesselgreaves (2002), Kirkpatrick, McIntire, & Characklis (1980), ASHRAE, Chapter 38: CONDENSERS (2008). Table 13 summarises these.

Table 13: Thermal conductivity of scale species used for foulant calculations in model.

Substance	Formula	Mineral name (as Hydrate)	Thermal Conductivity (25 deg c) (W/m/K)
Steel (1% Carbon)			46[1]
Magnetic Iron oxide	Fe_2	Magnetite	2.9[2]
Calcium Carbonate	$CaCO_3$	Calcite	2.26 to 2.93[3]
Calcium Phosphate	$Ca_3(PO_4)_2$		2.6[4]
Calcium Sulphate	$CaSO_4$	Gypsum	2.3[5]
Magnesium Phosphate	$MgPO_4$		2.2[6]
Combined CaCO3 + Biofilm			1.63[7]
Sodium Aluminium silicate	$NaAlSi_2O_6.H_2O$	Analcite	1.3[8]
Microbiological film (biofilm)			0.63[9]
Dicalcium silicate	Ca_2SiO_4	Lamite	0.057[10]

(Hesselgreaves, 2002)[2,4,5], (Kirkpatrick, McIntire, & Characklis, 1980)[9], (ASHRAE, Chapter 38: CONDENSERS , 2008)[1,3,6,7,8,10]

3.4.4 Energy balance rationalisation

The energy balance was determined using the relationship defined by equation **(1)**:

$$Q_c = Q_e + W_{comp} \qquad (1)$$

The balance was calculated in an Excel spreadsheet referred to as the 'Energy balance and efficiency spreadsheet' (refer 'Energy balance calculator.xls' on CD enclosed). The theoretical heat load on the condensers (calculated in this way) was compared to the apparent heat rejected over the evaporative condensers

(based on the psychrometric conditions) and the apparent heat rejected over the plate heat exchanger condensers (calculated from the I-history data). The Excel spreadsheet made use of a series of macros developed by Love et al (2007) and modified by the author to automate the calculation of energy use by the compressors for each of the hourly average data points. Isentropic efficiency and part load efficiency are calculated using compressor manufacturer's data.

Figure 17 is a flow diagram of the steps taken to calculate the energy balance in Excel.

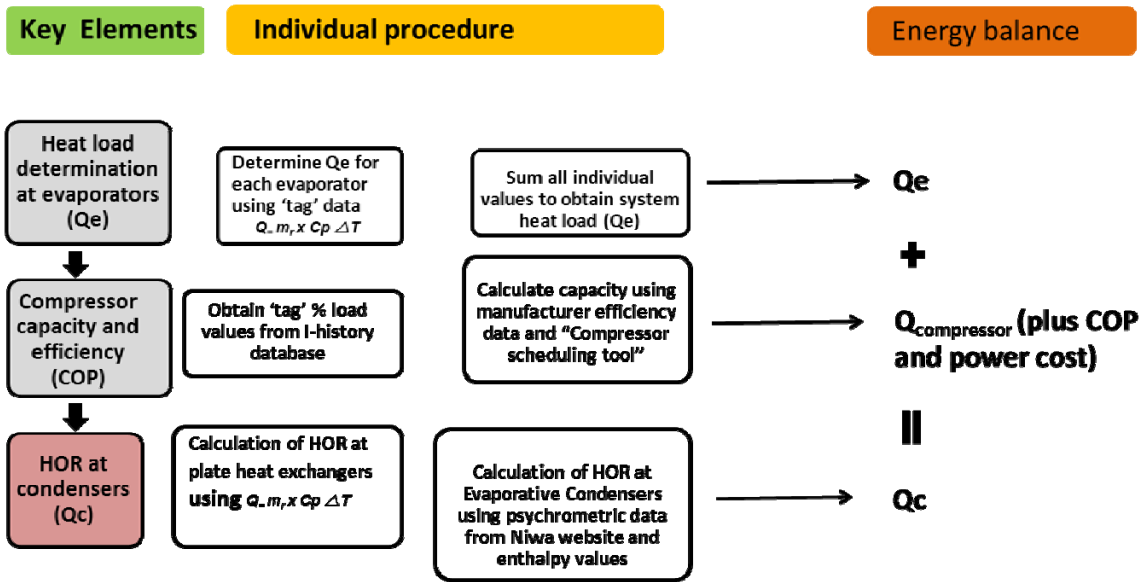

Figure 17: Flow diagram of the steps taken to calculate the energy balance in Excel

3.5 Modelling

The software 'Engineering Equation Solver' (EES), (S.A. Klein, F-Chart Software, 2009) was used to develop and test the Efficiency and Fouling model. The model can be accessed via the attached CD using the filename: Efficiency_and_Fouling_Model_Smilgate.EES".

Figure 18 provides a screen shot of the interactive diagram window of the model.

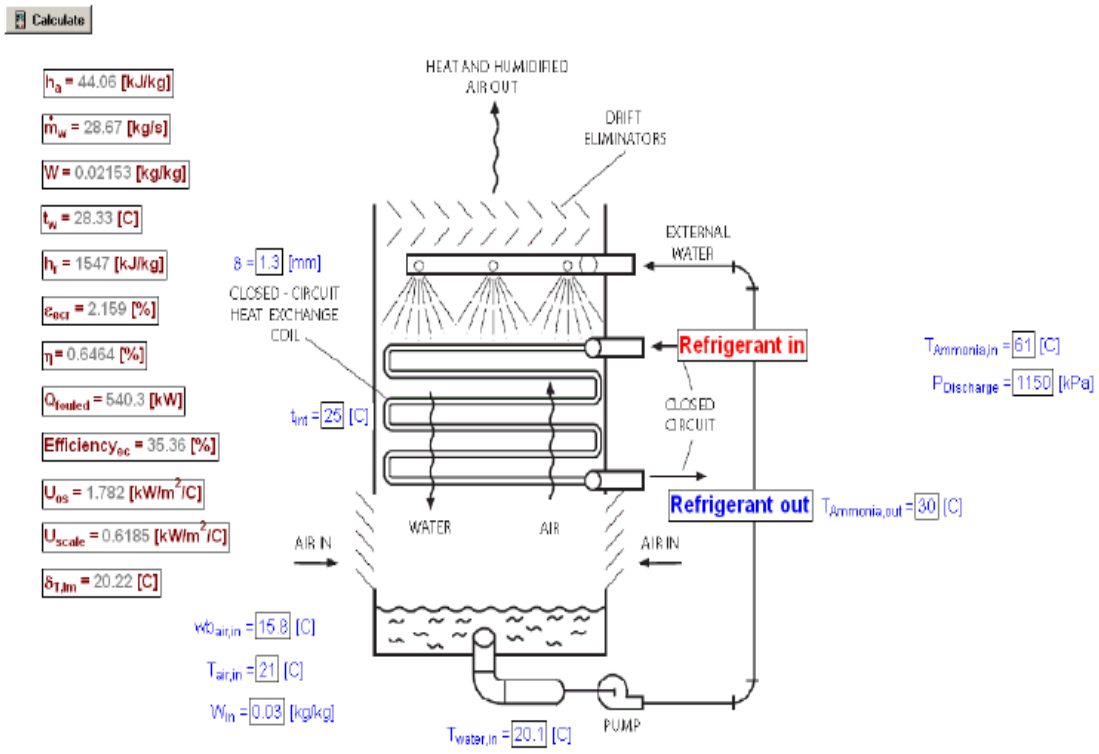

Figure 18: The interactive diagram window developed in EES for the Efficiency and fouling model.

Showing user inputs in blue and calculation outputs in grey.

The EES software was used to run sensitivity analysis on model variables and for 'what if?' queries. HOR capacity results from the EES "HOR calculator" were used as the Q_{fouled} (HOR for a fouled or below design load condenser bundle) value for efficiency calculations in the EES model.

Table 14 summarises outputs from the model:

Table 14: Summary of the outputs obtained from the EES Evaporative Condenser and Fouling Model.

Variable	Description
h_a	Enthalpy of air exiting Evaporative Condenser (kJ/kg)
W	Humidity ratio of moist air (kg water/ kg of air)
m_w	Mass flow rate of recirculating water (kg/s)
T_w	Temperature of water leaving tube bundle (°C)
h_r	Enthalpy of refrigerant leaving Evaporative Condenser (kJ/kg)
η	Condenser performance index
Q_{fouled}	Heat of rejection for fouled condenser tube bundle (kW)
U_{scale}	Heat transfer coefficient of fouled condenser (kW/ m^2/ °C)
U_{os}	Heat transfer coefficient at outside of tube bundle (kW/ m^2/ °C)
ε_{ec}	Efficiency of Evaporative Condenser (%)
$\Delta_{T,lm}$	Log mean temperature difference over tube bundle (°C)
T_{int}	Temperature at the water air interface (mm)
δ	Predicted thickness of foulant layer (°C)

3.6 Film thickness predictions

A major component of the project was to develop a model that would reliably predict the film thickness of the foulant on the outside of the evaporative condenser coils. As a precursor to predicting the film thickness it is necessary to determine the type of foulant material that is likely to create this film. This can be done by utilising one of two options.

The first option is to utilise a computer model that predicts the fouling material by analyzing the chemical environment of the system being assessed. The Nalco 3DT 'Optimiser' programme (refer to Appendix 8) could possibly be used for this purpose.

The second option is to analyse the actual scale if access can be arranged to the heat exchange surface. This is the most accurate option, although access to the condenser surfaces may be limited. Measurements of the condenser surfaces were made in this study.

Figure 19 provides a flow diagram of the process that was used to obtain these film thickness predictions.

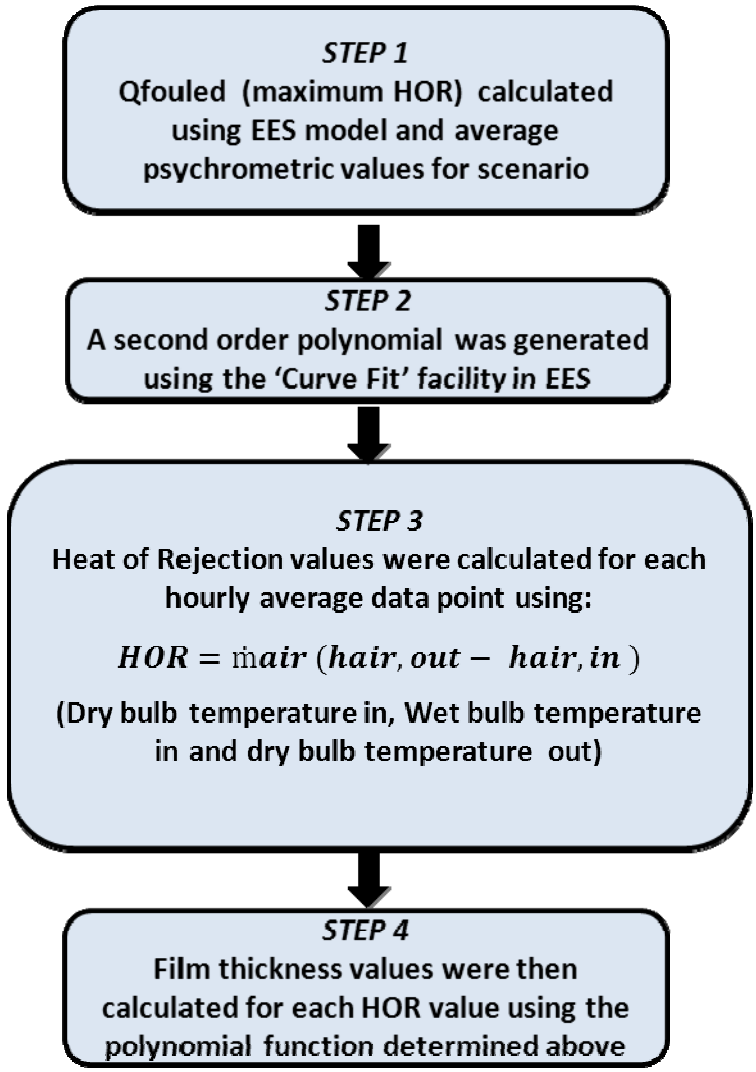

Figure 19: Flow diagram of the film thickness prediction procedure

Step 1 of the procedure employs the EES model to calculate the maximum HOR values for film thicknesses of 0 to 4mm (total scale thickness of 8mm), using the average dry bulb air temperature into the condenser, the average air wet bulb temperature into the condenser and the average dry bulb temperature out of the condenser for a particular data set. For the purposes of demonstration this example uses the February to April, 2010 scenario.

Figure 20 is a diagram of the first step in the procedure showing the EES parametric table and the corresponding inputs (in black) with the calculated outputs in blue.

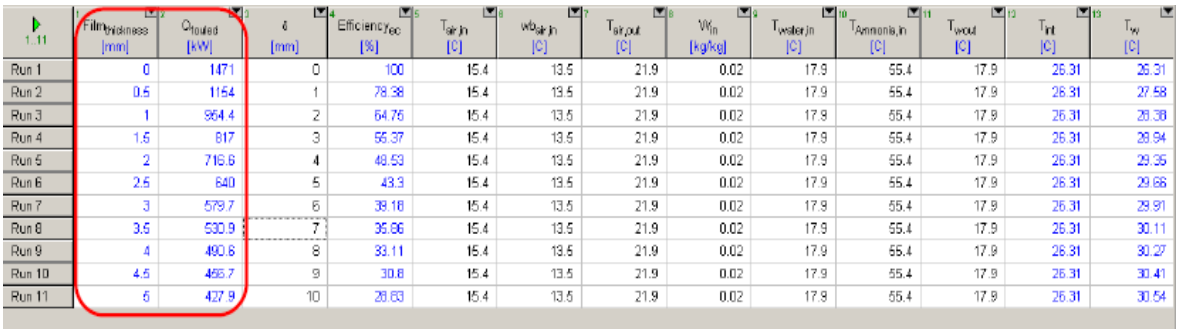

1..11	Film$_{thickness}$ [mm]	Q_{fouled} [kW]	δ [mm]	Efficiency$_{ec}$ [%]	$T_{air,in}$ [C]	$wb_{air,in}$ [C]	$T_{air,out}$ [C]	W_{in} [kg/kg]	$T_{water,in}$ [C]	$T_{Ammonia,in}$ [C]	T_{wout} [C]	T_{int} [C]	T_w [C]
Run 1	0	1471	0	100	15.4	13.5	21.9	0.02	17.9	55.4	17.9	26.31	26.31
Run 2	0.5	1154	1	78.38	15.4	13.5	21.9	0.02	17.9	55.4	17.9	26.31	27.58
Run 3	1	954.4	2	64.76	15.4	13.5	21.9	0.02	17.9	55.4	17.9	26.31	28.38
Run 4	1.5	817	3	55.37	15.4	13.5	21.9	0.02	17.9	55.4	17.9	26.31	28.94
Run 5	2	716.6	4	48.53	15.4	13.5	21.9	0.02	17.9	55.4	17.9	26.31	29.35
Run 6	2.5	640	5	43.3	15.4	13.5	21.9	0.02	17.9	55.4	17.9	26.31	29.66
Run 7	3	579.7	6	39.18	15.4	13.5	21.9	0.02	17.9	55.4	17.9	26.31	29.91
Run 8	3.5	530.9	7	35.86	15.4	13.5	21.9	0.02	17.9	55.4	17.9	26.31	30.11
Run 9	4	490.6	8	33.11	15.4	13.5	21.9	0.02	17.9	55.4	17.9	26.31	30.27
Run 10	4.5	456.7	9	30.8	15.4	13.5	21.9	0.02	17.9	55.4	17.9	26.31	30.41
Run 11	5	427.9	10	28.83	15.4	13.5	21.9	0.02	17.9	55.4	17.9	26.31	30.54

Figure 20: EES parametric table showing psychrometric data inputs (black) and the calculated outputs in blue.

For the February to April 2010 dataset. The red box highlights the film thickness and maximum HOR *values (*Q_{fouled}*).*

Step 2 utilises this data to create a curve fit with corresponding 2nd order polynomial in EES. Figure 21 provides an example of the curve fit procedure for the April, 2010 data set.

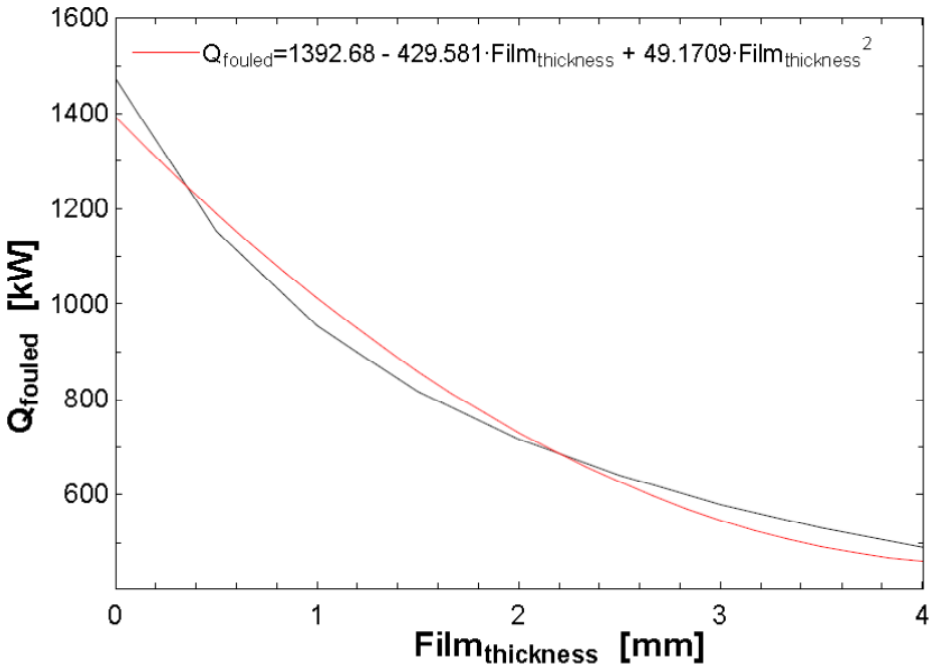

Figure 21: Curve fit and corresponding 2nd order polynomial for April, 2010 data set.

The next step (Step 3) is to calculate hourly average HOR values for the EC1 Evaporative Condenser from the I-history data for the February to April, 2010 period using the "Condenser capacity" portion of equation **(11)**:

$$HOR = m_a \left(h_{air,\,out} - h_{air,\,in}\right) \qquad \textbf{(38)}$$

Where m_a is the mass of air lowing through the condenser

$h_{air,\,in}$ is the enthalpy of ambient air drawn into the evaporative condenser.

$h_{air,\,out}$ is the enthalpy of air at the exit of the evaporative condenser.

Figure 22 provides an excerpt from EES showing the calculation results (HOR) for the first 10 data-points out of a total of 1873 in the April, 2010 data set.

1.1873	1 fan_{energy}	2 $T_{air,in}$ [C]	3 $T_{air,out}$ [C]	4 $T_{Ammonia,out}$ [C]	5 wb_{air}	6 $flow_{air}$	7 HOR	8 $h_{air,in}$ [kJ/kg]	9 $h_{air,out}$ [kJ/kg]	10 $h_{air,sat}$	11 $\dot{m}_{air}$	12 $Rair,out$
Run 1	1	20.6	24.8	30.24	18.1	32.6	751.9	51.14	75.6	101	31.75	1.148
Run 2	1	20.7	25.4	30.96	18.6	32.6	789.2	52.42	78.03	104.9	31.68	1.144
Run 3	1	21	25.4	30.28	18.4	32.6	800.2	52.09	78.03	101.2	31.7	1.144
Run 4	1	20.3	25.2	30.43	18.3	32.6	781.9	51.79	77.18	102	31.67	1.145
Run 5	1	19.5	25.2	30.19	17.7	32.6	838.3	49.92	77.18	100.8	31.56	1.145
Run 6	1	18.4	25.2	29.33	17	32.6	901.3	47.79	77.18	96.32	31.42	1.145
Run 7	1	17.4	24.2	28.8	16.3	32.6	837.4	45.72	73.04	93.66	31.46	1.151
Run 8	1	16.3	24.2	28.29	15.4	32.6	914.4	43.13	73.04	91.12	31.31	1.151
Run 9	1	16.4	23.8	28.37	15.6	32.6	848.5	43.7	71.43	91.55	31.4	1.154
Run 10	1	16.3	23.6	28.34	15.5	32.6	833	43.42	70.64	91.41	31.41	1.155

Figure 22: Excerpt from *HOR* EES calculator showing the first 10 results from the April, 2010 database.

For the Fonterra Whareroa scenario the resulting ***HOR*** values are the Capacity values for the Evaporative Condenser. This is due to the fact that the evaporative condensers at this plant are used for 'base load' heat rejection and are therefore assumed to be running at maximum capacity at all times when the air circulation fans are running. For other scenarios where this is not the case, it would be necessary to calculate the condenser capacity by iteration.

The final step (Step 4) calculates the predicted film thickness using the ***HOR*** values and the 2nd order polynomial equation relationship of ***HOR*** to film thickness. This operation was carried out using EES as shown in Figure 23 below:

1..1873	1 Film$_{scale}$ [mm]	2 HOR
Run 1	1.909	751.9
Run 2	1.759	789.2
Run 3	1.716	800.2
Run 4	1.788	781.9
Run 5	1.574	838.3
Run 6	1.354	901.3
Run 7	1.577	837.4
Run 8	1.31	914.4
Run 9	1.537	848.5
Run 10	1.593	833

Figure 23: Excerpt from EES film thickness calculation using the 'Curve fit' 2nd order polynomial equation for the relationship of Film thickness (Film$_{scale}$ = δ) to HO_R for the February to April, 2010 data set.

3.7 Economic and environmental evaluation of the model

Energy cost evaluations were calculated for fouled tube bundle scenarios and compared with the design energy cost.

The major costs associated with operating an evaporative condenser are due to the electricity costs of running the compressor(s), the forced air fan and the water circulation pump.

The electricity costs for running the compressor(s) were calculated using the cost result determined using the "Compressor Scheduling Tool", pro-rated for the load on the individual condenser (EC1):

$$E_{con} = \left(\sum_{Comp} \left(\frac{1,552}{25,703} \right) \right) + (E_{air\ fan} + E_{water\ pump}) \quad \textbf{(39)}$$

Where E_{con} = Electricity cost of condenser

$\frac{1,552}{25,703}$ represents the ratio of the ***HOR*** capacity for the evaporative condenser to the total ***HOR*** Capacity for the system

$\sum_{Comp}$ = Total cost of running compressors

+cost saving for heat recovery from compressors

$E_{air\ fan}$ = Electicity cost of running air fan = 22.0 kW × \$0.1

$E_{water\ pump}$ = Electicity cost of running water recirc pump = 4.0 kW × \$0.1

Where the total cost of running the compressors is calculated by the "Compressor Scheduling Tool" using:

$$(W_{calc} \ x \ E_{cost}) - (Q_{rec} \ x \ E_{cost}) \quad \textbf{(40)}$$

Where W_{calc} is a user defined function that calculates compressor work from suction pressure, discharge pressure, suction superheat, compressor load and pre-programmed manufacturer compressor data for the refrigerant (717).

E_{cost} is the cost per kW

Q_{rec} is the heat recovered from the compressor

$$Wcomp = m_r \left(\frac{\Delta h_{comp}}{\eta_i} \right) \quad \textbf{(41)}$$

Where m_r = mass flow rate of refrigerant (kg/s)

Δh_{comp} = Enthalpy over the compressor (kJ/kg)

η_i = isentropic efficiency of the compressor (equation 27)

Carbon dioxide equivalent values (CO_{2e}) were then calculated from this cost information to demonstrate the increase in environmental impact of fouled heat transfer surfaces (tube bundle of evaporative condenser).

3.8 Summary

The site chosen to use as a test site for the model development was Fonterra Whareroa. This site was chosen due to its accessibility and because of the quality of its data management system.

The project utilised the Whareroa I-history database to develop an energy balance for the reticulated ammonia refrigeration system (EC5). One of the three evaporative condensers in the refrigeration system was chosen as the focus for the project. Air temperatures out of the condenser were logged and utilised with psychrometric and I-history data to determine the efficiency of the condenser.

A model was developed that combined the dynamics model of Qureshi and Zubair with the thermal resistance relationships as defined by ASHRAE. This model was then used to predict the thickness of a foulant on the study condenser given the calculated efficiency of this unit.

CHAPTER 4 RESULTS

4.1 Introduction

The energy balance of the Refrigeration system at Whareroa was determined using an Excel spreadsheet to calculate the heat load entering the system from the processing plants at the evaporators: Powder 5, Energy Center 2, Milk Treatment (Supplementary), Cream Products and Whey Products.

The rejected heat load at the condensers was then calculated using a combination of 'tag' data from the Whareroa I-history database, Psychrometric data measured at the Evaporative Condensers, and data from the NIWA weather station using EES.

The amount of fouling was then predicted on the basis of how much the apparent heat of rejection varied from the clean value.

4.2 Condenser output validation study

It was thought pertinent to test the integrity of the I-history data for the condenser "% load" output for two reasons: one, it is significant in terms of the energy balance result and two, it is measurable and therefore potentially provides an indication of the accuracy of other I-history outputs.

The ampere and % load readings in the refrigeration room were monitored for all five operating condensers on an hourly basis for 8 hours. These results were then compared with the % load values from the I-history database (Table 15).

Table 15: Results for ampere (Amps) reading and % load taken at EC5 refrigeration room for the five working compressors and compared with % load from I-history database on the 3rd of August, 2009.

Time	Condenser 1 Tag 4520			Condenser 2 Tag 4440			Condenser 3 Tag 4280			Condenser 4 Tag 4360			Condenser 5 Tag 4700		
	Amps	%Load	I-history value	Amps	%Load	I-history value	Amps	%Load	I-history value	Amps	%Load	I-history value	Amps	%Load	I-history value
9am	626	100	100	343	99	99	269	91	91	133	99	99	133	98	98
10am	625	100	100	339	99	99	268	91	91	131	99	99	133	98	98
11am	625	100	100	341	99	99	267	91	91	132	99	99	133	98	98
12pm	620	100	100	311	85	85	253	87	87	131	99	99	130	98	98
1pm	610	100	100	276	62	62	220	68	68	129	99	99	128	98	98
2pm	600	100	100	178	23	23	153	34	34	127	99	99	127	98	98
3pm	594	100	100	156	7	7	141	24	24	126	99	99	127	98	98
4pm	613	100	100	174	16	16	163	33	33	130	99	99	131	98	98

Ampere and % load readings were obtained from the compressor ampere gauge and load gauge in the EC5 Compressor room. These observations were compared with the load results obtained through the I-history database for the corresponding time. As can be seen from Table 18 the observed values (the columns in **red**), are identical to two significant figures with those from the I-history database (the columns in **blue**). Therefore it is safe to assume that the I-history database is recording the compressor loading data accurately.

4.3 Determination of Heat Load (Q_e) into Refrigeration system

Data sets used to calculate the heat load on the refrigeration system encompassed two and a half seasons. Table 16 summarises the range of heat loads into the Whareroa refrigeration system for each of the five production plants.

Table 16: Typical values for high (peak) season (December, 2008) and low season (May, 2009) milk processing for each processing plant at Fonterra Whareroa.

Processing plant	Average Peak season heat load (kW)	Average Low season heat load (kW)
Powder 5	310	250
Energy Centre 2	2923	394
Milk Treatment	572	211
Cream Products	1015	242
Whey Products	3256	981
TOTAL	**8076**	**2078**

4.4 Determination of Rejected Heat Load (Q_c) out of the Refrigeration system.

Heat Of Rejection (HOR) values for the reticulated ammonia system were calculated from I-history data for the four plate heat exchanger condensers and psychrometric data for the evaporative condenser (EC1). The evaporative condenser HOR was then pro-rated for the two other evaporative condensers to provide a total HOR from all condensers as per equation 42:

$$HORtotal = HOR_{EC1}\left(\frac{HOR_{design,\,total}}{HOR_{design,\,EC1}}\right) \quad \textbf{(42)}$$

Where HOR_{total} = Heat of Rejection for all Evaporative Condensers

HOR_{EC1} = Heat of Rejection for Evaporative Condenser No. 1

$HOR_{design,total}$ = Total design Heat of Rejection

$HOR_{design,\ EC1}$ = Design Heat of Rejection for Evaporative Condenser No.1

Table 17 summarises the comparative *HOR's* for the heat loads stated in Table 16:

Table 17: Typical heat load and Heat of Rejection (*HOR*) values for the reticulated ammonia refrigeration system at Fonterra Whareroa.

*Processing period	Heat load (kW)	*HOR* (kW)	*COP*
Average peak season	8,076	10,706	4.07
Average low season	2,078	2,957	3.80

* Based on December 2008 for peak season and May 2009 for low season

The average peak season heat load and *HOR* are approximately four times the average low peak levels. The average *COP* (equation **(5)**) for the two periods are 4.07 and 3.80 respectively. The low season drop in *COP* maybe explained by the increased use of part loaded compressors to meet the cooling duty. Part loaded compressors are inherently less efficient than fully loaded machines (Dossat & Horan, 2001). For screw-type compressors the degree to which efficiency drops off as load on the compressor decreases is dependent on the ratio of discharge pressure to suction pressure. This ratio is called the 'pressure ratio' (*PR*). At high pressure ratios the drop off in efficiency as load reduces is more significant than compressors with low pressure ratios.

Average hourly data for heat load into the refrigeration system, $Q_{evaporator}$ ***(Qe)*** and Heat of Rejection, $Q_{condenser}$ ***(Qc)*** has been plotted in Figure 24 (low season: May 2009) and Figure 25 (high season: December, 2008).

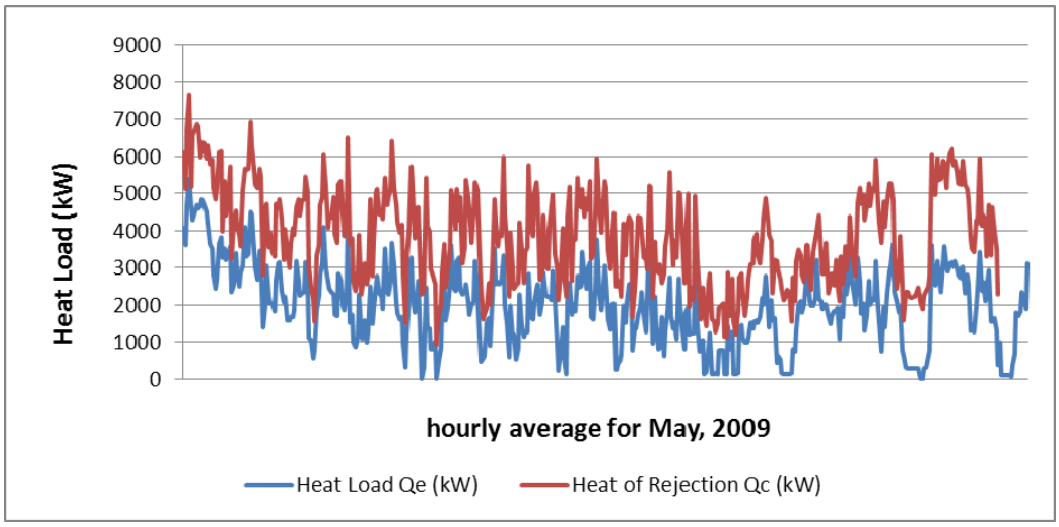

Figure 24: Graph of Heat Load and Rejected Heat for the low season period of May, 2009.

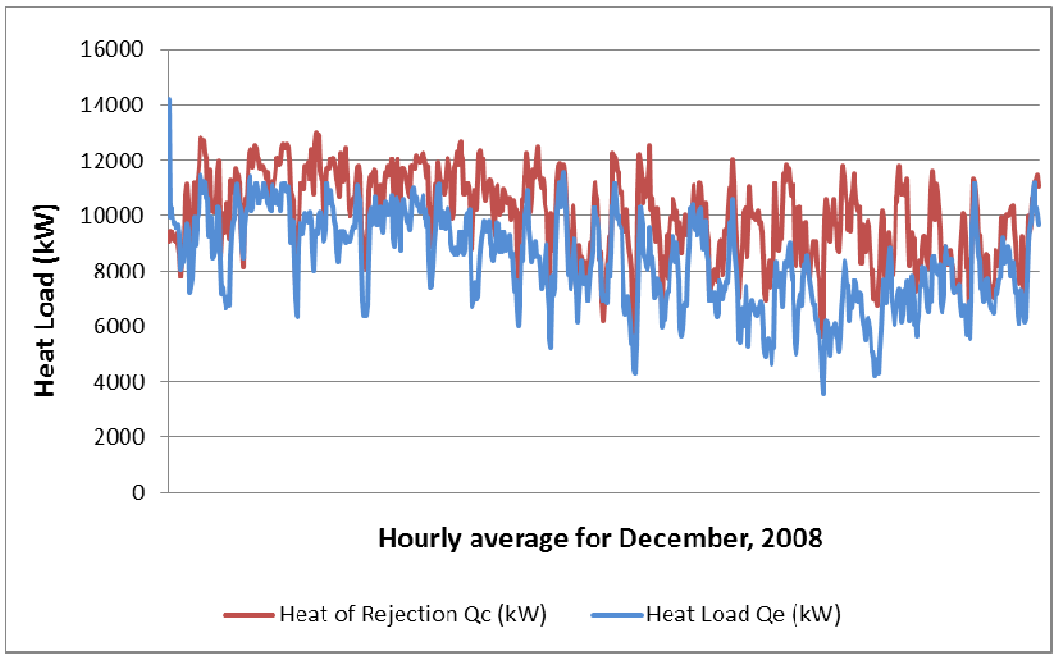

Figure 25: Graph of Heat Load and Rejected Heat for the high season period of December, 2008.

Figures 24 and 25 indicate that the calculations for heat load (Qe) and heat of rejection (Qc) are consistent for both periods as the heat load into the system follows the same trend as the heat of rejection from the system. This provides a

degree of confidence that the data from the data sources (I-history, NIWA and the data-logger) is consistent and therefore potentially provides a reasonable representation of the energy balance through the refrigeration system.

4.5 Energy Balance

An energy balance was completed for each data set acquired throughout the project. The heat load into the system (total heat load at evaporators) and energy used by the compressors were calculated (equation 3 and the Comp_Work user defined function in Excel). The resulting value of $Qe + W_{comp}$, which is the theoretical load on the condensers (equation 1) was then compared to the heat of rejection value calculated using psychrometric data (equation 11). Obviously these two values should be the same as they both represent the heat of rejection from the system (Qc). A match indicates that at least the two values calculated via different methods are consistent.

The resulting balance quantifies the magnitude of the heat associated with the production facility but also gives a valuable insight into the 'fit' of the data, i.e. the closer the agreement between the heat load and HOR (minus the energy used by the compressors) the more accurate the energy balance.

The energy balance was calculated in Excel. Figure 26 provides an example of the "energy summary" worksheet used for these calculations.

ENERGY SUMMARY		
Period to be analysed	**July to Sept, 2010**	
	Total for period	**Average (per hour)**
Total heat load at evaporators (kW)	**7,997,197.71**	**1,115.52**
Total energy used by Compressors (kWh)	**1,475,941.42**	**691.70**
Work done by compressor Ec (kWc)	**1,475,941.42**	**691.70**
COP for refrigeration system		**4.94**
Unit cost of electricity= 0.1 $/ kWh		
Total cost of electricity for compressors ($)	**120,264.55**	**57.18**
Theoretical load on condensers (Qe + W)	**9,473,139.13**	**1,807.22**
Apparent Heat Rejection		
Heat rejected at Condenser: PHX's (kW)	**5,363,347.37**	**662.26**
Evaporative condensers (kW)	**4,954,486.99**	**3,173.92**
Total Heat rejected at condensers (Qc)	**10,317,834.36**	**3,836.18**
%Difference Qe +W to Qc	**-8.92**	

Figure 26: An example of the Energy Summary calculation worksheet from the "July to September heat balance data set" spreadsheet.

The "% Difference between $Qe + W_{comp}$ and Qc" value provides an indication of the agreement between heat into and out of the refrigeration system.

Table 18: A summary of the energy balance results for each of the experimental data sets.

Period	Qe + W (kW)	Qc (kW)	% variance
1st Dec 2008 – 31st Dec 2008	**7,330,548**	**9,547,628**	**30.2**
29th Apr 2009 – 26th May 2009	**1,200,473**	**845,880**	**29.6**
18th Nov 2009 – 4th Feb 2010	**15,024,508**	**18,095,690**	**17.0**
4th Feb 2010 – 25th Apr 2010	**10,604,395**	**13,338,862**	**20.5**
3rd May 2010 – 24th May 2010	**1,645,497**	**1,867,303**	**13.5**
15th Jul 2010 – 30th Sep 2010	**9,473,139**	**10,317,834**	**8.9**
1st Nov 2010 – 15th Dec 2010	**11,222,297**	**13,140,865**	**14.6**

Table 18 summarises the energy balance results for each of the data sets. For the data sets analysed, the level of agreement ranged from 8.9 to 30.2%. The difference in energy balance agreement between data sets may be explained by the variability introduced by the fan speed control strategy utilised at Fonterra Whareroa and the errors introduced by each sensor. There were also several data sets where the fan 'energiser' tag, which indicated when the air fan was off or on, provided corrupted data to I-history. In these situations it was assumed that the fan was on. This will result in an over-estimation of the apparent heat of rejection at the evaporative condensers.

The Whareroa EC5 evaporative condensers use a 'fixed head pressure' control strategy. The controller attempts to maintain a single point head pressure regardless of the system load by controlling the fan speed of the condenser (refer Figure 27). Fan speed is controlled using an 'on/off 'strategy to maintain a discharge pressure of 12 bar.g. If the discharge pressure reduces, the control system will turn off the Evaporative Condenser fan to reduce the heat transfer efficiency of the condenser. The discharge pressure will then increase in an

attempt to reject more heat. The fan will then be turned back on when the discharge pressure reaches the pre-set control range.

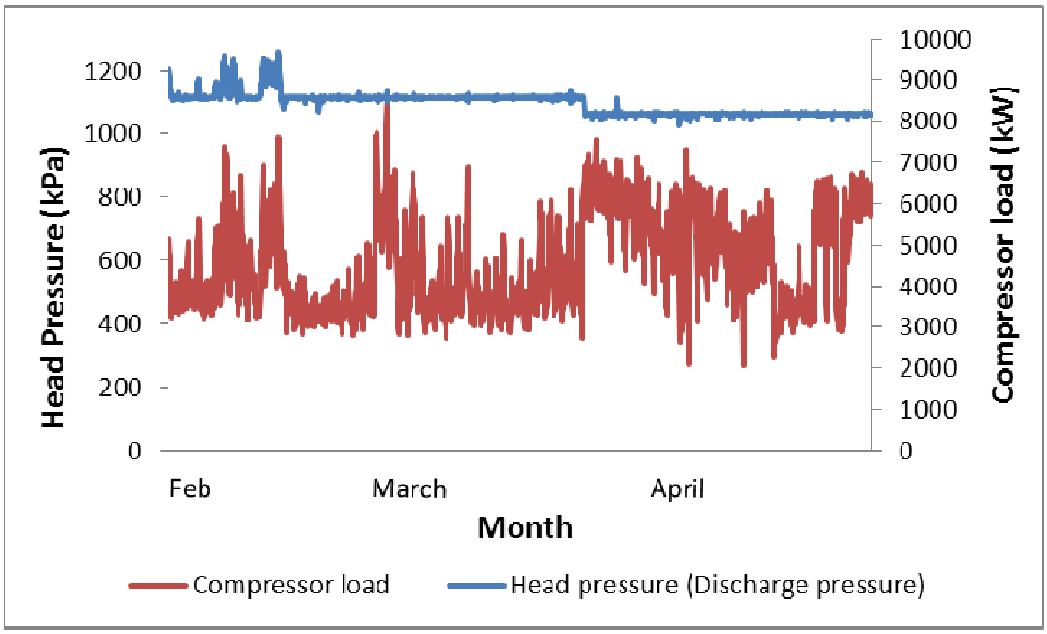

Figure 27: Graph showing the relationship of head pressure (compressor discharge pressure) to compressor load for the February to April, 2010 data set.

If the Evaporative Condenser efficiency is compromised in some way, e.g. fouling reducing heat transfer efficiency, the discharge pressure will continue to rise with the fan on at full speed when the heat load capacity of the evaporative condenser is exceeded.

We can use equation **4** ($\boldsymbol{Q = UA(\Delta T)_{lm}}$) to explain this behaviour. If we make $\boldsymbol{Q}$ equal to the $\boldsymbol{HOR}$ then the action of turning off the air fans reduces the heat transfer coefficient $\boldsymbol{U}$. This forces $\Delta\boldsymbol{T}$ to rise by increasing the discharge pressure corresponding to the saturation temperature in order to maintain the same value of $\boldsymbol{Q}$. In this case if $\boldsymbol{U}$ is too small, the fans cycle on, causing the pressure to fall back to10.7 bar.g. If $\boldsymbol{U}$ is too big, the fans cycle off causing the pressure to rise to 10.7

bar.g. If U is too small even when the fans are on full, then the pressure will rise above 10.7 bar.g until ΔT has been increased sufficiently to maintain Q. Fouling will also reduce U. As the level of fouling increases, U will decrease proportionally, until we reach the scenario where U is too small even when the fans are on full, forcing the pressure to rise above the head pressure set point. This will result in higher compressor use and increased energy costs.

The graph of head pressure to compressor load (Figure 27) indicates that head pressure is constant for the majority of the time regardless of heat load. The increases in late February may be due to a high wet bulb temperature, associated with summer conditions. Conversely, the step change reduction in head pressure in late March is due to the operators changing the set point for the condenser head pressure. This was probably due to an observed reduction in wet bulb temperature, associated with less humid, environmental conditions. These observations appear to be confirmed in Figure 28, which shows high wet bulb temperatures corresponding to the increase in head pressure in late February and a general trending decrease in wet bulb temperature from late March.

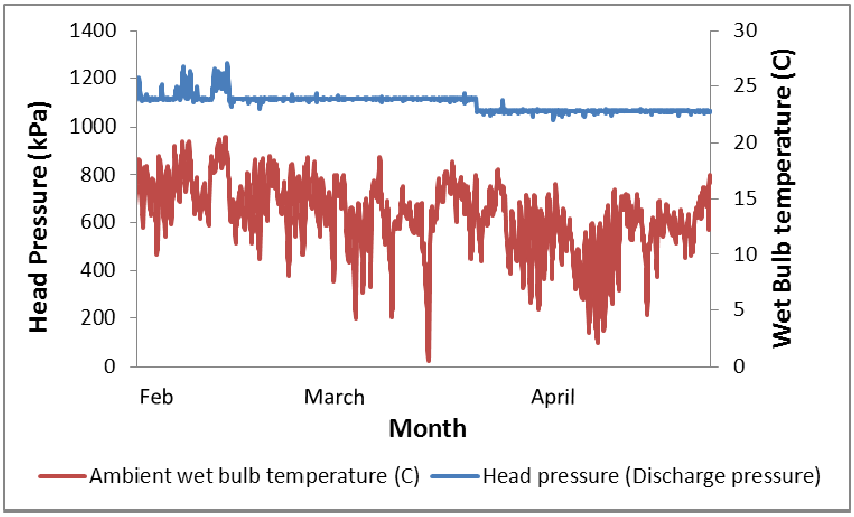

Figure 28: Graph showing the relationship of head pressure (compressor discharge pressure) to wet bulb temperature for the February to April 2010 data set.

The “Compressor scheduling tool” calculates the heat load into the system as defined by the load on the compressors and the isentropic efficiency characteristics of the compressors as defined by the manufacturer. This heat load can be compared with the heat load on the evaporators as calculated through the ‘energy balance’ exercise to obtain a sense of the variation between the two values.

Figure 29 and Figure 30 are graphs representing the comparison between the two values for peak season (November to January 2009/10) and low season (May 2010).

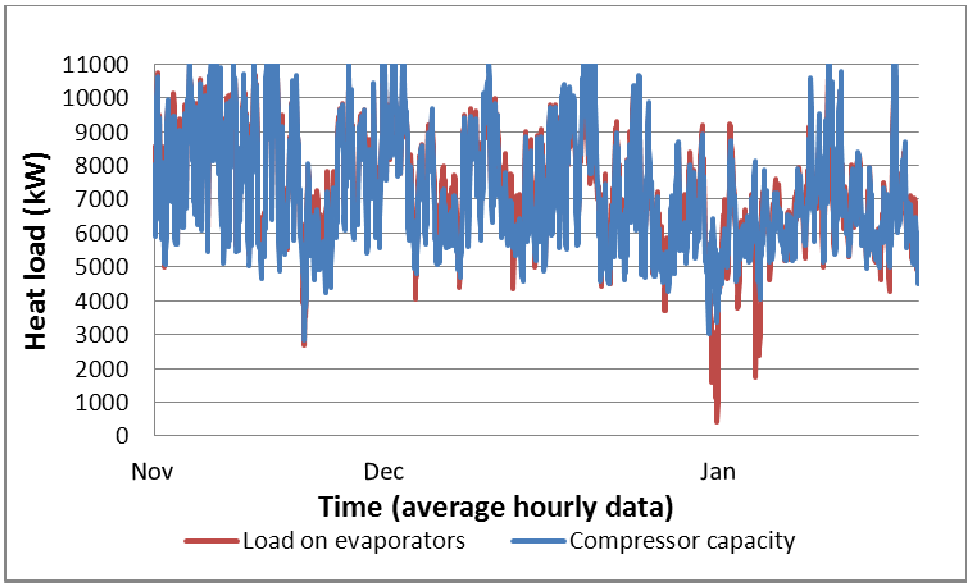

Figure 29: Comparison of compressor capacity calculated by “Compressor scheduling tool”, and Heat Load on Fonterra Whareroa reticulated ammonia refrigeration system.

Calculated as a component of the ‘Energy Balance’ exercise for peak season scenario (November to January, 2009/10).

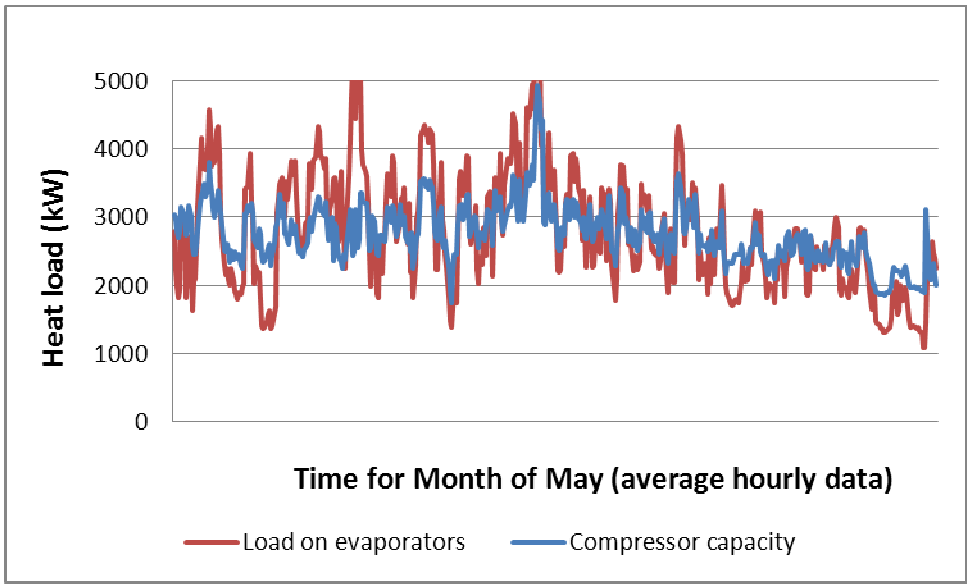

Figure 30: Comparison of compressor capacity calculated by "Compressor scheduling tool", and Heat Load on Fonterra Whareroa reticulated ammonia refrigeration system.

Calculated as a component of the 'Energy Balance' exercise for low season scenario (May, 2010).

The compressor capacity and the calculated heat load into the refrigeration system appear to be comparable for the high and low season scenarios. The higher level of variance for the evaporator load values in the low season scenario is possibly explained by an increased significance of the error associated with chilled water flow measurements used to calculate these load values (equation **3**).

4.6 Modelling

4.6.1 Sensitivity analysis

Each model scenario is defined by a small set of independent variables. In particular the design HOR rate determines the area, psychrometric and flow characteristics of each scenario.

Sensitivity analysis was carried out on the Whareroa scenario using design HOR capacity (1552 kW) and the manufacturer's other design parameters: wet bulb air temperature (21°C), saturated condensing temperature (35 °C), mass air flow (32.6 m^3/s), outside area of coil (292.44 m^2) and mass water flow (29 l/s) (refer to Appendix 7 for a copy of the design specifications).

The model contains 68 equations and there are a small number of independent variables that are listed in Table 19. Each independent variable was tested to determine how sensitive the model was to changes in this variable. The sensitivity was quantified in terms of change in the heat rejection capacity of the model scenario.

Table 19: List of independent variables and their effect on the efficiency of the design scenario for the Fonterra Whareroa EC1 evaporative condenser.

Sensitivity is determined by the magnitude of change in heat rejection capacity from design.

Variable	Explanation	Reference value	Range tested	Sensitivity (%)
$T_{air\ in}$	Temperature of air into condenser	25 °C	+/- 5 °C (20%)	0.00
W_{in}	Humidity Ratio of air into condenser	0.03 kg/kg	+/- 0.01 (33%)	0.0
$T_{water\ in}$	Temperature of recirculating water into condenser	26 °C	+/- 5 °C (20%)	26.06
$T_{Ammonia\ in}$	Temperature of ammonia into condenser	55 °C	+/- 5 °C (10%)	66.01
$T_{Ammonia\ out}$	Temperature of ammonia out of condenser	35 °C	+/- 5 °C (14%)	54.34
$T_{air\ out}$	Dry bulb temperature of air out of condenser	28 °C	+/- 5 °C (18%)	0.0
$P_{Discharge}$	Discharge pressure of ammonia	1351 kPa	+/- 100kPa (7%)	94.24
δ	Thickness of foulant	0.00 mm	10 mm (1000%)	62.09
$x_{quality}$	Quality of ammonia out of condenser (0=all liquid, 1=all vapour)	0.0	0.2 (200%)	183.6
d_{tower}	Area of tower that air is flowing through	6 m^2	+/- 5m^2 (83%)	62.09
m_r	Mass of refrigerant (kg/s)	1.83 kg/s	+/- 5 kg/s (273%)	22.28

The amount of condensation of ammonia ($X_{quality}$) has the largest effect on the performance of the modeled system. For the purposes of this study it was assumed that all the ammonia leaving the condenser was liquid. In addition, the discharge pressure ($P_{Discharge}$) and, as a consequence the temperature of ammonia into the condenser ($T_{Ammonia\ in}$) also have a significant effect on the performance of the modelled system. Temperature of ammonia out of the condenser ($T_{Ammonia\ out}$), the thickness of the foulant (δ), and the area of the tower that air is flowing through (D_{tower}), also have a very significant effect on the performance of the modelled system. The temperature of the recirculating water into the condenser ($T_{water\ in}$) and the mass flow rate of refrigerant (m_r) affect the performance, but to a lesser extent. In general terms the sensitivity analysis is indicating that it is extremely important to use accurate values for the independent variables listed in Table 22 when using the model to achieve a reliable output.

Another important factor affecting the accuracy of the results from the model is the estimation of thermal conductivity (k-value) for a composite fouling material. The model was used to quantify the variation in efficiency for a range of k-values using a film thickness of 2mm.

The results have been graphed in Figure 31 below. From the graph it can be seen that if we estimate a k-value of 1.0 W m^{-2} K^{-1} +/- 0.5 W m^{-2} K^{-1} the variation in efficiency will be 30.7 to 57.0 %. This significant variation indicates how important it is to determine the correct thermal conductivity before making predictions with the model.

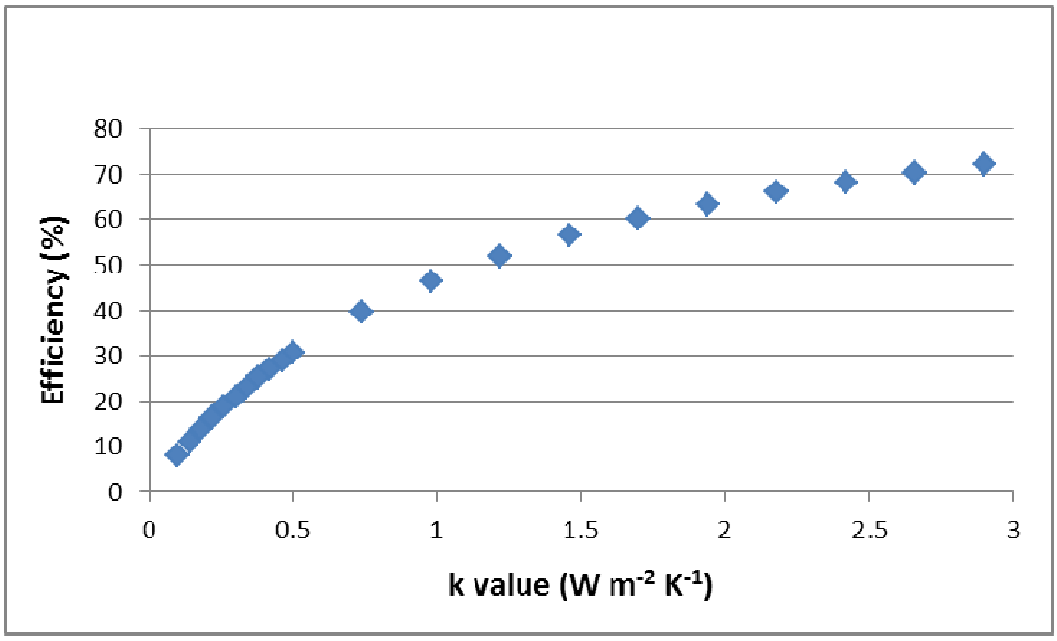

Figure 31: Model results for change in efficiency for k-value range of 0.1 to 3.0 W m^{-2} K^{-1}. Film thickness is 2.0mm.

4.6.2 Model validation

The primary challenge for this project was to develop a model that replicated the behaviour of the Whareroa refrigeration system and would also be applicable to other systems.

The model developed in EES was initially tested by attempting to replicate the normalised performance index (η) vs fouling thickness (δ) relationship determined by Qureshi & Zubair (2005). This validation test used their system characteristics: $T_{db,in}$ = 25°C, $T_{wb,in}$ = 18°C, T_r = 50°C, A = 9.7m^2, m_r = 0.11 kg/s, m_w = 2.67 kg/s, Q = 114.10 kW, m_a = 1.88 kg/s, δ = 3mm.

The resulting graph is shown as **Figure** 32:

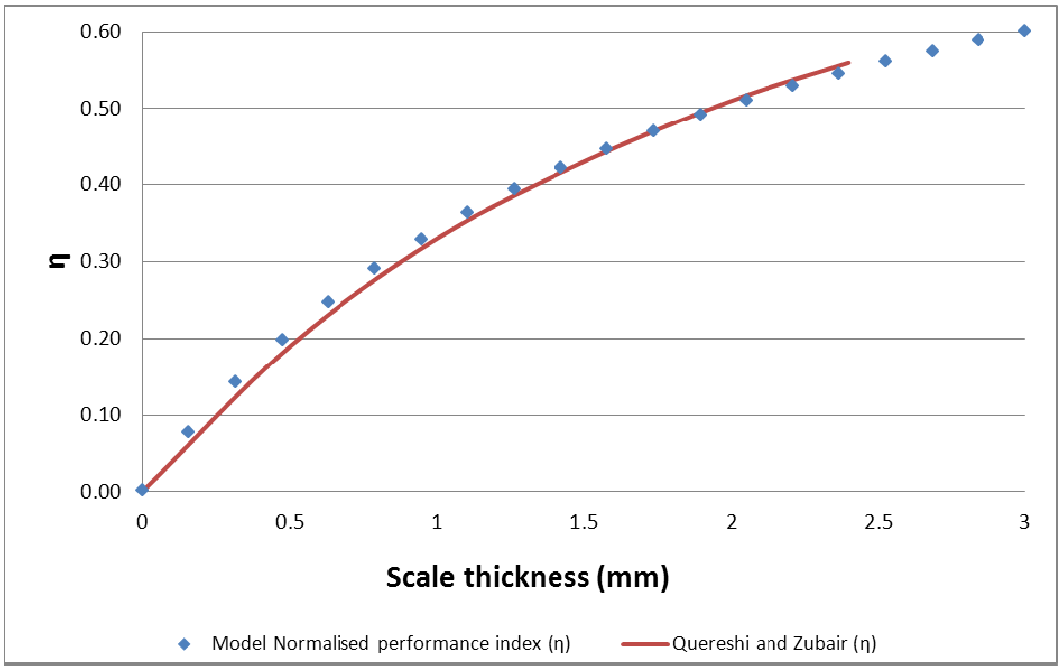

Figure 32: Comparison of normalised performance index (η) vs fouling thickness (δ) for Qureshi and Zubair (2005) values and the project model values.

The results from the model were then compared with the values proposed by Macleod-Smith (2002) for Calcium Carbonate that were subsequently confirmed by Qureshi & Zubair (2005). This relationship of change in heat transfer efficiency (effectiveness) to thickness of CaCO3 scale is shown in Figure 33, which provides a comparison of the Macleod-Smith values for Calcium Carbonate with the values obtained for the project model.

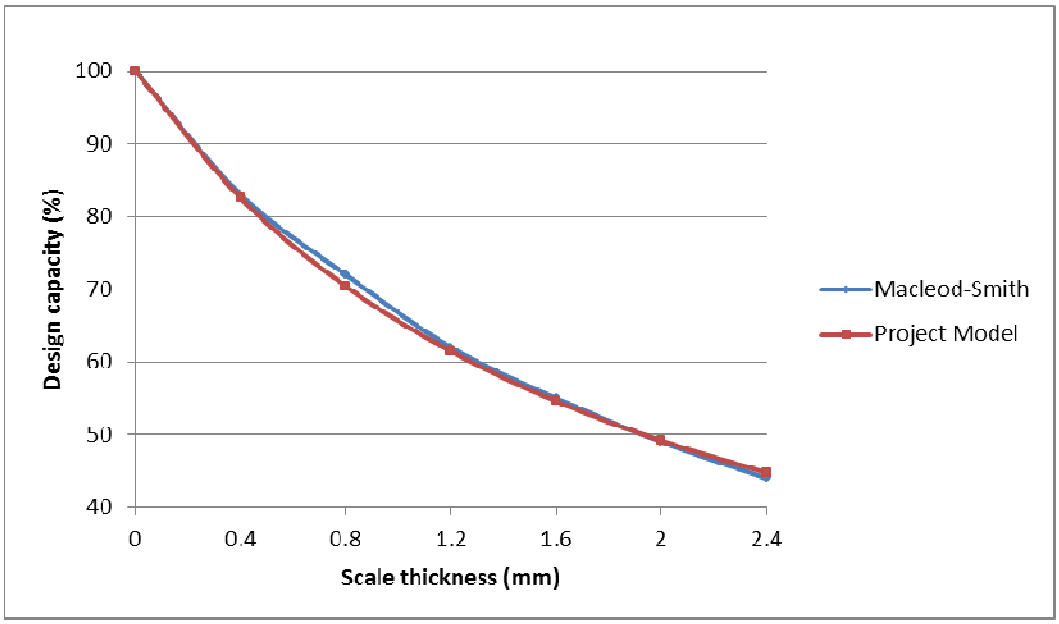

Figure 33: Comparison of fouling thickness (δ) in millimeters to change in percent design capacity (effectiveness) for calcium carbonate scale for the values proposed by Macleod-Smith (2002) and the values obtained with the project model.

The results of both comparisons indicate that the model developed for this project compared very well with the model developed by Queshi and Zubair. In addition, the model results were compared to the Carrier design data for heat transfer efficiency provided by Carrier (1965). The Carrier Handbook provides loss in efficiency predictions for Calcium Carbonate and Biofilm. Figure 34 provides graphs comparing the model results with those obtained from the Carrier Handbook.

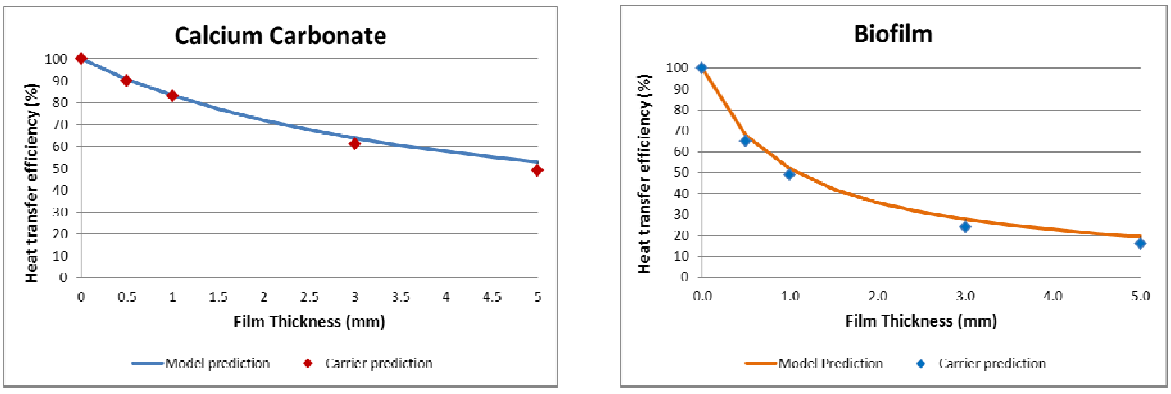

Figure 34: Comparison for change in percent heat transfer efficiency (effectiveness) with increased film thickness for Calcium Carbonate and Biofilm for Model predictions and Carrier Handbook predictions.

The model predictions are very close to those determined by Carrier.

Having verified the integrity of the model, the model was then used to determine the heat transfer efficiency to scale thickness relationship for other fouling substances using design parameters for the Whareroa EC1 Evaporative Condenser.

Table 20 summarises these results and Figure 35 provides graphs comparing the results for each substance. It should be noted at this stage that the Delta value used by Qureshi et al is the total foulant thickness across the diameter of the coil. The parameter that is of real interest is the film thickness of the fouling substance. This is half the delta value and will be referred to as 'Film thickness'.

Table 20: A comparison of the efficiency (effectiveness) vs film thickness relationship for a number of fouling substances using design characteristics for the Fonterra Whareroa evaporative condenser.

Efficiency is the measure of effective HOR capacity as compared to design HOR capacity.

% efficiency									
Film thickness (mm)	**Calcium Carbonate**	**Magnetite**	**Calcium Phosphate**	**Calcium Sulphate**	**Magnesium Phosphate**	**Calcium Carbonate + Biofilm**	**Analcite**	**Biofilm**	**Dicalcium Silicate**
0	100	100	100	100	100	100	100	100	100
0.5	90.73	90.73	89.77	88.59	88.13	84.62	81.44	68.01	16.13
1	83.26	83.26	81.69	79.78	79.05	73.66	69.04	51.94	8.908
1.5	77.12	77.12	75.13	72.77	71.88	65.45	60.17	42.27	6.213
2	71.97	71.97	69.71	67.06	66.08	59.07	53.51	35.81	4.804
2.5	67.59	67.59	65.15	62.32	61.27	53.96	48.32	31.18	3.938
3	63.82	63.82	61.26	58.31	57.23	49.78	44.16	27.7	3.351
3.5	60.54	60.54	57.9	54.88	53.78	46.3	40.74	24.99	2.927
4	57.65	57.65	54.96	51.92	50.8	43.35	37.9	22.82	2.606
4.5	55.09	55.09	52.38	49.32	48.21	40.81	35.48	21.04	2.355
5	52.81	52.81	50.09	47.03	45.92	38.62	33.41	19.56	2.153

.

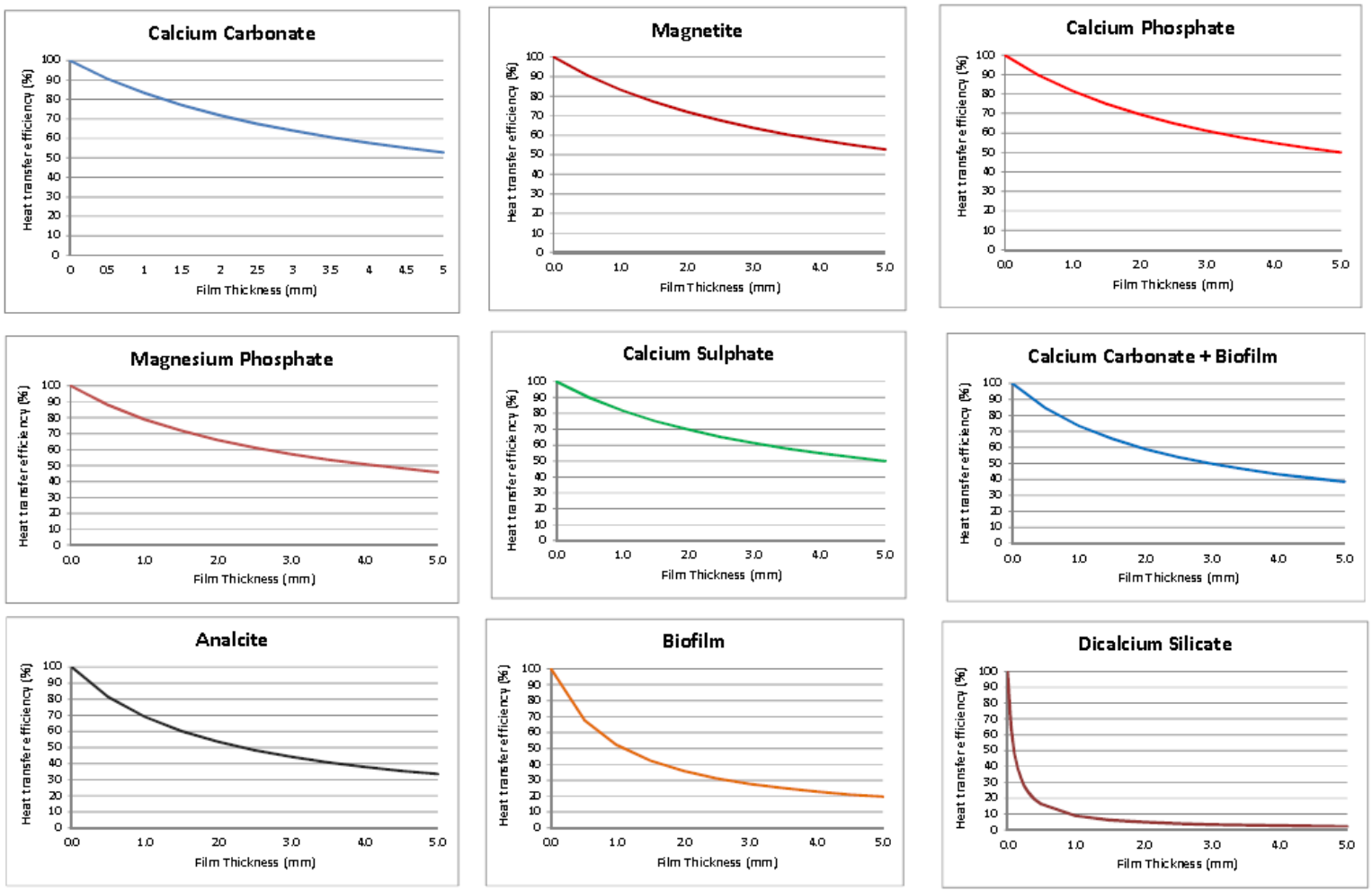

Figure 35: Graphs showing comparison of loss of heat transfer efficiency (effectiveness) with increasing film thickness for a range of fouling substances.

The determination of this efficiency to film thickness relationship for common fouling materials allows us to make predictions about real systems if we can measure the efficiency of a particular system.

4.6.3 Film thickness predictions from Heat of Rejection values

Heat of rejection values were calculated for the Fonterra Whareroa refrigeration system as part of the Energy Balance determination exercise using equation **(11)**. The resulting HOR values were then utilized as inputs to the EES model to predict the scale film thickness for this HOR level.

A preliminary analysis to identify the composition of the fouling material is required before the EES model can be used to predict the film thickness on the outside of the coil. This was completed on a sample of 'scale' removed from the coil on the 15th of March, 2010. The analysis by X-ray fluorescence indicates that the fouling material is predominantly silicon (35% by weight), Calcium Oxide (14% by weight) and iron (13% by weight). X-ray Diffraction also indicates the presence of Calcium Carbonate and Dicalcium Silicate. A copy of the analysis can be found in Appendix 8.

Because the foulant is a composite material it is difficult to accurately determine the conductive heat transfer coefficient of this material (k-value). The actual k-value will be in the range 2.9 to 0.057 W/m K. A k-value of 1.0 W/m K was selected by calculating the mass weight average of the individual components (0.90) plus a 10% adjustment to allow for the volatile components within the composite material.

The selected k-value was used in the EES model to calculate HOR values for a range of film thicknesses. The EES model was adjusted to represent the averaged February to April, 2010 I-history data for the EC1 Evaporative Condenser at Whareroa. This analysis is shown in Figure 36 .

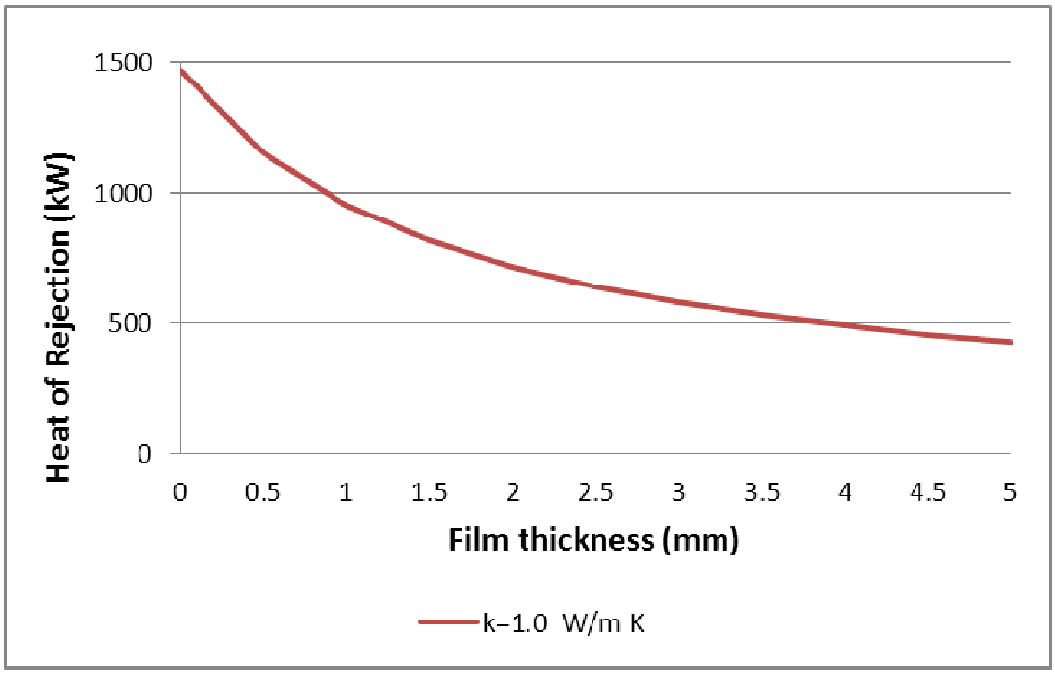

Figure 36: Heat of Rejection values for a k-value of 1.0 W/m K for film thicknesses of 0 to 5.0mm.

The scenario uses April, 2010 data from the Whareroa I-history database and NIWA environmental data.

The HOR values calculated from Psychrometric, NIWA and I-history data were averaged to provide a monthly HOR value. The average HOR for the month of April, 2010 is 793 kW. From the graph the film thickness that coincides with this HOR value is **1.73mm** which yields a total increase in coil outside diameter of 3.46mm, i.e. an outside diameter of **30.46 mm**.

The Whareroa Evaporative Condenser was opened for inspection on the 2nd of June. Figure 37 is a photograph taken during this inspection of the underside of the coils showing that scale is evident.

Figure 37: A photograph showing the underside of the Fonterra Whareroa EC1 coils.

The outside diameter of the coils was measured using a micrometer. Thirty measurements were taken to provide a good representation of the film thickness on the coils (Appendix 9). The average value was **30.24mm**, i.e. a film thickness of **1.62mm**.

The predicted value of 1.73mm compares favorably with the measured value of 1.62mm with a variance of 6.4%. The 95% confidence interval error for the measured values is +/- 0.61mm. The predicted value differs from the measured value by 0.11mm and therefore lies within the 95% confidence interval for the measurement.

There are two questions that require answering before we can be confident that the model is a useful tool for predicting foulant build-up on heat transfer surfaces. The first is: how accurate was the k-value 'guess' used in this example and the second is how will the model perform on other systems?

Both of these questions should be answered by applying the model to a number of other systems however, this exercise is beyond the time constraints of this project.

The Film Thickness prediction procedure described in section 3.6 was employed to produce the results that are seen in graph form in Figure 38 below:

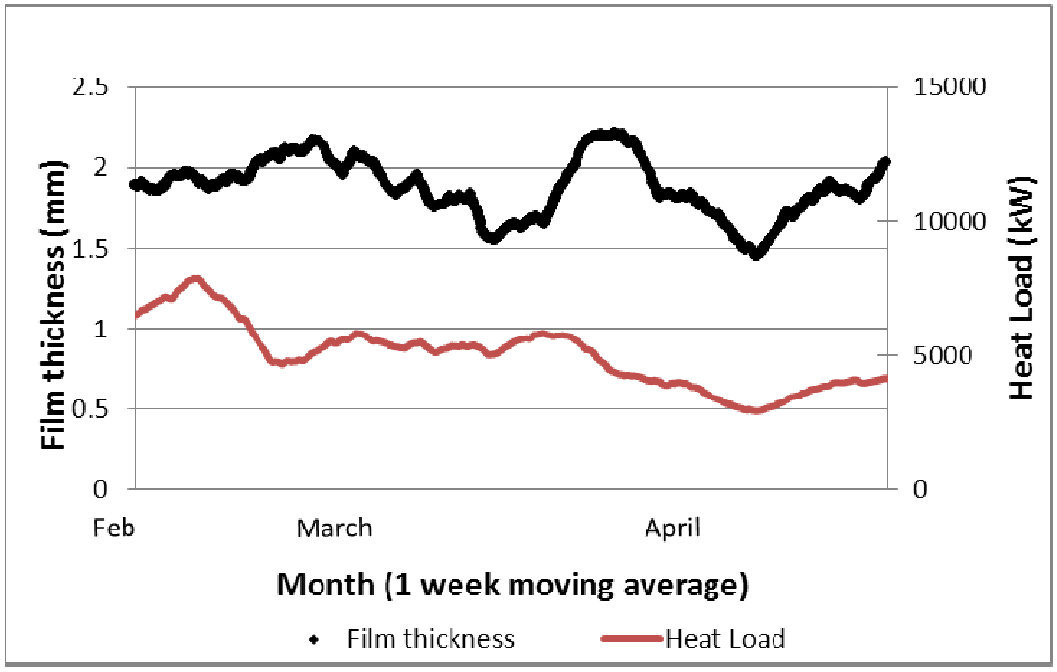

Figure 38: Film thickness predictions for the period February to April, 2010 based on *HOR* values calculated from Psychrometric, NIWA and I-history data.

The film thickness predictions are compared with the corresponding heat load calculated in the Energy Balance exercise.

The graph in Figure 38 appears to show that the heat load follows changes in thickness of the foulant layer. However, an XY scatter graph of the two variables indicates that there is essentially no relationship between the variables. R^2= 0.0979 (Refer to Figure 39 below). This is a realistic outcome as film thickness should be independent of heat load.

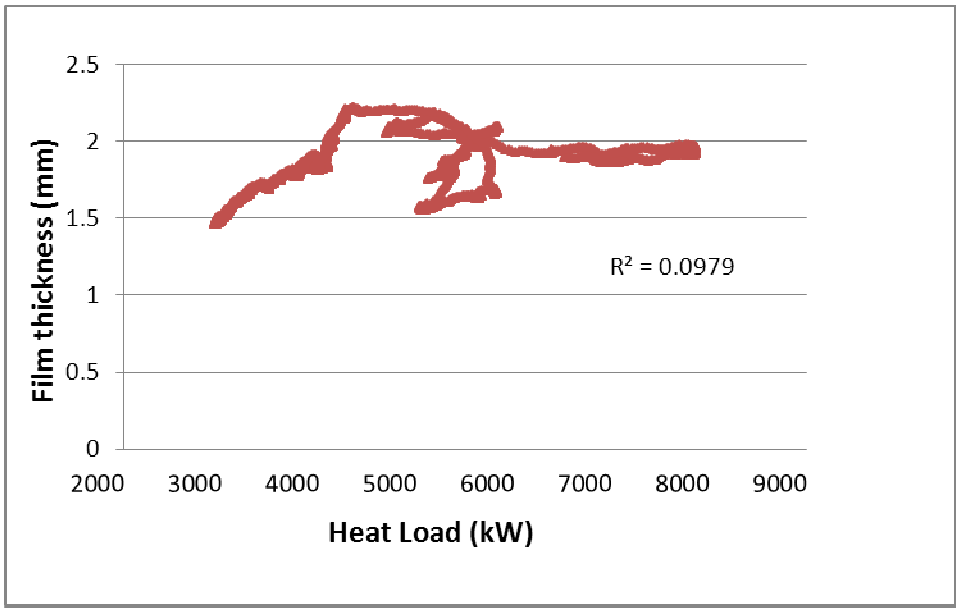

Figure 39: XY scatter plot comparing the two variables Film thickness of foulant and the corresponding heat load at the evaporators.

Data was combined from each of the datasets for the November 2009 to December 2010 period to provide a seasonal profile for foulant film thickness and heat load. The resulting graph (Figure 40) indicates that control of foulant deposition was consistent for the majority of the 2009 production season. Foulant deposition appears to decrease towards the end of the season and this trend continues into September of the 2010 production season. Foulant deposition then increases as the 2010 season progresses. The two factors that have a major influence on the level of deposition are the quality of the water treatment programme and the temperature of the heat transfer surface (*Nalco, 1988), (p 21.2).* This is due to the inverse solubility of most scale forming species as temperature increases. If the chemical programme is managed correctly microbio film development and foulant deposition will be minimised. The existing fouling will also slowly be removed with time. This is possibly what is being observed for the period November 2009 to June 2010. As the heat load increases the potential for mineral deposit fouling increases, consequently if the chemical treatment programme is not adjusted to allow for this then fouling will occur. This is possibly what is being observed for the period August 2010 to December 2010.

It is important to note that it is the trend that is of primary importance with this data and not the absolute values. This is due to the fact that there may be some variability in the absolute values due to measurement and computational errors but the trend is an indicator of changes in the system.

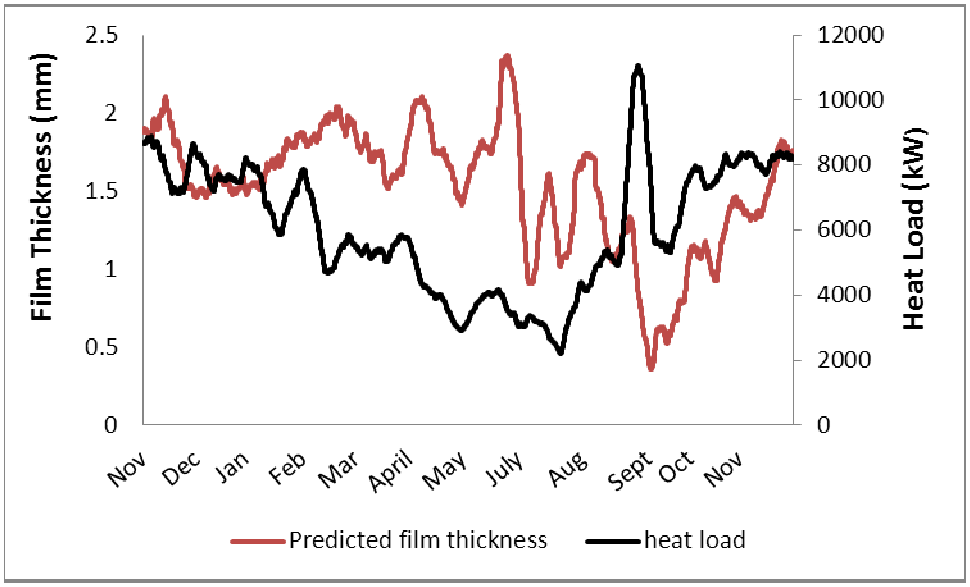

Figure 40: Film thickness predictions for the period November 2009 to December, 2010 based on *HOR* values calculated from Psychrometric, NIWA and I-history data.

The film thickness predictions are compared with the corresponding heat load calculated in the Energy Balance exercise.

4.6.4 Change in Efficiency with change in relative area of foulant film on coil

One of the observations when manipulating data in the model was that efficiency appeared to decrease as the relative area of the foulant layer increased, i.e. there is a 'geometry effect' associated with the relationship between relative surface area and reduction in efficiency. To test this hypothesis the model was run using Calcium Carbonate as the fouling material and the ratio of area outside the tube ($A_{outside}$) to area inside the tube (A_{inside}) was varied to test what the efficiency would

change by for a constant fouled thickness of 1mm. Table 21 provides the results obtained from the model.

Table 21: EES model calculation results for change in efficiency with change in relative areas of area outside ($A_{outside}$) to area inside (A_{inside}) as represented by the Area ratio ($Area_{ratio}$)[4]

A_{inside} (m^2)	$A_{outside}$ (m^2)	Area Ratio	Q_{clean} (kW)	Q_{fouled} (kW)	L (m)	Efficiency %
0.63	1.26	2.000	54.5	11.04	10	20.25
2.99	5.13	1.714	203.6	44.89	34	22.05
6.56	10.20	1.556	362.0	87.95	58	24.29
11.33	16.49	1.455	517.4	138.8	82	26.82
17.32	23.98	1.385	663.6	195.9	106	29.51
24.50	32.67	1.333	798.3	257.9	130	32.31
32.90	42.57	1.294	921.0	323.6	154	35.14
42.50	53.68	1.263	1032.0	391.8	178	37.97
53.31	66.00	1.238	1133.0	461.7	202	40.75
65.32	79.52	1.217	1224.0	532.2	226	43.48
78.54	94.25	1.200	1307.0	602.8	250	46.13

The results of the change in efficiency versus relative area change were plotted in Figure 41. This supports the observation that heat transfer efficiency does decrease with increase in relative area of the foulant (scale) film, i.e. geometric effects impact on the heat transfer efficiency.

[4] For the purpose of this exercise $A_{outside}$ and A_{inside} were both allowed to vary. Alternatively one of the variables could have been set but this would not have affected the results generated by the model in terms of $Area_{ratio}$.

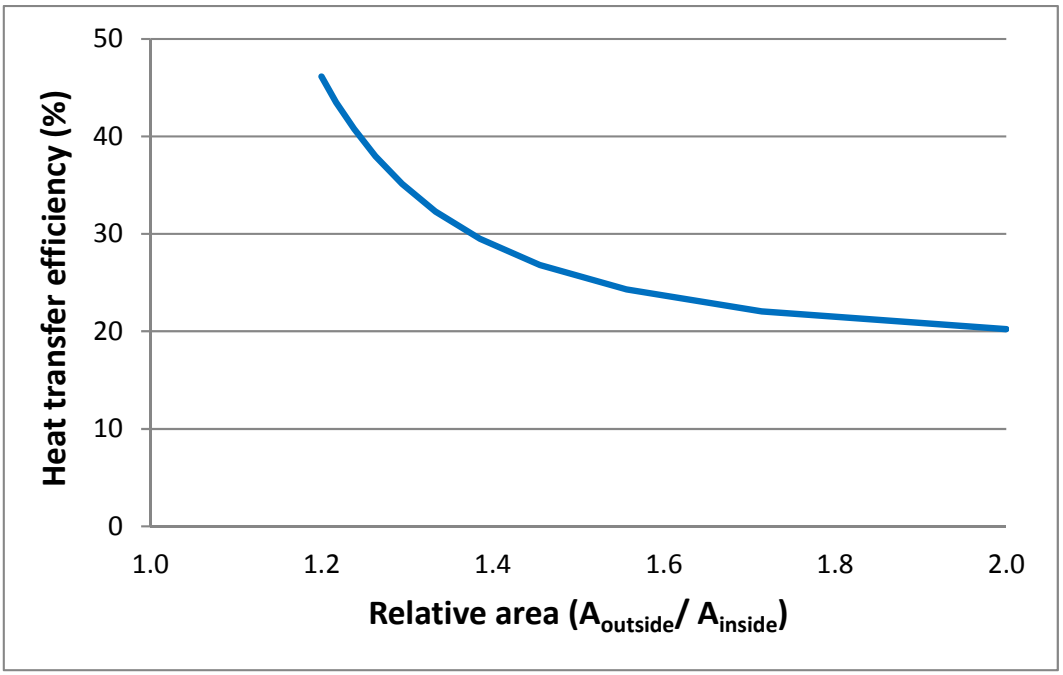

Figure 41: Change in efficiency with change in relative area of a coil with a Calcium Carbonate scale film thickness of 1mm.
Relative area is defined as the ratio of the outside area of the coil (scale surface) to the inside area of the coil.

4.7 Cost analysis

The major costs associated with operating an evaporative condenser are due to the electricity costs of running the compressor, the forced air fan and the water circulation pump.

The electricity cost of running the EC1 condenser was calculated using equation **(39)**. Figure 42 provides a graph of the cost of running the condenser per kW of heat rejected by the compressor compared to the predicted film thickness and Figure 43 is an XY scatter graph of these two variables with the associated regression analysis.

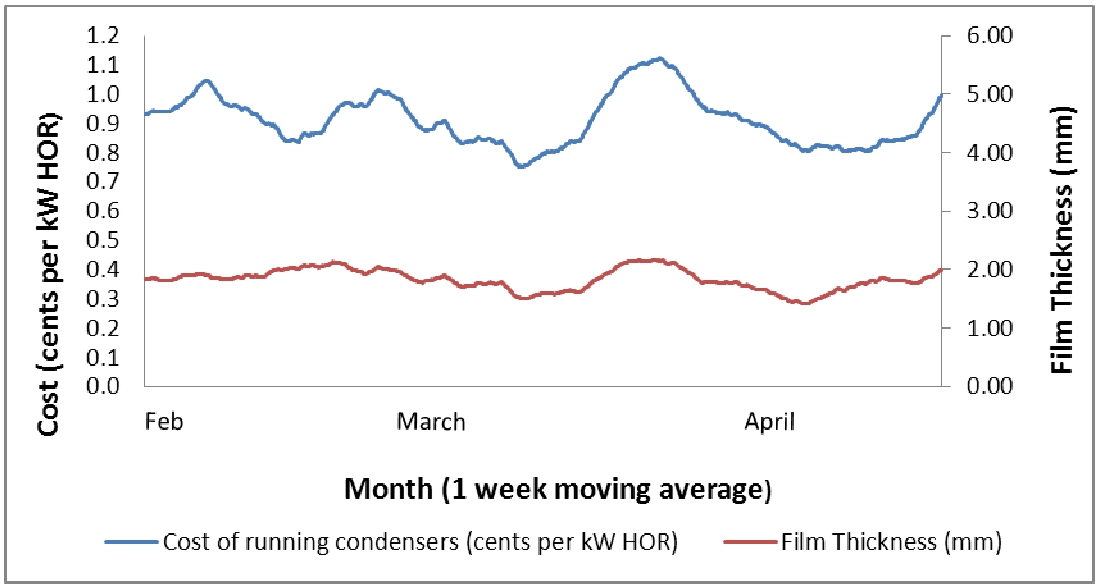

Figure 42: Cost of running the EC1 condenser compared to the film thickness prediction for the February to April, 2010 data set.

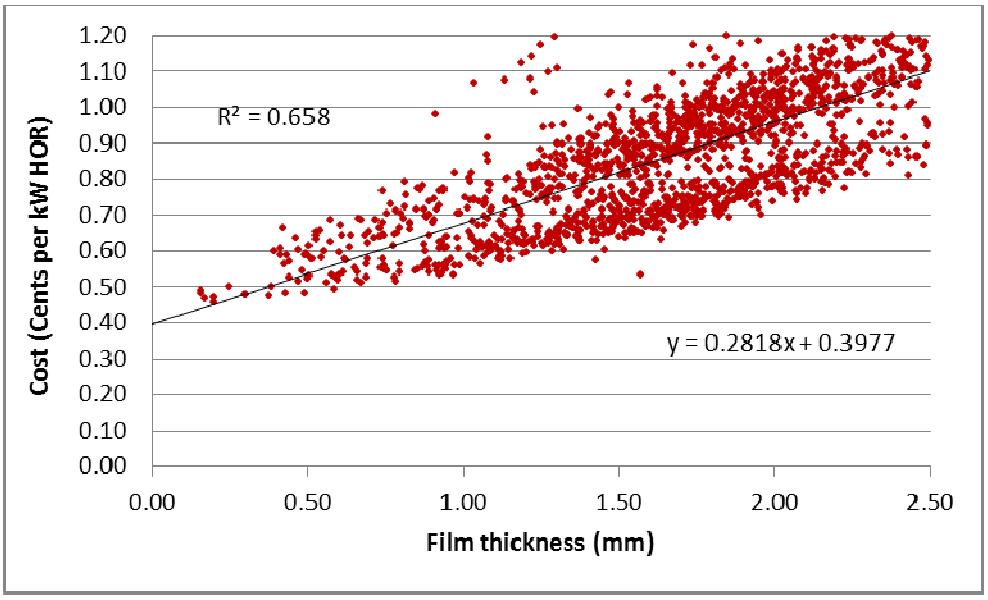

Figure 43: Cost of running the EC1 condenser and film thickness prediction for the February to April, 2010 data set.

*Marginal cost per kW **HOR** (y) equals 0.2818 times the film thickness. Where the deposit is known and k=1.0 W/m^2 K.*

The regression analysis result of **0.658** indicates that there is a weak correlation between running cost and film thickness. Other variables affecting the cost of running the EC1 condenser, i.e. environmental conditions such as humidity must be explored further for their contribution to strengthening the correlation.

Although the regression analysis indicates the cost to film thickness relationship is not perfect we can still project from the XY Scatter Graph with some confidence that the cost per kW HOR will increase by approximately 150% when the scale layer on the EC1 condenser coil increases in thickness from 0 to 2.5mm, i.e. an increase in cost from **0.398** cents per kW HOR to **1.10** cents per kW HOR. For this scenario where the average HOR per hour is 793 kW the total cost of running the condenser would increase from **$75.75** per day to **$209.35** per day.

The cost increase associated with the scale thickness measured during the June shut (1.62mm) is **0.46** cents per kW HOR. Using the average HOR per of 793 kW this would indicate a cost per day of **$162.63**; an increase of **115%**. If we extrapolated this to a cost per day for the total refrigeration system, the clean system would cost $1254.51 per day to manage a heat load of 6.73MW per hour and $2693.35 per day at a scale film thickness of 1.62mm for the same heat load.

In general we can hypothesise from this correlation that the cost of running the evaporative condenser increases at a rate of (0.2818 x the film thickness) + 0.398 cents per kW HOR, i.e. a marginal cost for fouling of 0.2818 cents per mm of foulant per kW of HOR. Figure 43 illustrates the cost to film thickness relationship.

Because the Whareroa evaporative condensers are run as 'baseline' HOR equipment, i.e. they are running at full load when they are on, we can also assume that the HOR efficiency (ε_{ec}) to cost relationship will be constant for this system. If the efficiency of the condenser drops by a set amount the cost of rejecting the heat load will increase by an amount equal to the value set by the equation for the correlation. For this scenario the correlation is $y = 96.686 * x^{-1.192}$ as determined by

the curve fit function shown in Figure 44: Cost to Efficiency correlation for the EC1 evaporative condenser at Fonterra Whareroa..

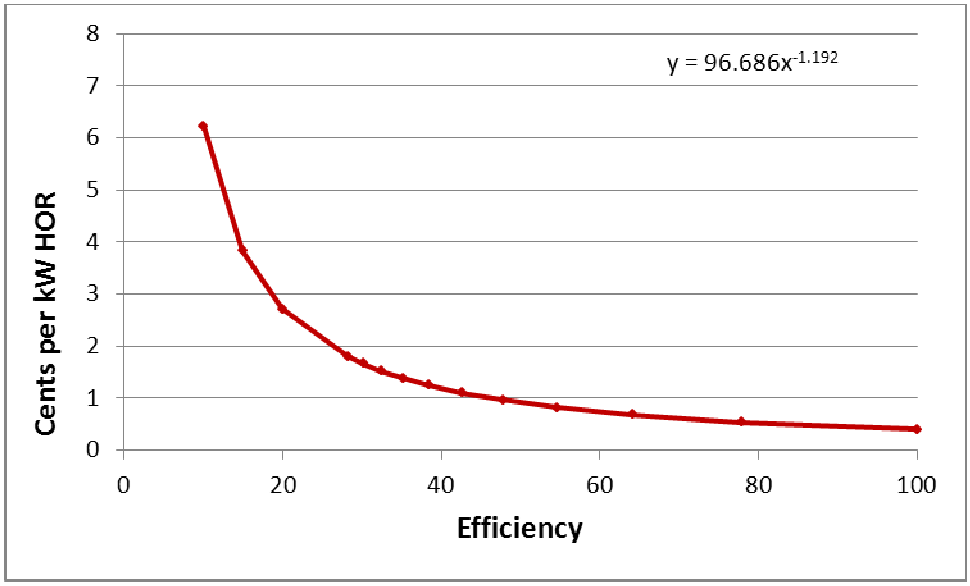

Figure 44: Cost to Efficiency correlation for the EC1 evaporative condenser at Fonterra Whareroa.

The electrical cost to run the Evaporative Condenser can also be viewed in terms of Carbon Dioxide emissions (or equivalents). Figure 45 represents the actual running costs as t-CO_2-e per hour of electricity used and is compared with the predicted film thickness for this period. The CO_2 emission rate is calculated by multiplying the energy usage by the set rate for Fonterra Whareroa of 0.634t per MWhr. The average for the period is 1.069 t-CO_2-e per day and can be compared to the emission rate when there is no fouling present 0.480 t-CO_2-e per day, i.e. an increase of 123%.

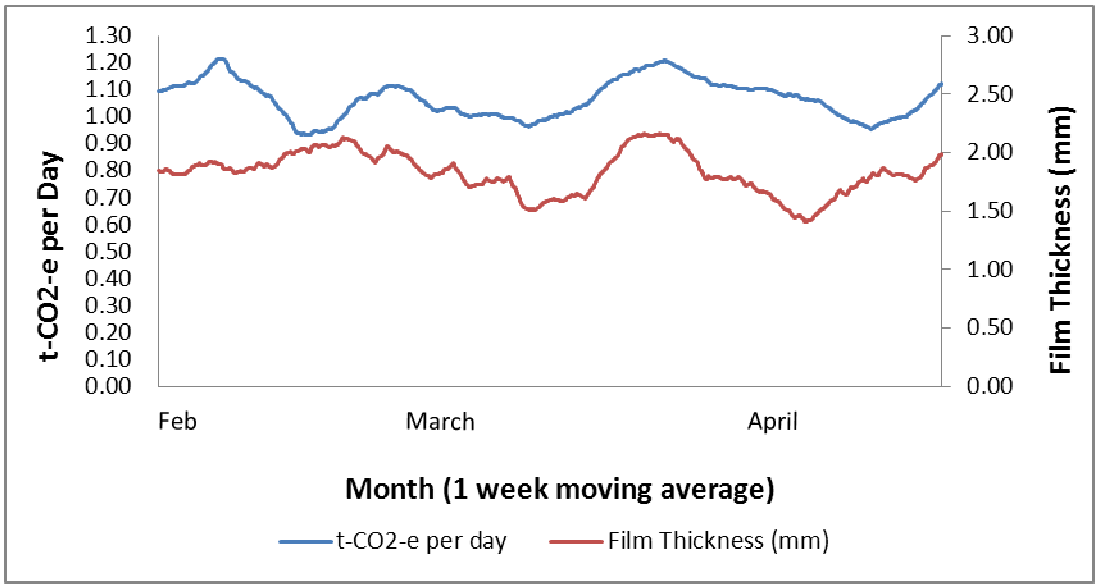

Figure 45: t-CO_2-e per day for electricity consumed to run the EC1 condenser compared to film thickness for the February to April, 2010 data set.

(Based on emission rate for Whareroa of 0.634t per MWhr of electricity).

t-CO_2-e emission rates for the electricity used to run the refrigeration system compressors were compared to the heat load and predicted film thickness for the composite seasonal data. The result is shown as Figure 46 below. The CO_2 emission trend appears normal for the heat load, i.e. emissions follow heat load.

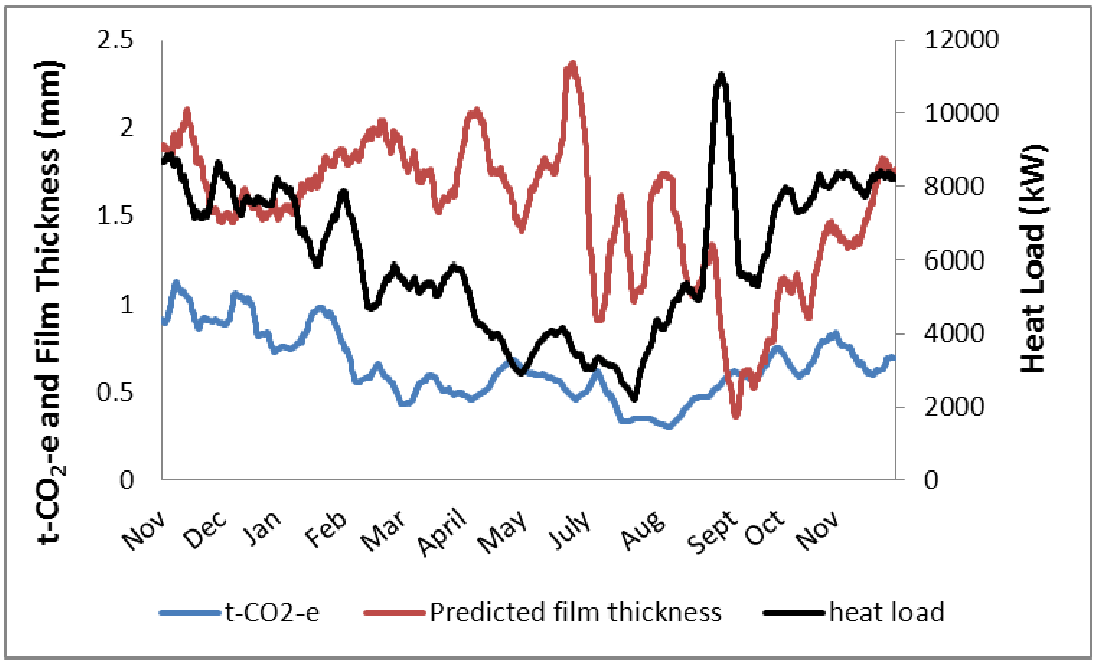

Figure 46: t-CO_2-e electricity consumed to run the refrigeration system compressors compared to predicted film thickness and system heat load for the period November 2009 to December 2010 *(Based on emission rate for Whareroa of 0.634t per MWhr of electricity).*

4.8 Summary

The results of the energy balance exercise indicate that there are some significant errors in the data that is captured on site. A potential source of this could be the flow meter values for the chilled water flow rates through the evaporators and the plate heat exchanger condensers. Another potential source is the fan speed strategy utilised to manage the air flow through the evaporative condenser(s).

The model was tested by comparing outputs for efficiency with those obtained by Macleod- Smith, Qureshi and Zubair and Carrier design data. The model produced results that were within 5% of the results obtained by the other three sources.

A prediction of fouling thickness was then made for the study evaporative condenser based on efficiencies determined from temperature measurements over the evaporative condenser that were then used by the model to predict film thickness. The evaporative condenser was opened for its annual shut and the thickness of the foulant was measured. Results obtained for the model prediction differed from the actual measured result by 6.4%.

Theoretical energy costs for running the total refrigeration system were extrapolated to determine the cost relationship associated with running the system in a fouled state. Energy costs for the 1.73mm scale film thickness measured during the inspection show that the costs increased by 115% when compared to design. CO2-e emissions are directly proportional to energy cost so there would be a 115% increase in emissions as well.

Chapter 5 DISCUSSION

The results of this research have shown that the predictive efficiency model developed here closely replicates the results of Qureshi and Zubair, The Carrier Refrigeration Handbook and Macleod-Smith. The model was used to predict the film thickness of scale buildup on an existing evaporative condenser. The model predicted the scale build-up to within 6.4% of the build-up measured when the condenser was opened for inspection. The predicted scale thickness was determined at 1.73mm and the actual thickness was found to be 1.62mm. It was determined that the prediction value was within the 95% confidence interval for the coil measurements.

A potential limitation of this model is the requirement to estimate the thermal conductivity (k-value) of a fouling material when the material is a combination of two or more substances comprising of minerals and/or biofilm. As an example, to emphasis the importance of accurate thermal conductivity determination, if we use the same range of k-values that were used for the sensitivity analysis (refer section 4.6), for k-values of 0.5 to 1.5 W m^{-2} K^{-1} the model predicts a film thickness of between 0.82 and 2.63mm, i.e. a variation of +/- 52% to the predicted value of 1.73mm. This outcome highlights that the model will only be accurate if the k-value determination is accurate.

There are a limited number of models in the literature that are used to predict the morphology of a composite material. An example can be found in the 4th edition of Perry's Chemical Engineers' Handbook (Perry, 1963). Such models could potentially be used to enhance the capabilities of this project. However, rigorous assessment would be required to determine their reliability. Although the project model is possibly limited by the necessity to identify the fouling material before the film thickness can be predicted, this is the most accurate option at this point in time.

Another limitation of the project is the inability to reconcile the energy balance to less than 30% difference between heat load plus work done by the compressors, and heat of rejection. A combination of the variability introduced by the fan speed control strategy utilised at Fonterra Whareroa and the errors introduced by each sensor, particularly the fan 'energiser' and water flow meters are thought to be the main causes of this high margin of error.

Regardless of the limitations, this methodology can still be used to monitor the heat transfer efficiency of a refrigeration system in real time if there is capability to monitor heat load into the system and psychrometric variables over the condenser. If a system is known to be clean then the model can be 'calibrated' to show Q_{clean}, any subsequent loss in efficiency could then be addressed as a reduction in efficiency is observed. Loss in apparent efficiency could be caused by a number of issues including: water-side fouling of heat transfer surfaces, fouling of the refrigerant side with oil or air, mechanical failure of fans, pumps or compressors and malfunctioning sensors.

The minimum variables that are required to monitor a system with this model are described in Table 22. Dry bulb temperature out of the condenser is probably the one variable that will require additional equipment to allow continuous monitoring.

Table 22: Variables required to monitor a refrigeration system with the predictive efficiency model.

Evaporator side variables	Unit
Temperature into heat exchanger	°C
Temperature out of heat exchanger	°C
Flow rate of chilled water through heat exchanger	Kg/s
Temperature or pressure of refrigerant into heat exchanger	°C or kPa
Evaporation temperature	°C
Condenser side variables	
Thermal conductivity of deposits (k-value)	W/m/K
Dry bulb ambient air temperature	°C
Wet bulb ambient air temperature	°C
Dry bulb air temperature out of condenser	°C
Cold well water temperature	°C
Suction pressure of refrigerant	kPa
Discharge pressure of refrigerant	kPa*
Discharge temperature of refrigerant (superheat)	°C*
Air flow rate in the tower	Kg/s*
Water flow rate in the tower	Kg/s

*The sensitivity analysis (refer 4.6.1) indicates that it is critical that these variables are measured as accurately as possible.

This project has focused on only one refrigeration system. As a consequence the question of transferability still requires answering. Testing this model on another refrigeration system would also increase the credibility of the results obtained for the Fonterra Whareroa system. Further, the application of the model to a refrigeration system where the evaporative condensers is not fully loaded is also required to test the full capability of this model.

This project has highlighted the cost of running a fouled refrigeration system. Although the fouling was only moderate the predicted cost to cool the processing plant increased by 115%. Given that this represents a significant increase in revenue it makes sense to resource the appropriate chemical treatment programme so that fouling is minimised.

The business community is slowly recognising the importance of sustainability but few are taking real action to demonstrate it. The potential impacts of global warming have motivated responsible businesses to take action to optimise energy use. In addition, the financial crisis of 2008 has forced businesses to become more financially sustainable. Many organisations are using this focus on environmental and financial sustainability as a means of differentiating themselves from their competitors. As an example Nalco are now employing energy and sustainability indicators internally in their business plans and externally as a means of demonstrating value creation for their customers. Figure 47 is an excerpt from a strategy paper from Nalco (Williams, 2010) showing the sustainability and value creation flow path for 'Optimized Cooling Water Treatment'. This is of particular relevance to this project and highlights the value that is created for the customer from good fouling mitigation.

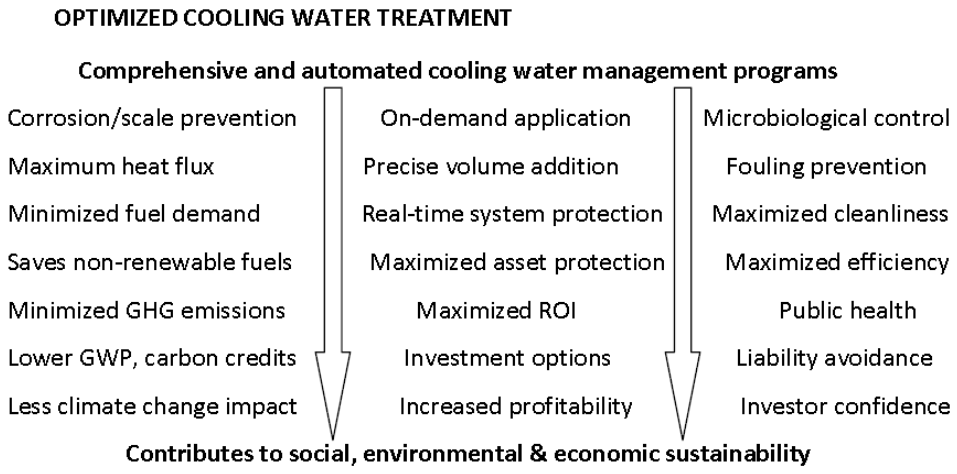

Figure 47: Example of sustainability indicators flow diagram produced by Nalco

Using sustainability as a marketing tool is currently useful but ultimately is only effective if rigorous research and case studies exist to show that the organisation in question is ‘walking the talk’. Anything less is likely to be recognized as ‘green washing’.

Using sustainability indicators to support measurable economic and environmental impacts is a (far more) powerful position for a business reliant on industrial processing. Development of such predictive models for businesses reliant on energy intensive processes such as refrigeration can deliver tangible economic and environmental benefits. These are a better basis for marketing products and services to industry.

CHAPTER 6: CONCLUSIONS AND RECOMMENDATIONS

This project has produced a predictive efficiency model that has the potential to be a useful tool for real time monitoring of refrigeration systems and potentially other industrial cooling systems.

Currently the model developed during this project is not in a form that is 'user friendly'. The steps required to enhance the capability of the model and create a tool that could be 'universally' used to monitor refrigeration systems are:

1. Enhancing capability by using the commercial version of Engineering Equation Solver (EES) so that the macro function in this version can be utilised to transfer data to and from of databases such as Excel. This would allow the model to be largely automated and potentially mean that the model could be incorporated into a process control system and used for continuous monitoring.

2. Testing the model on refrigeration systems with variable loads to determine the model's accuracy for partial load situations.

3. Reviewing the performance of the model on systems with a range of fouling materials.

The energy balance exercise completed during this project indicated that there is potentially an issue with the calibration of monitoring sensors situated at the Fonterra Whareroa plant. It is recommended that the calibration schedule of these sensors be reviewed. Particular emphasis should be placed on the chilled water flow meters at each of the process plant evaporator plate heat exchangers.

Industrial plants that take the opportunity to utilise monitoring tools such as the one developed during this project are being proactive about optimising their financial and environmental sustainability.

APPENDICES

Appendix 1:

Procedure for Determining Optimum Relation Between Condensing Pressure and Outdoor Wetbulb

The trajectory of optimum condensing pressures for corresponding outside air wet bulb temperatures shown in Figure 11 is specific to the existing ammonia system. Each system will have its own unique trajectory. However, the following procedure can be used to empirically develop the trajectory of optimum condensing pressures. Note, this procedure needs to be executed during off-design periods of the year (during relatively low outside air wet bulb conditions). The procedure also requires the ability to continuously monitor the outdoor air wet bulb temperature, condensing pressure, and the engine room total electrical demand. We also recommend that other system state variables (such as suction pressures, superheat – if applicable, etc.) be monitored to ensure reliable system operation during the procedure.

1. Measure the outdoor air wet bulb temperature.
2. Note the current condensing pressure and system electrical demand.
3. Reset the condensing pressure down 5 psig (35 kPa) and allow the system to equilibrate.
4. Note the new system electrical demand.
5. Continue steps 3 and 4 until the lower limit in condensing pressure setpoint is reached.
6. Plot the system electrical demand vs. the condensing pressure and note the condensing. pressure that corresponds to the point of minimum system electrical demand (like Figure 6).
7. Plot that single "optimum" condensing pressure point on a optimum condensing pressure vs. outdoor air wet bulb temperature curve.
8. Repeat steps 1-7 on one or more days with different wet-bulb conditions to more fully develop a curve analogous to Figure 11.

Once the optimum condensing pressure trajectory curve is developed, it can be programmed into a system PLC or supervisory controller to yield optimum system performance throughout the year. Bear in mind that the procedures 1-6 above need to be executed in a relatively short period of time (1-2 hrs) as the outside air wet bulb will change throughout the day. In general, the outside air wet bulb temperature has a daily range of between 7-10°F (4 – 5.5°C). Step 3 above is important. The period to achieve equilibrium operation will be longer for larger systems (on the order of tens of minutes). Finally, constrain the condensing pressure from dropping below a lower limit that will degrade the operation of a system (due to expansion valves, hot gas defrost, etc.).

Appendix 2: HRF Selection data and Procedure (BAC)

SELECTION DATA AND PROCEDURE / AUSLEGUNGS VERFAHREN

GENERAL INFORMATION

OPERATING CONDITIONS

Evaporative Condensers are designed for operating conditions specified below. The operator must ensure that during operation of the equipment these conditions are not exceeded.
Acceptable Refrigerants: R-717, Halocarbon Refrigerants and HFC's.
Coil design pressure: 22 bar max. (Note that high pressure coils with a design pressure of 28 bar are available upon request.)
Maximum temperature of superheated vapour: 120 °C
Minimum temperature of refrigerant in coil(s): - 20°C

ALLGEMEINE INFORMATION

BETRIEBSBEDINGUNGEN

Verdunstungsverflüssiger sind für nachstehende Betriebs-bedingungen entworfen. Der Betreiber hat sicherzustellen, daß diese Bedingungen während des Betriebs eingehalten werden.
Akzeptierte Kältemittel: R717, FKW, HFC.
Max. Betriebsdruck: 22 bar (Rohrschlangen für 28 bar Betriebsdruck als Option verfügbar)
Max. Temperatur des überhitzten Dampfes: 120°C
Min. Temperatur Kältemittel im Rohrbündel: -20°C

TABLE 1 - BASE HEAT REJECTION VXC (kW)
TABELLE 1 - VERFLÜSSIGERNENNLEISTUNG VXC (kW)

MODEL NO VXC MODELL VXC	HEAT REJECTION KONDENSATOR NENNLEISTUNG (kW)	MODEL NO VXC MODELL VXC	HEAT REJECTION VERFLÜSSIGER-NENNLEISTUNG (kW)
14	61	S455	1961
18	78	S482	2077
25	108	495	2132
28	121	S504	2172
36	156	516	2227
45	194	552	2422
52	225	S578	2492
59	250	S600	2585
65	281	620	2672
72	311	S656	2826
86	371	680	2930
97	418	S700	3016
110	474	734	3076
125	539	716	3087
135	582	772	3326
150	647	738	3438
166	716	804	3464
185	796	S806	3473
205	884	S858	3697
221	953	908	3913
250	1078	S910	3921
265	1142	S954	4153
S288	1241	990	4265
S300	1293	S1010	4352
S326	1413	1032	4448
S350	1508	1124	4843
357	1538	1240	5343
393	1719	1360	5862
S403	1737	1430	6161
S429	1849	1544	6652
454	1956	1608	6928

NOTE / BEMERKUNG:
• Models (& capacities) in italics have a unit width of 3,6 meters.
• Typen (& Leistungen) im Kursivdruck haben eine Gerätebreite von 3,6 Metern.

TABLE 2 - HEAT REJECTION CAPACITY FACTORS
TABELL 2 - KORREKTURFAKTOR

A. REFRIGERANT R22 & 134A / KÄLTEMITTEL R22 & 134A

Cond. Temp. / Verfl. Temp. (°C)	Entering Air Wet Bulb Temperature (°C) / Feuchtkugeltemperatur der Luft beim Eintritt (°C)											
	10	12	14	16	18	20	22	23	24	26	28
29	1.12	1.31	1.39	1.48	1.69	1.83	2.00	2.21	2.49	2.98	–	–
31	0.99	1.05	1.15	1.30	1.41	1.60	1.81	1.74	1.99	2.36	3.19	–
33	0.89	0.94	1.01	1.09	1.20	1.26	1.34	1.43	1.53	1.81	2.35	3.04
35	0.80	0.85	0.90	0.96	1.04	1.09	1.16	1.20	1.27	1.46	1.72	2.14
37	0.73	0.76	0.81	0.85	0.92	0.95	0.99	1.04	1.09	1.21	1.38	1.65
39	0.67	0.69	0.73	0.77	0.82	0.84	0.87	0.91	0.94	1.04	1.15	1.32
41	0.61	0.64	0.66	0.69	0.73	0.75	0.78	0.80	0.83	0.90	0.99	1.10
43	0.56	0.58	0.61	0.63	0.66	0.68	0.70	0.72	0.74	0.79	0.86	0.94
45	0.52	0.54	0.56	0.58	0.60	0.62	0.63	0.65	0.67	0.71	0.76	0.82

B. REFRIGERANT R717 (Ammonia) / KÄLTEMITTEL R717 (Ammoniak)

Cond. Temp. / Verfl. Temp. (°C)	Entering Air Wet Bulb Temperature (°C) / Feuchtkugeltemperatur der Luft beim Eintritt (°C)											
	10	12	14	16	18	20	22	23	24	26	28
29	0.98	1.08	1.19	1.32	1.51	1.68	1.75	1.90	2.21	2.98	–	–
31	0.88	0.94	1.02	1.12	1.25	1.34	1.43	1.58	1.68	2.10	2.84	–
33	0.79	0.84	0.90	0.97	1.07	1.13	1.19	1.27	1.36	1.61	2.00	2.70
35	0.71	0.75	0.80	0.86	0.93	0.97	1.02	1.07	1.13	1.30	1.53	1.90
37	0.65	0.68	0.72	0.76	0.82	0.85	0.88	0.93	0.97	1.08	1.23	1.48
39	0.59	0.62	0.65	0.68	0.73	0.75	0.78	0.83	0.84	0.92	1.05	1.19
41	0.54	0.57	0.59	0.63	0.66	0.67	0.69	0.72	0.74	0.86	0.96	0.98
43	0.50	0.52	0.54	0.56	0.59	0.61	0.62	0.64	0.66	0.71	0.77	0.84
45	0.47	0.49	0.50	0.52	0.54	0.55	0.56	0.58	0.59	0.63	0.68	0.73

SELECTION EXAMPLE

Given

R717 refrigerant, open reciprocating compressor

	Alt. ≠ 1	Alt. ≠ 2
Total Heat Rejection :	950 kW	950 kW
Condensing Temperature :	35°C	35°C
Wet Bulb Temperature :	22°C	22°C
Suction Temperature :	--	-5°C

Solution

Alt. ≠ 1
1. Determine heat rejection capacity factor for R717 at 35°C condensing temperature and 22°C wet bulb temperature from Table 2B which is 1,13.
2. Multiply 950 kW x 1,13 = 1074 kW.
3. From Table 1 select a unit with a base total heat rejection equal to or greater than 1074 kW.
4. Select a VXC-250 with a heat rejection rating of 1078 kW.

Alt. ≠ 2
1. See Alt. ≠ 1.
2. See Alt. ≠ 1.
3. Determine ammonia desuperheater capacity factor for -5°C from Table 3 which is 0,920.
4. Multiply 950 kW x 0,920 x 1,13 = 988 kW.
5. Selection : VXC-250.

AUSWAHLBEISPIEL

Gegeben

Kältemittel R717 offener Kolbenverdichter

	Alt. ≠ 1	Alt. ≠ 2
Verflüssigerleistung :	950 kW	950 kW
Verflüssigungstemperatur :	35°C	35°C
Feuchtkugeltemperatur :	22°C	22°C
Saugtemperatur :	--	-5°C

Lösung

Alt. ≠ 1
1. Bestimmung des Korrekturwertes für R717 bei 35°C Verflüssigungstemperatur und 22°C Feuchtkugeltemperatur (Tabelle 2B). Der Faktor ist 1,134.
2. Man multipliziere : 950 x 1,13 = 1074 kW.
3. Aus Tabelle 1 wählt man einen Verdunstungsverflüssiger, dessen Verflüssigernennleistung größer oder gleich 1074 kW ist. Man wähle hier einen VXC 250 mit einer Verflüssigernennleistung von 1078 kW.

Alt. ≠ 2
1. Siehe Alt. ≠ 1.
2. Siehe Alt. ≠ 1.
3. Mann bestimme den Ammoniakenthitzerkorrekturfaktor für -5°C nach Tabelle 3, nämlich 0,920.
4. Man multipliziere : 950 kW x 0,920 x 1,13 = 988 kW.
5. Auslegung : VXC-250.

TABLE 3 - R717 DESUPERHEATER HEAT REJECTION CAPACITY FACTORS
TABELLE 3 - KORREKTURWERTE FÜR R717 BEI ENTHITZERBETRIEB

Suction Temp. Saugtemperatur (°C)	Capacity Factor Korrekturfaktor
-25	0.915
-20	0.886
-15	0.857
-10	0.828
- 5	0.920
0	0.785
+ 5	0.954

Appendix 3: Nomenclature

A	area (m^2)
$A1$	mean surface are of coil (m^2)
A_{inside}	inside area of coil (m^2)
$A_{outside}$	outside area of coil (m^2)
$A(x)$	manufacturer's performance factors
$B(x)$	manufacturer's performance factors
$C1$	represents increase in performance index as fouling reaches its asymptotic value
$C2$	constant used in asymptotic fouling model (equation 29)
COP	Coefficient of performance
Cp	specific heat at constant pressure (KJ kg^{-1} C^{-1})
Cp_w	specific heat of water (KJ kg^{-1} C^{-1})
D	diameter (m)
d_{tower}	diameter of tower (m)
E_{cost}	is the cost per kW
E_f	is the effectiveness of an evaporative condenser
FLC	percent full load capacity
G	mass velocity ($kg/(s.m^2)$)
h	specific enthalpy (kJ kg^{-1})
h_a	enthalpy of air (kJ kg^{-1})
$h_{air,in}$	enthalpy of ambient air drawn into the evaporative condenser (kJ kg^{-1})
$h_{air,out}$	enthalpy of air at the exit of the evaporative condenser (kJ kg^{-1})
$h_{air,out}(refrigerant,\ SCT)$	enthalpy of saturated air at the refrigerant condensing temperature (kJ kg^{-1})
Δh_{comp}	Enthalpy over the compressor (kJ/kg)
h_D	convective mass transfer coefficient kg m^{-2} s^{-1})
$h_{f,w}$	specific enthalpy of water evaluated at T_w (kJ kg^{-1})
h_{inside}	convective heat transfer coefficient inside coil (kW m^{-2} C^{-1})

$h_{outside}$	convective heat transfer coefficient outside coil (kW m^{-2} C^{-1})
HOR	Heat of rejection (kW)
HOR_{total}	Heat of Rejection for all Evaporative Condensers (kW)
HOR_{EC1}	Heat of Rejection for Evaporative Condenser No. 1 (kW)
$HOR_{design,total}$	Total design Heat of Rejection (kW)
$HOR_{design,\ EC1}$	Design Heat of Rejection for Evaporative Condenser No.1(kW)
h_r	enthalpy of refrigerant (kJ kg^{-1})
HRF	is the heat rejection factor at a particular wet bulb temperature and saturation condensing temperature
h_{rin}	enthalpy of refrigerant at inlet air temperature and pressure (kJ kg^{-1})
h_{rout}	enthalpy of refrigerant at outlet air temperature and pressure (kJ kg^{-1})
h_{sint}	enthalpy of saturated moist air at water, air interface (kJ kg^{-1})
h_{win}	enthalpy of refrigerant at inlet air wet bulb temperature and pressure (kJ kg^{-1})
k	thermal conductivity (kW m^{-1} C^{-1})
$k_{ammonia,\ discharge}$	thermal conductivity of ammonia at discharge pressure from the compressor (kW m^{-1} C^{-1})
k_{steel}	thermal conductivity of steel coil (kW m^{-1} C^{-1})
k_{scale}	thermal conductivity of fouling material (kW m^{-1} C^{-1})
L	Length of coil (m)
m_a	mass flow rate of air (kg/s)
m_r	mass flow rate of refrigerant (kg/s)
m_w	mass flow rate of water (kg/s)
$M_{Velocity}$	mass velocity of ammonia (kg/s)
N_c	is the Nominal capacity is the design capacity defined by the manufacturer of the evaporative condenser.
Nu	Nusselt number
P	pressure (kPa)
$P_{air,\ out}$	pressure of air out of evaporative condenser (kPa)
Pc	critical thermodynamic pressure of ammonia (kPa)

$P_{Discharge}$	the compressor discharge pressure (kPa)
P_{rl}	Prandtl number
Pr	= reduced pressure (kPa)
PR	pressure ratio (discharge pressure (kPa) / suction pressure (kPa))
Q	heat transfer (kW)
Q_c	heat transfer at condenser (kW)
Q_{clean}	heat of rejection for evaporative condenser at design (kW)
Q_e	heat transfer at evaporator (kW)
Q_{fouled}	heat of rejection for evaporative condenser at design (kW)
Q_{rec}	is the heat recovered from the compressor (kW)
R	resistance of the fouling layer (kW/ m^2 .C)
Re	Reynolds number
Re_a	Reynolds number of air
R_{eamm}	Reynolds number for ammonia
Re_{pr}	
r_{id}	inside diameter of coil (m)
r_{od}	outside diameter of coil (m)
T	temperature (°C)
$T_{db,in}$	Dry bulb temperature of air into the condenser (°C)
$T_{wb,in}$	Wet bulb temperature of air into the condenser (°C)
T_{dis}	temperature of refrigerant at discharge (°C)
T_{int}	temperature of water at water, air interface (°C)
T_r	temperature of refrigerant (°C)
T_w	temperature of water (°C)
$T_{w,in}$	temperature of water out of evaporative condenser (°C)
$T_{w,out}$	temperature of water out of evaporative condenser (°C)
U	overall heat transfer coefficient (kW m^{-2}. °C)
U_{clean}	heat transfer coefficient for clean system (kW m^{-2}. °C)
U_{fouled}	heat transfer coefficient for fouled system (kW m^{-2}. °C)
U_{os}	heat transfer coefficient for outside of coil (kW m^{-2}. °C)

V_{air}	velocity of air in evaporative condenser (m/s)
W	humidity ratio of moist air ($kg_w\ kg_a^{-1}$)
W_{calc}	Work done by the compressor using the "Work _Comp" tool (kW)
W_{in}	humidity ratio of air into evaporative condenser
W_{sint}	humidity ratio of air at water air interface
W_{comp}	work done by compressor (kW)
x	Thickness of layer (m)
$x_{quality}$	mass fraction of vapour
ΔTlm	log mean temperature difference (°C)
$\triangle T$	change in temperature at condenser or evaporator (°C)
δ	total thickness of fouling layer (m)
$\rho_{air,in}$	density of air into evaporative condenser (kg/m^3)
ε_{ec}	efficiency of evaporative condenser
η	Condenser performance index
η_i	isentropic efficiency
η_p	part load efficiency
$\eta_{Q,norm}$	normalized cooler/ condenser performance index
μ	fluid dynamic viscosity (Pa.s)
$\mu_{air,in}$	dynamic viscosity of air (Pa.s)
μ_{amm}	fluid dynamic viscosity of ammonia (Pa.s)
λ	thermal conductivity of material ($kW\ m^{-1}\ C^{-1}$)
$\triangle$	"change in"
$\sum Comp$	Total cost of running compressors + cost saving for heat recovery ($)

Appendix 4: Fonterra Whareroa Instrument works report

Whareroa Instrument Works Report

Position ID	Position Name	Device ID	Func ID	SP	Strategy	Error limit	Calibration period	As Found / As Left	Calibration Date	Last Error	Due Date	Cal Count	Input 0%	Input 100%	Input Unit
47-BCFT4060	Chilled water to Cream Products	47-0860181304	FTy	47-SP 305 Rosemount Magflow meters		2.00 % of span	80 years	As Found 1	9/06/2005	0.00 % of span	9/06/2085	2	0	2000	Pulses
47-BCFT4060	Chilled water to Cream Products	47-0860181304	FTm	47-SP 305 Rosemount Magflow meters	None	2.00 % of span	80 years	As Found 1	9/06/2005	0.17 % of span	9/06/2085	1	0	360	m3/hr
47-BCFT4924	"Cp,Wpc,Cheese Chilled water Supply Flow Rate"	47-BCFT4924	FTy	Procedure	Priority 1	2.00 % of reading	80 years				1/04/2085	0	0	2000	Pulses
47-BCFT4924	"Cp,Wpc,Cheese Chilled water Supply Flow Rate"	47-BCFT4924	FTm	47-None yet. Refer to Manufacturers Manual	Priority 1	2.00 % of span	80 years				1/04/2085	0	0	700	m3/hr
47-BCFTC655	Chilled water to Cream Products through SSHEC640 -	47-0860183968	FTy	47-SP 305 Rosemount Magflow meters		2.00 % of span	80 years	As Found 1	9/06/2005	-0.20 % of span	9/06/2085	1	0	2000	Pulses
47-BCFTC655	Chilled water to Cream Products through SSHEC640 -	47-0860183968	FTm	47-SP 305 Rosemount Magflow meters		2.00 % of span	80 years	As Found 1	9/06/2005	-0.04 % of span	9/06/2085	1	0	360	m3/hr
47-BCTT4902	Cooling Water Return To Pipe Bridge At Milk Treatm	47-20736	TTD	47-SP 107 Dip testing Temperature probes	Priority 2	0.30 % of span	80 years				31/07/2085	0	0	100	°C
47-BCTT4902	Cooling Water Return To Pipe Bridge At Milk Treatm	47-20736	TT	47-SP 101 Temperature Transmitter	Priority 2	0.45 % of span	80 years				31/07/2085	0	0	100	°C
47-BCTTC631	Phe No.1 Ch. Water Inlet Temperature	47-9724058	TTD	47-SP 107 Dip testing Temperature probes	None	0.30 % of span	80 years	As Left 2	17/07/2003	0.00 % of span	17/07/2083	1	10	40	°C
47-BCTTC631	Phe No.1 Ch. Water Inlet Temperature	47-9724058	TT	47-SP 101 Temperature Transmitter	None	0.45 % of span	80 years	As Left 2	17/07/2003	-0.43 % of span	17/07/2083	1	10	40	°C
47-BCTTC636	Phe No.1 Ch. Water Outlet Temperature	47-9724054	TT	47-SP 101 Temperature Transmitter	None	0.45 % of span	80 years	As Left 2	17/07/2003	-0.36 % of span	17/07/2083	1	10	40	°C
47-BCTTC636	Phe No.1 Ch. Water Outlet Temperature	47-9724054	TTD	47-SP 107 Dip testing Temperature probes	None	0.30 % of span	80 years	As Left 2	17/07/2003	0.00 % of span	17/07/2083	1	10	40	°C

Report : Fonterra Instrument Works Report

Print date:Friday, 5.6.2009

Position ID	Position Name	Device ID	Func ID	SP	Strategy	Error limit	Calibration period	As Found / As Left	Calibration Date	Last Error	Due Date	Cal Count	Input 0%	Input 100%	Input Unit
47-BCTTC841	Phe No.2 Ch. Water Inlet Temperature	47-9724057	TTD	47-SP 107 Dip testing Temperature probes	None	0.30 % of span	80 years				1/01/2099	0	20	40	°C
47-BCTTC841	Phe No.2 Ch. Water Inlet Temperature	47-9724057	TT	47-SP 101 Temperature Transmitter	None	0.45 % of span	80 years				1/01/2099	0	20	40	°C
47-BCTTC846	Phe No.2 Ch. Water Outlet Temperature	47-9724055	TT	47-SP 101 Temperature Transmitter	None	0.45 % of span	80 years				1/01/2099	0	20	40	°C
47-BCTTC846	Phe No.2 Ch. Water Outlet Temperature	47-9724055	TTD	47-SP 107 Dip testing Temperature probes	None	0.30 % of span	80 years				1/01/2099	0	20	40	°C
47-BCTTC867	Phe Ch. Water Inlet Temperature	47-9724062	TTD	47-SP 107 Dip testing Temperature probes	None	0.30 % of span	80 years				1/01/2099	0	20	40	°C
47-BCTTC867	Phe Ch. Water Inlet Temperature	47-9724062	TT	47-SP 101 Temperature Transmitter	None	0.45 % of span	80 years				1/01/2099	0	20	40	°C
47-BCTTC870	Phe Ch. Water Outlet Temperature	47-9724049	TTD	47-SP 107 Dip testing Temperature probes	None	0.30 % of span	80 years				1/01/2099	0	20	40	°C
47-BCTTC870	Phe Ch. Water Outlet Temperature	47-9724049	TT	47-SP 101 Temperature Transmitter	None	0.45 % of span	80 years				1/01/2099	0	20	40	°C
47-CATT9246	Ctw To Hx9246 Return Temp Xmitter	47-CATT9246	TT	47-SP 101 Temperature Transmitter	None	0.45 % of span	80 years				1/01/2099	0	0	100	°C
47-CATT9246	Ctw To Hx9246 Return Temp Xmitter	47-CATT9246	TTD	47-SP 107 Dip testing Temperature probes	None	0.30 % of span	80 years				1/01/2099	0	0	100	°C
47-CGTTQ724	ST Condenser Cooling Water Outlet Temp.	47-444636	TTD	47-SP 107 Dip testing Temperature probes	None	0.30 % of span	80 years	As Left 2	7/12/1999	-0.10 % of span	7/12/2079	1	0	100	°C
47-CGTTQ724	ST Condenser Cooling Water Outlet Temp.	47-444636	TT	47-SP 101 Temperature Transmitter	None	0.45 % of span	80 years	As Found 1	20/01/2000	0.12 % of span	20/01/2080	2	0	100	°C
47-CPTTF037	F Tech Cooling Water Return Temperature	47-CPTTF037	TTD	47-SP 107 Dip testing Temperature probes	Priority 2	0.30 % of span	80 years				1/01/2099	0	0	100	°C

Position ID	Position Name	Device ID	Func ID	SP	Strategy	Error limit	Calibration period	As Found / As Left	Calibration Date	Last Error	Due Date	Cal Count	Input 0%	Input 100%	Input Unit
47-CPTTF037	F Tech Cooling Water Return Temperature	47-CPTTF037	TT	47-SP 101 Temperature Transmitter	Priority 2	0.45 % of span	80 years	As Left 2	26/07/2005	0.00 % of span	26/07/2085	2	0	100	°C
47-E2FT4095	Chilled Water Ammonia Hx #2	47-W30088/3/1	FTm	47-SP 305 Rosemount Magflow meters	None	2.00 % of span	80 years				29/09/2099	0	0	700	m3/hr
47-E2TTC209	Chilled Phx Inlet Temperature	47-E2TTC209	TTD	47-SP 107 Dip testing Temperature probes	None	0.30 % of span	80 years				1/01/2099	0	20	40	°C
47-E2TTC209	Chilled Phx Inlet Temperature	47-E2TTC209	TT	47-SP 101 Temperature Transmitter	None	0.45 % of span	80 years				1/01/2099	0	20	40	°C
47-E2TTC212	Chilled Phx Outlet Temperature	47-E2TTC212	TTD	47-SP 107 Dip testing Temperature probes	None	0.30 % of span	80 years				1/01/2099	0	20	40	°C
47-E2TTC212	Chilled Phx Outlet Temperature	47-E2TTC212	TT	47-SP 101 Temperature Transmitter	None	0.45 % of span	80 years				1/01/2099	0	20	40	°C
47-E2TTC311	Chilled Water	47-E2TTC311	TT	47-SP 101 Temperature Transmitter	None	0.45 % of span	80 years	As Left 2	5/11/1999	0.13 % of span	5/11/2079	1	4	20	°C
47-E2TTC311	Chilled Water	47-E2TTC311	TTD	47-SP 107 Dip testing Temperature probes	None	0.30 % of span	80 years				1/01/2099	0	4	20	°C
47-E5FT4127	P5Nh3 Chilling Return Flow Transmitter	47-E5FT4127	FTy	Procedure	None	2.00 % of reading	80 years				1/01/2099	0	0	2000	Pulses
47-E5FT4127	P5Nh3 Chilling Return Flow Transmitter	47-E5FT4127	FTm	Procedure	None	2.00 % of span	80 years	As Found 1	19/11/1999	0.00 % of span	19/11/2079	1	0	1000	l/sec
47-E5FT4154	Dcw Make Up Flow Transmitter To Cooling Towers	47-E5FT4154	FTm	47-	None	2.00 % of span	80 years				1/01/2099	0	0	500	m3/hr
47-E5FT4154	Dcw Make Up Flow Transmitter To Cooling Towers	47-E5FT4154	FTy	47-	Priority 2	2.00 % of reading	80 years				10/04/2083	0	0	2000	Pulses
47-E5FTS863	Chilled Water Flowmeter	47-E5FTS863	FTm	Procedure	None	2.00 % of span	80 years				1/01/2099	0	0	0	m3/hr
47-E5PT4804	Separator No.1 Suction Pressure	47-E5PT4804	PT	47-SP 202 Pressure TXs - Local sensors	None	2.00 % of span	80 years				1/01/2099	0	0	0	bar

Position ID	Position Name	Device ID	Func ID	SP	Strategy	Error limit	Calibration period	As Found / As Left	Calibration Date	Last Error	Due Date	Cal Count	Input 0 %	Input 100 %	Input Unit
47-E5PT4813	Separator No.1 Liquid Pump Pressure	47-E5PT4813	PT	47-SP 202 Pressure TXs - Local sensors	None	2.00 % of span	80 years	As Found 1	24/05/2001	-0.06 % of span	24/05/2081	1	1	12	bar
47-E5PT4904	Separator No.2 Suction Pressure	47-E5PT4904	PT	47-SP 202 Pressure TXs - Local sensors	None	2.00 % of span	80 years				1/01/2099	0	0	0	bar
47-E5PT4913	Separator No.2 Liquid Pump Pressure	47-E5PT4913	PT	47-SP 202 Pressure TXs - Local sensors	None	2.00 % of span	80 years				1/01/2099	0	0	0	bar
47-E5TT4120	Basin 1 Outlet Temperature Transmitter	47-E5TT4120	TTD	47-SP 107 Dip testing Temperature probes	None	0.30 % of span	80 years	As Left 2	8/01/2002	-0.20 % of span	8/01/2082	1	0	100	°C
47-E5TT4120	Basin 1 Outlet Temperature Transmitter	47-E5TT4120	TT	47-SP 101 Temperature Transmitter	None	0.45 % of span	80 years	As Left 2	8/01/2002	0.15 % of span	8/01/2082	1	0	100	°C
47-E5TT4126	P5\Nh3 Chilling Temperature Transmitter (Return Li	47-E5TT4126	TTD	47-SP 107 Dip testing Temperature probes	None	0.30 % of span	80 years				1/01/2099	0	0	100	°C
47-E5TT4126	P5\Nh3 Chilling Temperature Transmitter (Return Li	47-E5TT4126	TT	47-SP 101 Temperature Transmitter	None	0.45 % of span	80 years				1/01/2099	0	0	100	°C
47-E5TT4135	P5 Temperature Transmitter (Return Line)	47-0625067	TTD	47-SP 107 Dip testing Temperature probes	None	0.30 % of span	80 years				1/01/2099	0	0	100	°C
47-E5TT4135	P5 Temperature Transmitter (Return Line)	47-0625067	TT	47-SP 101 Temperature Transmitter	None	0.45 % of span	80 years	As Left 2	9/08/2007	-0.03 % of span	9/08/2087	1	0	100	°C
47-E5TTS853	Phe No1 Chilled Water Inlet Temperature	47-E5TTS853	TTD	47-SP 107 Dip testing Temperature probes	None	0.30 % of span	80 years				1/01/2099	0	0	100	°C
47-E5TTS853	Phe No1 Chilled Water Inlet Temperature	47-E5TTS853	TT	47-SP 101 Temperature Transmitter	None	0.45 % of span	80 years				1/01/2099	0	0	100	°C
47-E5TTS855	Phe No1 Chilled Water Outlet Temperature (Indicati	47-E5TTS855	TTD	47-SP 107 Dip testing Temperature probes	None	0.30 % of span	80 years				1/01/2099	0	0	100	°C
47-E5TTS855	Phe No1 Chilled Water Outlet Temperature (Indicati	47-E5TTS855	TT	47-SP 101 Temperature Transmitter	None	0.45 % of span	80 years				1/01/2099	0	0	100	°C

Appendix 5: Tag list

Compressors		Tag name	Unit
1	Ammonia compressor # 1 Motor current	E5FC4200	amps
2	Ammonia compressor # 2 Motor current	E5FC4520	amps
3	Ammonia compressor # 3 Motor current	E5FC4440	amps
4	Ammonia compressor # 4 Motor current	E5FC4280	amps
5	Ammonia compressor # 5 Motor current	E5FC4360	amps
6	Ammonia compressor # 6 Motor current	E5FC4700	amps
7	Ammonia compressor # 1 % full capacity		%
8	Ammonia compressor # 2 % full capacity		%
9	Ammonia compressor # 3 % full capacity		%
10	Ammonia compressor # 4 % full capacity		%
11	Ammonia compressor # 5 % full capacity		%
12	Ammonia compressor # 6 % full capacity		%

Refrigeration system pressures

13	Separator #1 outlet pressure	E5PT4813	Bar
14	Separator #2 outlet pressure	E5PT4913	Bar
15	Separator #1 inlet pressure	E5PT4804	Bar
16	Separator #2 inlet pressure	E5PT4904	Bar
17	Average compressor discharge pressure	E5PT4694	Bar

Powder 5 # 1 Heat Exchanger (HEC500)

18	Flow switch	S856	on/off
19	Flow rate	E5FTS863	m^3/hr
20	Inlet temperature	E5TTS853	deg C
21	outlet temperature	E5TTS855	deg C
21A	Ammonia outlet pressure	SSPTC514	bar

Powder 5 # 2 Heat Exchanger (HEC520)

22	Flow switch	S861	on/off
19	Flow rate	E5FTS863	m^3/hr
23	Inlet temperature	E5TTS858	deg C
24	outlet temperature	E5TTS860	deg C
	Ammonia outlet pressure	SSPTC534	bar

EC2 #1 Heat Exchanger (HEC300)

25	Flow switch		C313	on/off
26	Flow rate		E2FT4095	m^3/hr
27	Inlet temperature		E2TTC309	deg C
28	outlet temperature		E2TTC311	deg C
	Ammonia outlet pressure		SSPTC314	bar

EC2 #2 Heat Exchanger (HEC200)

29	Flow switch		C213	on/off
30	Flow rate		E2FT4093	m^3/hr
31	Inlet temperature		E2TTC209	deg C
32	outlet temperature		E2TTC212	deg C
	Ammonia outlet pressure		SSPTC214	bar

Milk Treatment Heat Exchanger (HEC640)

33	Flow switch		C671	on/off
34	Flow rate	Fixed @ 186 m^3/hr	BCFTC655	
35	Inlet temperature		BCTTC667	deg C
36	outlet temperature		BCTTC670	deg C
	Ammonia outlet pressure		SSPTC654	bar

Cream Products #1 Heat Exchanger (HEC620)

37	Flow switch		C637	on/off
38	Flow rate			
39	Flow rate		BCFT4060	m^3/hr
40	Inlet temperature		BCTTC631	deg C
41	outlet temperature		BCTTC636	deg C
41A	Ammonia outlet pressure		SSPTC634	bar

Cream Products #2 Heat Exchanger (HEC600)

42	Flow switch		C647	on/off
38	Flow rate		BCFT4924	m^3/hr
39	Flow			

	rate		
	Inlet		
43	temperature	BCTTC641	deg C
	outlet		
44	temperature	BCTTC646	deg C
44A	Ammonia outlet pressure	SSPTC614	bar

WPC #1 Heat Exchanger (HEC820)

45	Flow switch	F057	on/off
	Flow		
46	rate	WPFTF058	m^3/hr
	Inlet		
47	temperature	WPTTF051	deg C
	outlet		
48	temperature	WPTTF056	deg C
48A	Ammonia outlet pressure	SSPTC834	bar

WPC #2 Heat Exchanger (HEC800)

49	Flow switch	F047	on/off
	Flow		
46	rate	WPFTF058	m^3/hr
	Inlet		
50	temperature	WPTTF041	deg C
	outlet		
51	temperature	WPTTF046	deg C
51A	Ammonia outlet pressure	SSPTC814	bar

Data to be recorded for trending purposes

	EC5 cooling tower average return water		
52	temperature	E5TT4126	deg C
53	EC5 cooling tower basin temperature	E5TC4120	deg C
	Make up flow		
54	rate	E5FT4154	m^3/hr
55	EC5 Baltamore # 1 basin temperature	E5TT4593	deg C
56	EC5 Baltamore # 2 basin temperature	E5TT4592	deg C
57	EC5 Baltamore # 3 basin temperature	E5TT4591	deg C
	EC5 fan # 1		
58	speed	E5VS4011	%
	EC5 fan # 2		
59	speed	E5VS4021	%
	EC5 fan # 3		
60	speed	E5VS4031	%
	EC5 fan # 4		
61	speed	E5VS4041	%
	EC5 fan # 5		
62	speed	E5VS4051	%
63	Cogen return temperature	CGTTQ724	deg C

64	Powder 3 and 4 return temperature	P4TT9300	deg C
65	Casein return temperature	CATT9245	deg C
66	Milk Treatment return temperature	BCTT4902	deg C
67	Cream products return temperature	CPTTF037	deg C
68	Whey Products return temperature	WPTTF808	deg C
69	Powder 5 return temperature	E5TT4135	deg C
70	Ammonia chillers return flow	E5FT4127	Lt/sec
71	Site return flow	E5FT4130	Lt/sec

Appendix 6: Plant commissioning documentation

Kiwi Co-operative Dairies
Hawera

Ammonia Chilled Water Refrigeration
Operating and Maintenance Manual

C7189-OM-Rev 1

Factory Chilled Water Plate Heat Exchanger Units

The first stage development of this project had equipped the following factories with chilled water plate heat exchangers which are connected back to the **AER**.

Factory	Designation	Units	Size / unit	Drg Ref.
Powder 5	P5	2	1.5MW	C7189-03
Energy Centre 2	EC2	1	1.8MW	C7189-04
Milk Treatment (Supplementary)	MT	1	1.25MW	C7189-05
Cream Products	CP	2	1.75MW	C7189-06
Whey Products	WPC	2	3.75MW	C7189-07

Factories P5, EC2, MT and CP are connected to the **AER** through one set of ammonia refrigerant mains to Separator Vessel No. 1.

WPC is connected to Separator Vessel No. 2 via a separate set of ammonia refrigerant mains.

Ammonia refrigerant is pumped to the plate exchanger units from the separator vessels. The refrigerant temperature/pressure is regulated at the plate heat exchanger by an evaporator pressure regulating valve and the outlet of each plate heat exchanger.

The chilled water transfers heat to the refrigerant as it passes through the plate heat exchanger due to the temperature difference between the two mediums.

This results in a portion of the ammonia refrigerant evaporating inside the plate heat exchanger. The wet vapour returns to the separator vessel.

Performance data and base infomation about the factory chilled water plate heat exchangers is attached.

Kiwi Co-operative Dairies
Hawera

Ammonia Chilled Water Refrigeration
Operating and Maintenance Manual

C7189-OM-Rev

Ammonia Engine Room

Plant Description	Design Data
Evaporative Condensers	**BAC VXC N400** 2+3=VXCN800
• No of units	3 off
• Rated capacity per unit	1552 kW HOR
• Condensing temp. / ambient wet bulb temp.	35C / 21C
• Airflow	32.6 m^3/s
• Fan motor capacity	22 kW, 415 V, 50 Hz
• Water flow	29 l/s
• Pump motor capacity	4.0 kW, 415 V, 50 Hz
Plate Heat Exchanger Condensers	**Alfa Laval A15 - BWFD**
• No. of units	2 off (with provision for one future)
• Rated capacity per unit	4500 kW HOR
• Water flow rate per unit	153.7 l/s
• Pressure drop (water side)	85 kPa
• Water inlet temperature	26C
• Water outlet temperature	33C
• Condensing temperature	35C

Agent: Johnson controls NZ Ltd
09 444 6434

Kiwi Co-operative Dairies Hawera

Ammonia Chilled Water Refrigeration Operating and Maintenance Manual

C7189-OM-Rev

Ammonia Engine Room

Plant Description

Design Data

Compressor Unit No. 1.	**Stal SVA 89**
• Rated capacity	3180 kWR
• Drawn power (full load)	685 kW
• Saturated suction temperature / pressure	- 4C (268 kPa)
• Saturated condensing temperature / pressure	+ 35C (1255 kPa)
• Oil separator	Stal TAS 1300
• Oil cooler	Flotech WPR340-4000
• Oil temperature	+ 45C
• Oil charge	600 litres
• Oil type	Mobil SHC226
• Motor size	Weg 750 kW, 3300V, 50Hz
Compressor Unit No. 2.	**Stal SVA 87**
• Rated capacity	2177 kWR
• Drawn power (full load)	455 kW
• Saturated suction temperature / pressure	- 4C (268 kPa)
• Saturated condensing temperature / pressure	+ 35C (1255 kPa)
• Oil separator	Stal TAS 1000
• Oil cooler	Flotech HP180-3000
• Oil temperature	+ 45C
• Oil charge	500 litres
• Oil type	Mobil SHC226
• Motor size	Teco 525 kW, 415V, 50Hz
Compressor Unit No. 3.	**Stal SVA 83**
• Rated capacity	1089 kWR
• Drawn power (full load)	235 kW
• Saturated suction temperature / pressure	- 4C (268 kPa)
• Saturated condensing temperature / pressure	+ 35C (1255 kPa)
• Oil separator	Stal TAS 700
• Oil cooler	Flotech HP180-2000
• Oil temperature	+ 45C
• Oil charge	300 litres
• Oil type	Mobil SHC226
• Motor size	Teco 265 kW, 415V, 50Hz

Ammonia Engine Room

Plant Description

Design Data

Compressor Unit No. 4.	**Mycom 200VMD**
• Drawn power (full load)	200 kW
• Rated capacity	900 kWR
• Saturated suction temperature / pressure	- 4C (268 kPa)
• Saturated condensing temperature / pressure	+ 35C (1255 kPa)
• Oil separator	Weldtrade WT-OS-478
• Oil cooler	Flotech HP100-3000
• Oil temperature	+ 45C
• Oil charge	350 litres
• Oil type	Mobil SHC226
• Motor size	Teco 220 kW, 415V, 50Hz
Compressor Unit No. 5.	**Stal SVA 89**
• Rated capacity	3180 kWR
• Drawn power (full load)	665 kW
• Saturated suction temperature / pressure	- 4C (268 kPa)
• Saturated condensing temperature / pressure	+ 35C (1255 kPa)
• Oil separator	Stal TAS 1300
• Oil cooler	Flotech WPR340-4000
• Oil temperature	+ 45C
• Oil charge	600 litres
• Oil type	Mobil SHC226
• Motor size	Weg 750 kW, 3300V, 50Hz
Pump-out compressor unit	**Stal A2N**
• Motor size	Weg 11 kW, 400V, 50Hz, IP55
• Running speed	970 rpm

Ammonia Engine Room

Plant Description

Design Data

Separator Vessel No. 1.

• Vessel size	2743 mm ID x 4000 mm strake
• Liquid make-up valve	Masoneilan Camflex II 80NB (C_v = 54)
• Liquid level indicator	E & H DC11 TEN 4750mm AAIIBIBKAI
• Liquid level switches	E & H FTL 260 (DC supply)
• Operating level	25 %
• High high (HH) level	43 %
• High (H) level	40 %
• Low (L) level	15 %
• Low low (LL) level	12 %
• Suction pressure switch	RT 1A
• Suction pressure transmitter	AKS 33, - 1 to 9 bar
• Design operating pressure	268 kPa
• High pressure warning	330 kPa
• Low pressure warning	255 kPa
• Low low pressure alarm	241 kPa

Ammonia Liquid Pumps	**Hermetic CNF 65-200/1**
• No of pumps	2
• Rated duty	61.4 m^3/hr @ 48m
• Pump liquid pressure	568 kPa (300 kPa differential press)
• Motor	12 kW, 400 V, 50 Hz
• Pump pressure transmitter	AKS 33, -1 to 9 bar

Appendix 7: 3DT Optimiser programme example

Program Optimization Report

Company: **PanPac**
Plant: **Napier**
City: **Napier**
State: **Hawkes Bay**
Attention: **Customer Contact**
Copy: **Other Contact Names**

Date: **25-Nov-10**
Prepared by:
NALCO Copy to:

Summary and Recommendations	Program Performance	System Parameters	Value	Unit
This is the space where the Nalco Rep will write a summary of the program description and recommendations.	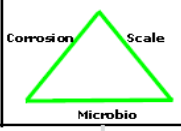	Recirculating Rate	10	m3/hr
		Delta T	9	C
		Volume	3	m3
		Cycles	2.7	
		Evaporation Rate	0	m3/hr
		Blowdown Rate	0	m3/hr
		Makeup Rate	0	m3/hr
		Holding Time Index	26	Hrs

Product Category or Control Parameter	Product Number or Control Parameter	Dosage or Control Set Point	Control Method	Product Description
Cycles of Concentration	2.7		Conductivity Set Point	na
pH	0		None	na
Multifunctional	3DT188	118.30	TRASAR	TM2, o-PO4, PSO, BZT, TT, THSP
Scale Inhibitor				
Copper Corrosion Inhibitor				
Mild Steel Corrosion Inhibitor				
Oxidizing Biocide	ST-70	0.66	Timer Control	Aqueous, one drum, stabilized bromine biocide that is already active and ready to feed for control of microorganisms and slime.
Bromine				
Non-Oxidizing Biocide	7330	100.00		This isothiazolin biocide is effective in a wide pH range against a broad spectrum of microorganisms. It is especially effective in combination with halogens, but may be inactivated by reduced sulfur species like sulfide.
Algaecide	90001	85.00		Non-oxidizing quaternary biocide for controlling algae and bacteria in recirculating cooling systems
Biodispersant	73551	20.00		Biodetergent 73551 is a non-biocidal compound that helps remove and prevent soft bacterial and silt deposits by solubilization and scrubbing with entrained air bubbles. 73551 should be used with a biocide, since it is not biocidal.
Bioreporter				

Performance Details		Model Value	Model Units	Recommendation
Corrosion	Mild Steel Cathodic Inhibitor (Ver: 1.5)	106.00	weight percent	The system has mild steel components. The program includes cathodic inhibitor components:, PSO(4.3 ppm). The total cathodic inhibitor residual is 106% of the recommended minimum for inhibiting pitting corrosion of mild
Corrosion	MS Anodic Corrosion (PO4 levels) (Ver: 1.6)	100.00	weight percent	The minimum PO4 required to inhibit MS corrosion at pH=8.51, Ca=68, total Zn=0 is 8.5 ppm PO4. System has 8.5 ppm or 100% of the minimum. PO4 level in system is above the requirement.
Corrosion	MS Corrosion PSO Products (Ver: 1.9)	0.40	mils per year	Corrosion threshold set to 2 by user. The mild steel corrosion rate is below the limit of 2 mpy.
Scale	Al Fouling (Ver: 1.2)	0.00	ppm Aluminum as Al	The program contains the following Al dispersant polymers: HSP. The cycled Al concentration is within the program limit of 2 ppm.
Scale	CaCO3 Scale Control (Ver: 1.24)	1,180.00	Unitless	The CaCO3 inhibitor is PSO. The CaCO3 saturation is 5. The scale inhibitor program is capable of safely handling saturations up to 59. The inhibition factor is 1180%. CaCO3 is adequately inhibited. Scale formation factors for
Scale	CaF2 Saturation (Ver: 1.0)	0.00	Unitless	Calcium fluoride (CaF2) is subsaturated and will not scale.
Scale	CaPO4/Trace Ion Inhibition (Ver: 1.9)	304.00	weight percent	Scale Temperature is 25C. The inhibitor threshold below 54 Degrees C is 90%. Calcium Phosphate and/or trace ions are adequately inhibited. The program contains dispersants ; HSP. Factors causing dispersant demand
Scale	CaSO4 Scaling (Ver: 1.6)	0.00	Unitless	The CaSO4 inhibitor is PSO(4.2588ppm). Gypsum saturation (CaSO4-2H2O) (D) at the basin temperature (25C/77F) is within acceptable limits (2) for this program.
Scale	HTT Limits (Ver: 1.2)	26.00	hours	Fouling considerations typically limit HTT to under 150 hours for systems having deposit/fouling issues with moderate cooling water contamination problems. Current HTT of 26 hours is acceptable.
Scale	Iron Fouling (Ver: 1.2)	0.00	ppm as Iron	The program contains the following iron dispersant polymers: HSP. The cycled Fe concentration is within the program limit of 5 ppm.
Scale	MgSiO3 Scaling potential (Ver: 1.2)	0.49	Unitless	MgSiO3 is subsaturated and will probably not scale.
Scale	Mn Fouling (Ver: 1.2)	0.00	ppm Manganese as Mn	The program contains the following Mn dispersant polymers: HSP. The cycled Mn concentration is within the program limit of 2 ppm.
Scale	SiO2 Scaling (Ver: 1.5)	0.97	Unitless	The ratio of the lower silica (185 ppm SiO2) to the silica limit under these conditions is 0.97. SiO2 scaling is unlikely as long as other deposits (CaCO3, Fe, etc) are well-controlled.
Microbio	Algae (Ver: 1.1)	0.50	Unitless	The tower has a history of algae fouling.
Microbio	Biocide Antagonisms (Ver: 1.2)	0.00	Unitless	The microbiological program contains a specific algaecides.
				There are 0 identified problems with the selected biocides.

Appendix 8: Deposit scale analysis

NALCO
Analytical Resources
21 Gul Lane Jurong Singapore 629416
Phone: 65-6505-6642 Fax: 65-6505-6781 Email: analyticallabsingapore@nalco.com

Final - Report Number: 168681

FONTERRA - WHAREROA
PO BOX 459
HAMILTON - - 3240 - NEW ZEALAND
Sold To: 0150142159 **Ship To:**
Representative: Alicia Stephens
Sample taken from: ECS BAC#2 Tower Scale

Batch Number:	SAB0962
Sample number:	SD002491
Date Sampled:	15-Mar-2010
Date Received:	23-Mar-2010
Date Completed:	30-Mar-2010
Date authorised:	31-Mar-2010

Deposit Analysis

Elemental analysis by X-ray Fluorescence

The sample preparation was: Dried at 105 °C

Silicon (SiO_2)	35 wt %
Calcium (CaO)	14 wt %
Iron (Fe_2O_3)	13 wt %
Magnesium (MgO)	4 wt %
Zinc (ZnO)	3 wt %
Aluminum (Al_2O_3)	2 wt %
Phosphorus (P_2O_5)	1 wt %
Total From XRF:	74 wt %

Total From XRF + Loss at 925 °C = 100%

The following elements were not detected or were below the reporting limit (< 0.5%):

Sb Ar As Ba Bi Br Cd Ce Cs Cl Cr Co Cu Dy Er Eu F Gd Ga Ge Au Hf Ho In I Ir La Pb Lu Mn Hg Mo Nd Ni Nb Os Pd Pt K Pr Re Rh Rb Ru Sc Sm Se Ag Na Sr S Ta Te Tb Sn Tm Ti V Tl Th U Yb Y Zr

Gravimetric Tests

Loss at 925 °C	26 wt %

The Loss at 925 °C includes water of hydration, CH_2Cl_2 extractables, all organics (carbon, hydrogen, nitrogen), many sulfur compounds and the CO_2 from most carbonates, and some volatile compounds.

Analysis by X-Ray Diffraction

The XRD was performed on: Dried at 105 °C
Calcium Carbonate (Calcite) - $CaCO_3$
Calcium Silicate (Larnite) - Ca_2SiO_4

Infrared Analysis

FT-IR analysis indicated that sample contained some carbonate and silicate.

Authorized by Tao Wen

Appendix 9: Coil diameter measurements made on 2nd of June, 2010

Measurement	Diameter (mm)	Measurement	Diameter (mm)
1	29.1	16	31.21
2	31.53	17	30.11
3	31.36	18	28.98
4	28.87	19	28.67
5	31.41	20	28.47
6	32.16	21	31.32
7	30.88	22	30.63
8	26.43	23	32.85
9	28.56	24	31.96
10	30.79	25	27.29
11	31.86	26	30.54
12	30.94	27	33.14
13	29.65	28	29.49
14	31.73	29	28.41
15	29.67	30	29.15

REFERENCES

International business forum. (2009). Retrieved May 11th, 2009, from APEC.

ASHRAE. (2008). Chapter 38: CONDENSERS . In ASHRAE, *2008 HANDBOOK* (pp. 38.1- 38.20). ASHRAE.

ASHRAE. (2008). CONDENSERS. In ASHRAE, *2008 ASHRAE HANDBOOK-HVAC Systems and Equipment (SI)* (p. 38.14). ASHRAE.

ASHRAE. (2008). COOLING TOWERS. In ASHRAE, *ASHRAE HANDBOOK: HVAC systems and equipment* (p. 39.1 to 39.20). ASHRAE.

ASHRAE. (2009). Chapter 4: Heat Transfer. In ASHRAE, *ASHRAE HANDBOOK* (pp. 4.1 - 4.34). ASHRAE.

ASHRAE. (2009). CHAPTER 5: Two Phase Flow. *ASHRAE Handbook 2009*.

Broeck, N. V. (2007). *Power Quality and Utilization.* Laborelec: Leonardo Energy.

Brownell, K. (1998). *"Investigation of the Field Performance for Industrial Refrigeration Systems", M.S. Thesis, Mechanical Engineering, Solar Energy Laboratory, University of Wisconsin.* Madison: University of Wisconsin.

Carrier. (1965). *Carrier Handbook of Air Conditioning System Design.* New York: McGraw-Hill.

Cleland, D., Love, R., & Merts, I. (2005). *Clandeboye powder chilled water model.* Palmerston North: Institute of Food, Nutrition and Human Health, Massey University.

Crowther, H., & Furlong, J. (2004). Optimisating Chillers & Towers. *ASHRAE Journal*, July, 34 to 40.

Dossat, R. J., & Horan, T. J. (2001). *PRINCIPLES OF REFRIGERATION FIFTH EDITION.* London: Prentice Hall.

Dreyer, A. A. (1988). *Analysis of evaporative coolers and condensers, MSc thesis, University of Stellenbosch, SA.* Cape Town: University of Stellenbosch.

Elsarrag, E. (2006). Experimental study and predictions of an induced draft ceramic tile packing cooling tower. *Energy Conservation and Management*, (47) 2034 to 2043.

Ettouney, H., El-Dessouky, H., Bouhamra, W., & Al-Azmi, B. (2001). Performance of evaporative condensers. *Heat Transfer Eng 22*, 41-55.

Fonterra, W. (2009). *Whareroa Instrument Works Report.* Hawera: Fonterra.

Gehan, K. (2005). *Wet Surface Air Cooler (WSAC) Performance Monitoring.* Melbourne: Gehan, K;.

Gehan, K., & Hook, A. (2007). *Greenhouse Gas Reduction from fossil fuel power stations- The effect of surface condenser and cooling tower performance.* Melbourne: Nalco.

Goodman, W. (1938). The evaporative condenser. *Heat Piping Air Cond 10*, 165-328.

Halasz, B. (1998 (37)). A general mathmatical model of evaporative cooling devices. *Rev G'en Therm*, 245-255.

Hesselgreaves, J. (2002). An approach of fouling allowances in the design of compact heat exchangers. *Applied Thermal Engineering 22*, 755-762.

Hosoz, M., & Kilicarslan, A. (2004). Performance evaluations of refrigeration systems with air-cooled, water-cooled and evaporative condensers. *International journal of energy research*, (28) 683 to 696.

Kern, D., & Seaton, R. (1959). A theoretical analysis of thermal surface fouling. *Journal Chem Eng 4, (5)*, 258-262.

Khan, J., Qureshi, B., & Zubair, S. (2004). A comprehensive design and performance evaluation study of counterflow wet cooling towers. *Int J Refrigeration 27*, 914-923.

Kirkpatrick, J., McIntire, L., & Characklis, W. (1980). Mass and heat transfer in a circular tube with biofouling. *Water Research Vol 14*, 117-127.

Love, R. J., & Cleland, D. (2007). *Chilled water-it's too cold!-the problem of return water temperature depression and strategies to solve it.* Palmerston North: Centre for Postharvest and Refrigeration Research, Massey University.

Love, R., & Cleland, D. (2006). Modelling the performance of industrial chilled water systems. *IIR-IRHACE Conference, University of Auckland* (p. 580 to 587). Auckland: Centre of Postharvest and Refrigeration Research, Massey University.

Love, R., & Cleland, D. (2007). *Heat Recovery Modifications to EC5 Compressor Scheduling Tool.* Palmerston North: Massey University.

Love, R., Cleland, D., & Merts, I. (2008). *What is the optimum compressor discharge pressure setpoint for condensers?* c.

Macleod-Smith, R. (September, 2003). Controlling Legionella without damaging your Evaporative Condenser. *Health Estate Journal*, 50-56.

Maiya, M. (1995). Analysis of modified counter-flow cooling towers. *Heat recovery systems and CHP*, Vol. 15, no 3, 293 to 303.

Manske, K., Reindl, D., & Klein, S. (2001). Evaporative Condenser Control in Industrial Refrigeration Systems. *International Journal of Refrigeration*, pp. Vol. 24; No 7; pp.676-691.

Mizushina, T., Ito, R., & Miyashita, H. (1967). Experimental study of an evaporative cooler. *Int Chem Eng 7 (4)*, 727-732.

Morris, T., & Blaine, S. (2008). Chiller Plant Optimisation tool. *ASHRAE Journal*, July, 54 to 59.

Nalco. (1988). *The NALCO Water Handbook Second Edition.* New York: McGraw Hill.

New Zealand Ministry of Economic Development. (2008). *New Zealand Green House Gas Emissions 1990-2007.* Wellington: MED.

Panjeshahi, M., Ataei, A., Gharaie, M., & Parand, R. (2009). Optimum design of cooling water systems for energy and water conservation. *Chemical Engineering Research and Design*, (87) 200-209.

Parker, R., & Treybal, R. (1961). The heat, mass transfer characteristics of evaporative coolers. *AIChE Chem Eng Prog Symp Ser57 (32)* (pp. 138-149). AIChE.

Perry, R. (1963). *Perry's Chemical Engineer's Handbook.* Mew York: McGraw Hill.

Peterson, D., Glasser, D., & Williams, D. (1988). Predicting the performance of an Evaporative Condenser. *ASME trans., Journal of Heat Transfer vol 110, no. 3*, 748-753.

Peterson, J. (1993). An Effectiveness Model for Indirect Evaporative Coolers. *ASHRAE Trans.,vol 99*, 392-399.

Qureshi, B., & Zubair, S. (2005). The impact of fouling on performance evaluation of evaporative coolers and condensers. *International Journal of Energy Research*, 19:1313-1330.

Qureshi, B., & Zubair, S. (2006). A comprehensive design and rating study of evaporative coolers and condensers. Part I. Performance evaluation. *International Journal of Refrigeration 29*, 645-658.

Qureshi, B., & Zubair, S. (2007). Second-law-based performance evaluation of cooling towers and evaporative heat exchangers. *International Journal of Thermal Sciences*, (46) 188 to 198.

Stabat, P., & Marchio, D. (2004). Simplified model for indirect-contact evaporative cooling-tower behaviour. *Applied Energy*, (78) 433-451.

Thompsen, E. (1946). Heat transfer in an evaporative condenser. *Refrigeration Eng 51 (5)*, 425-431.

Webb, R., & Villacres, A. (1984). Algorithms for performance simulation of cooling towers, evaporative condensers fluid coolers. *ASHRAE Trans 90 (Part 2B)*, 416-458.

Williams, P. (2010). *Nalco Eco Reference Guide.* Chicargo: Nalco.